


Doctoral Dissertation
Doctoral Program in Electrical, Electronic and Communications Engineering
(36^{th} cycle)

Scaling Optical Transport using Multi-band Photonic Integrated Switching Systems

Muhammad Umar Masood

* * * * *

Supervisors
Prof. Vittorio Curri, Supervisor
Prof. Andrea Carena, Co-supervisor
Prof. Paolo Bardella, Co-supervisor

Doctoral Examination Committee:
Prof. Francesco Musumeci, Referee, Politecnico di Milano
Prof. Francesco DA ROS, Referee, Technical University of Denmark - DTU

Politecnico di Torino
2024

I hereby declare that, the contents and organisation of this dissertation constitute my own original work and does not compromise in any way the rights of third parties, including those relating to the security of personal data.

. . . . . .

Muhammad Umar Masood

Turin, 2024

Acknowledgements

I extend my deepest gratitude to Prof. Vittorio Curri for the privilege of joining the PLANET group, marking the commencement of my Ph.D. journey. His mentorship has been a guiding beacon throughout my academic exploration.

I am equally thankful to my co-supervisors, Prof. Andrea Carena and Prof. Paolo Bardella, for their invaluable support and insights.

A special acknowledgment goes out to Ihtesham Khan, Bruno Correia, Lorenzo Tunesi, and all my colleagues at the Department of Electronics and Telecommunications—our camaraderie and shared moments have truly enriched my experience. I extend a warm thank you to Rasoul Sadeghi, Emanuele Virgilito, Andrea D'Amico, Giacomo Borraccini, Elliot London, and Shahzad Alam for being an integral part of my journey.

Above all, I owe the completion of this chapter to my family, whose unwavering support and love have been my foundation. My mother deserves a heartfelt mention for her emotional strength and constant encouragement; my father, for his perseverance and wisdom; and to my wife, whose boundless support and presence have been my constant encouragement over these pivotal three years.

Abstract

This thesis explores the growth of optical transport networks using a novel Reconfigurable Optical Add-Drop Multiplexer (ROADM) design that incorporates a photonic integrated multi-band Wavelength Selective Switch (WSS). This sophisticated technology was designed specifically to greatly improve the capability and effectiveness of multi-band optical transport networks. It achieves this by facilitating operations across the S, C, and L bands, hence enabling transfers ranging from 400G to 1.2T. The architecture utilizes the existing fiber infrastructure and incorporates real-world network topologies from different countries such as Germany, Italy, Spain, and the USA. It aims to demonstrate the practical advantages of transitioning from traditional C-band only systems to more flexible multi-band configurations. This change not only attempts to enhance network performance and capacity, but also effectively decreases capital costs by decreasing the requirement for further fiber deployments.

In addition to enhancing this study, machine learning methods are used to forecast control and routing states in the photonic switching systems, enabling the dynamic administration of network traffic. These algorithms are specifically developed to be independent of network topology and technology, allowing them to be applied in various network contexts and improving their effectiveness in controlling switch planes in real-time. The machine learning technique enhances data flow efficiency and enhances the Quality of Transmission (QoT) by evaluating viable pathways and improving network element design.

Comprehensive network simulations and performance assessments have shown that the utilization of the multi-band method, coupled with the WSS amd WBSS, not only fulfills but surpasses the limits of traditional networks. This technique effectively manages higher volumes of data traffic with improved efficiency and decreased operational expenses. The findings of this study emphasize the significant and revolutionary effect of incorporating advanced photonic and machine learning technology into optical networking. The results emphasize the most effective network setups that optimize both performance and capacity, providing a future-oriented viewpoint on network administration. This study lays the foundation for future progress in optical networking technology, with a focus on scalability and efficiency in situations with high demand. It also offers useful insights into the

strategic implementation of next-generation optical transport systems.

Contents

List of Tables

List of Figures

List of Scientific Contributions

A list of the scientific contributions, with special focus on publications, carried out during the PhD are described here.

Original publications included in this PhD thesis

Peer Reviewed International Journals

[1] M. U. Masood, L. Tunesi, I. Khan, C. Bruno, R. SADEGHI YAMCHI, E. Ghillino, P. Bardella, A. Carena, V. Curri, et al., "Networking assessment of roadm architecture based on photonics integrated wss for 800g multi-band optical transport," Journal of Optical Communicaitons and Networking, 2023 doi: 10.1364/JOCN.489754.

[2] L. Tunesi, I. Khan, M. U. Masood, E. Ghillino, V. Curri, A. Carena, and P. Bardella, "Design and performance assessment of modular multi-band photonic-integrated wss," Opt. Express, vol. 31, no. 22, pp. 36 486–36 502, Oct. 2023. doi: 10.1364/OE.498596.

[3] I. Khan, L. Tunesi, M. U. Masood, E. Ghillino, P. Bardella, A. Carena, and V. Curri, "Optimized management of ultra-wideband photonics switching systems assisted by machine learning," Optics Express, vol. 30, no. 3, pp. 3989–4004, 2022.

[4] I. Khan, L. Tunesi, M. U. Masood, E. Ghillino, P. Bardella, A. Carena, and V. Curri, "Performance evaluation of data-driven techniques for the softwarized and agnostic management of an n× n photonic switch," Optics Continuum, vol. 1, no. 1, pp. 1–15, 2022.

[5] I. Khan, M. Bilal, M. U. Masood, A. D'Amico, and V. Curri, "Lightpath qot computation in optical networks assisted by transfer learning," Journal of Optical Communications and Networking, vol. 13, no. 4, B72–B82, 2021.

[6] I. Khan, L. Tunesi, M. U. Masood, E. Ghillino, P. Bardella, A. Carena, and V. Curri, "Automatic management of n× n photonic switch powered by machine

learning in software-defined optical transport," IEEE Open Journal of the Communications Society, vol. 2, pp. 1358–1365, 2021.

[7] F. Usmani, I. Khan, M. U. Masood, A. Ahmad, M. Shahzad, and V. Curri, "Convolutional neural network for quality of transmission prediction of unestablished lightpaths," Microwave and Optical Technology Letters, vol. 63, no. 10, pp. 2461–2469, 2021.

[8] F. Usmani, I. Khan, M. Siddiqui, M. Khan, M. Bilal, M. U. Masood, A. Ahmad, M. Shahzad, and V. Curri, "Cross-feature trained machine learning models for qot-estimation in optical networks," Optical Engineering, vol. 60, no. 12, pp. 125 106–125 106, 2021.

[9] I. Khan, A. Ahmad, M. U. Masood, A. W. Malik, N. Ahmed, and V. Curri, "Impact of data center placement on the power consumption of flexible-grid optical networks," Optical Engineering, vol. 59, no. 1, pp. 016 115–016 115, 2020

Contributions to International Conferences

[1] Masood, M.U., Khan, I., Correia, B., Tunesi, L., Marchisio, A., Ghillino, E., Bardella, P., Carena, A. and Curri, V., 2024, July. Impact of Waveband and Wavelength Switching in the Next-Generation Optical Networks. In 2024 24th International Conference on Transparent Optical Networks (ICTON) (pp. 1-4). IEEE.

[2] Masood, Muhammad Umar, Ihtesham Khan, Lorenzo Tunesi, Bruno Correia, Andrea Marchisio, Enrico Ghillino, Paolo Bardella, Andrea Carena, and Vittorio Curri. "Waveband selective switch: a network analysis for advanced optical transport networks in 6G and beyond technologies." In Next-Generation Optical Communication: Components, Sub-Systems, and Systems XIII, p. PC128940D. SPIE, 2024.

[3] I. Khan, A. Marchisio, L. Tunesi, M. U. Masood, E. Ghillino, V. Curri, A. Carena, and P. Bardella, "A machine learning-based model for characterizing stationary-and-dynamic behavior of vcsel," in CLEO: Fundamental Science, Optica Publishing Group, 2023, JW2A–141

[4] I. Khan, M. U. Masood, L. Tunesi, E. Ghillino, A. Carena, V. Curri, and P. Bardella, "Two-step machine learning assisted extraction of vcsel parameters," in Physics and Simulation of Optoelectronic Devices XXXI, SPIE, vol. 12415, 2023, pp. 159–162.

[5] A. Marchisio, I. Khan, L. Tunesi, M. U. Masood, E. Ghillino, V. Curri, A. Carena, P. Bardella, et al., "Automated model for characterization of vcsel circuit-level parameters using machine learning," in European Conference on Integrated Optics, European Conference on Integrated Optics, 2023, pp. 264–266.

[6] M. U. Masood, I. Khan, L. Tunesi, B. Correia, E. Ghillino, P. Bardella, A. Carena, and V. Curri, "Multiband photonic integrated wss beyond 1tb/s data center interconnect technology," in 2023 International Conference on Photonics in Switching and Computing (PSC), 2023, pp. 1–3. doi: 10.1109/PSC57974.2023.10297220.

[7] M. U. Masood, L. Tunesi, I. Khan, B. Correia, E. Ghillino, P. Bardella, A. Carena, and V. Curri, "A comprehensive network performance analysis of multi-band photonic integrated wss for 400g and 800g transmission," in 2023 23rd International Conference on Transparent Optical Networks (ICTON), IEEE, 2023, pp. 1–4.

[8] M. U. Masood, L. Tunesi, I. Khan, B. Correia, E. Ghillino, P. Bardella, A. Carena, and V. Curri, "Multi-band photonic integrated wss for 800g optical data center interconnect systems," in 2023 IEEE Photonics Society Summer Topicals Meeting Series (SUM), IEEE, 2023, pp. 1–2.

[9] M. U. Masood, L. Tunesi, I. Khan, B. Correia, E. Ghillino, P. Bardella, A. Carena, and V. Curri, "Network performance analysis of a pic-based reconfigurable add-drop multiplexer for multiband applications," in Next-Generation Optical Communication: Components, Sub-Systems, and Systems XII, SPIE, vol. 12429, 2023, pp. 81–86.

[10] H. Tariq, F. Usmani, I. Khan, M. U. Masood, A. Ahmad, and V. Curri, "Iterative transfer learning approach for qot prediction of lightpath in optical networks," in 2023 23rd International Conference on Transparent Optical Networks (ICTON), IEEE, 2023, pp. 1–4.

[11] L. Tunesi, I. Khan, M. U. Masood, E. Ghillino, A. Carena, V. Curri, and P. Bardella, "Integrated multi-band wss: From design to performance evaluation," in 2023 International Conference on Photonics in Switching and Computing (PSC), 2023, pp. 1–4. doi: 10.1109/PSC57974.2023.10297184.

[12] L. Tunesi, I. Khan, M. U. Masood, E. Ghillino, A. Carena, V. Curri, and P. Bardella, "Photonic-integrated wavelength selective switch for s+ c+ l applications," in Optical Components and Materials XX, SPIE, vol. 12417, 2023, pp. 149–153.

[13] L. Tunesi, I. Khan, M. U. Masood, A. Marchisio, E. Ghillino, V. Curri, A. Carena, and P. Bardella, "Machine learning aided prediction of fabrication uncertainties in integrated multi-ring filters," in CLEO: Science and Innovations, Optica Publishing Group, 2023, STh4H–2.

[14] F. Usmani, I. Khan, M. U. Masood, A. Ahmad, and V. Curri, "Knowledge distillation-based compression model for qot estimation of an unestablished lightpaths," in 2023 23rd International Conference on Transparent Optical Networks (ICTON), IEEE, 2023, pp. 1–4.

[15] I. Khan, N. U. H. Ajmal, H. Tariq, L. Tunesi, M. U. Masood, E. Ghillino, P. Bardella, A. Carena, A. Ahmad, and V. Curri, "Multi-labeled random-forest enabled softwarized management for photonics switching systems," in 2022 Asia Communications and Photonics Conference (ACP), IEEE, 2022, pp. 498–502.

[16] I. Khan, L. Tunesi, M. U. Masood, E. Ghillino, P. Bardella, A. Carena, and V. Curri, "Machine learning aided characterization of multi-stage integrated ring resonator filters," in Integrated Photonics Research, Silicon and Nanophotonics, Optica Publishing Group, 2022, IM3B–4.

[17] I. Khan, L. Tunesi, M. U. Masood, E. Ghillino, P. Bardella, A. Carena, and V. Curri, "Optimal control of beneš optical networks assisted by machine learning," in Next-Generation Optical Communication: Components, Sub-Systems, and Systems XI, SPIE, vol. 12028, 2022, pp. 102–111.

[18] I. Khan, L. Tunesi, M. U. Masood, E. Ghillino, A. Carena, P. Bardella, and V. Curri, "Performance analysis of novel multi-band photonic-integrated wss operated on 400zr," in 2022 IEEE Photonics Society Summer Topicals Meeting Series (SUM), IEEE, 2022, pp. 1–2.

[19] I. Khan, L. Tunesi, M. U. Masood, E. Ghillino, A. Carena, V. Curri, and P. Bardella, "Machine learning assisted extraction of vertical cavity surface emitting lasers parameters," in 2022 IEEE Photonics Conference (IPC), IEEE, 2022, pp. 1–2.

[20] I. Khan, L. Tunesi, M. U. Masood, E. Ghillino, V. Curri, A. Carena, and P. Bardella, "Autonomous data-driven model for extraction of vcsel circuit-level parameters," in 2022 Asia Communications and Photonics Conference (ACP), IEEE, 2022, pp. 1530–1533.

[21] I. Khan, L. Tunesi, M. U. Masood, E. Ghillino, V. Curri, A. Carena, and P. Bardella, "Machine learning-based model for defining circuit-level parameters of vcsel," in 2022 International Conference on Software, Telecommunications and Computer Networks (SoftCOM), IEEE, 2022, pp. 1–6.

[22] M. U. Masood, I. Khan, L. Tunesi, B. Correia, E. Ghillino, P. Bardella, A. Carena, and V. Curri, "Network performance of roadm architecture enabled by novel wideband-integrated wss," in GLOBECOM 2022-2022 IEEE Global Communications Conference, IEEE, 2022, pp. 2945–2950.

[23] M. U. Masood, I. Khan, L. Tunesi, B. Correia, E. Ghillino, P. Bardella, A. Carena, and V. Curri, "Network traffic analysis of modular multiband integrated wss based roadms," in 2022 IEEE Photonics Conference (IPC), IEEE, 2022, pp. 1–2.

[24] M. U. Masood, I. Khan, L. Tunesi, B. Correia, R. Sadeghi, E. Ghillino, P. Bardella, A. Carena, and V. Curri, "Networking analysis of photonics integrated multiband wss based roadm architecture," in 2022 International Conference on Software, Telecommunications and Computer Networks (SoftCOM), IEEE, 2022, pp. 1–6.

[25] M. U. Masood, L. Tunesi, B. Correia, I. Khan, E. Ghillino, P. Bardella, A. Carena, and V. Curri, "Photonics integrated multiband wss based roadm architecture: A networking analysis," in 2022 Asia Communications and Photonics Conference (ACP), IEEE, 2022, pp. 1243–1247.

[26] L. Tunesi, I. Khan, M. U. Masood, E. Ghillino, A. Carena, P. Bardella, and V. Curri, "Novel design and operation of photonic-integrated wss for ultra-wideband applications," in 2022 IEEE Photonics Society Summer Topicals Meeting Series (SUM), IEEE, 2022, pp. 1–2.

[27] L. Tunesi, I. Khan, M. U. Masood, E. Ghillino, A. Carena, V. Curri, and P. Bardella, "Modular photonic-integrated device for multi-band wavelength-selective switching," in 2022 27th OptoElectronics and Communications Conference (OECC) and 2022 International Conference on Photonics in Switching and Computing (PSC), IEEE, 2022, pp. 1–3.

[28] F. Usmani, I. Khan, M. U. Masood, A. Ahmad, M. Shahzad, and V. Curri, "Qot-estimation assisted by transfer learning in extended c-band network operating on 400zr," in 2022 IEEE Photonics Society Summer Topicals Meeting Series (SUM), IEEE, 2022, pp. 1–2.

[29] F. Usmani, I. Khan, M. U. Masood, A. Ahmad, M. Shahzad, and V. Curri, "Transfer learning aided qot computation in network operating with the 400zr standard," in 2022 International Conference on Optical Network Design and Modeling (ONDM), IEEE, 2022, pp. 1–6.

[30] F. Usmani, I. Khan, H. Tariq, M. U. Masood, M. Shahzad, A. Ahmad, and V. Curri, "Performance analysis of transfer-learning approaches for qot estimation of network operating with 400zr," in 2022 Asia Communications and

Photonics Conference (ACP), IEEE, 2022, pp. 1238–1242.

[31] S. Alam, I. Khan, M. U. Masood, A. Ahmad, S. Ghafoor, and V. Curri, "Routing and spectrum allocation heuristic for sliced elastic optical network system," in 2021 IEEE Photonics Society Summer Topicals Meeting Series (SUM), IEEE, 2021, pp. 1–2.

[32] S. Alam, M. U. Masood, I. Khan, A. Ahmad, S. Ghafoor, and V. Curri, "Modeling off-line routing and spectrum allocation problem in elastic optical network," in 2021 International Conference on Electrical, Communication, and Computer Engineering (ICECCE), IEEE, 2021, pp. 1–6.

[33] I. Khan, M. U. Masood, L. Tunesi, P. Bardella, E. Ghillino, A. Carena, and V. Curri, "A neural network-based automatized management of n× n integrated optical switches," in Photonic Networks and Devices, Optica Publishing Group, 2021, NeF2B–2.

[34] I. Khan, M. U. Masood, L. Tunesi, P. Bardella, E. Ghillino, A. Carena, and V. Curri, "Machine learning assisted management of photonic switching systems," in CLEO: Science and Innovations, Optica Publishing Group, 2021, JTu3A–32.

[35] I. Khan, M. U. Masood, L. Tunesi, E. Ghillino, P. Bardella, A. Carena, and V. Curri, "A data-driven approach to autonomous management of photonic switching system," in 2021 IEEE Photonics Society Summer Topicals Meeting Series (SUM), IEEE, 2021, pp. 1–2.

[36] I. Khan, M. U. Masood, L. Tunesi, E. Ghillino, P. Bardella, A. Carena, V. Curri, et al., "Softwarized and autonomous management of photonic switching systems using machine learning," in 2021 International Conference on Optical Network Design and Modeling (ONDM), IFIP, 2021.

[37] I. Khan, L. Tunesi, M. Chalony, E. Ghillino, M. U. Masood, J. Patel, P. Bardella, A. Carena, and V. Curri, "Machine-learning-aided abstraction of photonic integrated circuits in software-defined optical transport," in Next-Generation Optical Communication: Components, Sub-Systems, and Systems X, SPIE, vol. 11713, 2021, pp. 145–150.

[38] I. Khan, L. Tunesi, M. U. Masood, E. Ghillino, P. Bardella, A. Carena, and V. Curri, "Autonomous control model for c+ l multi-band photonic switch system using machine learning," in Asia Communications and Photonics Conference, Optica Publishing Group, 2021, T4A–163.

[39] I. Khan, L. Tunesi, M. U. Masood, E. Ghillino, P. Bardella, A. Carena, and V. Curri, "Machine learning assisted accurate estimation of qot impairments of

photonics switching system on 400zr," in Asia Communications and Photonics Conference, Optica Publishing Group, 2021, T2B–2.

[40] I. Khan, L. Tunesi, M. U. Masood, E. Ghillino, P. Bardella, A. Carena, and V. Curri, "Machine learning assisted model of qot penalties for photonics switching systems," in Photonics in Switching and Computing, Optica Publishing Group, 2021, M2A–3.

[41] I. Khan, L. Tunesi, M. U. Masood, E. Ghillino, P. Bardella, A. Carena, and V. Curri, "Machine learning driven model for software management of photonics switching systems," in 2021 IEEE Global Communications Conference (GLOBECOM), IEEE, 2021, pp. 1–6.

[42] F. Shahzad, I. Khan, M. U. Masood, A. Ahmad, M. Imran, M. Ruffini, and V. Curri, "Impairment-aware virtual network embedding using time domain hybrid modulation formats in optical networks," in 2021 International Conference on Optical Network Design and Modeling (ONDM), IEEE, 2021, pp. 1–6.

[43] F. Usmani, I. Khan, M. Siddiqui, M. Khan, M. Bilal, M. U. Masood, A. Ahmad, M. Shahzad, and V. Curri, "Evaluating cross-feature trained machine learning models for estimating qot of unestablished lightpaths," in 2021 International Conference on Electrical, Communication, and Computer Engineering (ICECCE), IEEE, 2021, pp. 1–6.

[44] I. Khan, M. Chalony, E. Ghillino, M. U. Masood, J. Patel, D. Richards, P. Mena, P. Bardella, A. Carena, and V. Curri, "Effectiveness of machine learning in assessing qot impairments of photonics integrated circuits to reduce system margin," in 2020 IEEE Photonics Conference (IPC), IEEE, 2020, pp. 1–2.

[45] I. Khan, M. Chalony, E. Ghillino, M. U. Masood, J. Patel, D. Richards, P. Mena, P. Bardella, A. Carena, and V. Curri, "Machine learning assisted abstraction of photonic integrated circuits in fully disaggregated transparent optical networks," in 2020 22nd International Conference on Transparent Optical Networks (ICTON), IEEE, 2020, pp. 1–4.

[46] M. U. Masood, I. Khan, A. Ahmad, M. Imran, and V. Curri, "Smart provisioning of sliceable bandwidth variable transponders in elastic optical networks," in 2020 6th IEEE Conference on Network Softwarization (NetSoft), IEEE, 2020, pp. 85–91

Chapter 1

Introduction

In recent years, optical communication systems have experienced revolutionary progress, with notable improvements in their capacity, reliability, and adaptability. The development of these systems has been closely connected to breakthroughs in optical fiber technology and progress in photonic devices, both of which are crucial in manipulating light to enhance signal integrity. This thesis explores the potential of utilizing a more comprehensive knowledge of photonic technologies and their influence on signal quality to optimize the design and efficient expansion of optical network capabilities. The optical network infrastructure, which is essential for transmitting data, is presently facing an unprecedented level of strain due to the increasing need for greater bandwidth.

This demand is driven by a wide range of applications that require large amounts of data: from the exchange of terabytes of data between research institutions, to the movement of enterprise services and data storage to the cloud, the transfer of high-definition medical images between hospitals, to the increasing use of advanced educational technologies, among other examples. These advancements are coming together to form an intricate problem marked by escalating expenses and heightened network intricacy. Data transmission relies on the extensive, pre-existing network of optical fibers. Instead of investing a lot of money and inflexibly expanding the physical network infrastructure, an alternate approach may entail integrating technologies that improve the efficiency of the current fiber network, without making any changes to the existing infrastructure. An excellent method to enhance network performance is to tap into underutilized optical spectrum bands, hence increasing capacity and providing a cost-effective solution. This thesis explores these options, analyzing their impact on network performance and assessing them from both an energy consumption and a techno-economic perspective.

1.1 Motivation

In recent years, there has been a significant and steady annual increase in internet traffic, with a growth rate above 30%. This growth may be attributed mostly to the increasing number of devices linked to the internet. Projections indicate that there would be a sustained rise in the demand for communications network capacity on a global scale. The driving forces behind this include cloud computing, high-definition video streaming, immersive virtual reality experiences, and the emergence of 5G/6G technology.

Optical communication technologies have played a crucial role in the fast expansion of data traffic. Nevertheless, they are already approaching the theoretical maximum information capacity referred to as the nonlinear Shannon limit [1]. This limit represents the maximum achievable data rates for point-to-point fiber optic transmission. As a result, optical systems are facing difficulties in keeping pace with the rapid increase in IP traffic. This is a major problem for the telecommunications sector, as it has to find cost-efficient methods to fulfill the surging need for bandwidth. This difficulty is exacerbated by the fact that telecommunications operators have been seeing a decrease in income over the past decade, and it is expected that expenses per bit will soon surpass operator revenues.

Telecom businesses are forced to choose between supporting more traffic and successfully handling their finances. It is important to assess the impact of photonic communication technologies on network capacity expansion, improved network management, and the cost-effectiveness. Operators are required to select the appropriate technologies for designing and improving network topologies, while suppliers must decide on their priorities for future product development. Typically, the impact of transmission layer technology is evaluated for point-to-point connections that are running at maximum capacity, which is considered the most favorable situation. Due to limitations such as wavelength and spectrum competition, it is not possible to fully utilize all of the available spectrum in fiber networks.

Developing sustainable and economically viable methods to manage the growing traffic in the optical transport network while simultaneously decreasing energy consumption is of utmost importance. Wavelength Division Multiplexing (WDM) is proposed as an effective approach for managing the fast increase in traffic in optical communication networks [2]. WDM improves the effectiveness of fiber infrastructure by enabling many data streams to be transmitted simultaneously across a single optical connection. This optimizes the utilization of available bandwidth and leads to cost reduction. This is accomplished by partitioning the available frequency spectrum into narrower WDM channels, which enhances the efficiency of fiber utilization and streamlines network investments [3]. Telecommunication operators often operate within a WDM bandwidth of 4.8 THz, commonly in the optical fiber's C-band frequency range [4]. Multi-band transmission (MBT) is a

strategic approach that can fulfill capacity requirements without necessitating substantial modifications to existing optical fiber networks. This approach involves use a broader range of wavelengths, namely inside the low-loss zone of the frequently used single-mode optical fibers, specifically the ITU-T G.652.D variant. This enables the possibility of transmitting data at a bandwidth of around 50 THz [4, 5]. Multiple studies have clarified the effectiveness of MBT in different ranges of wavelengths, ranging from the O-band to the L-band [6, 7, 8]. Commercial solutions for MBT in the C+L-band have already been shown [9]. Consequently, studies have focused on these specific frequency ranges in order to obtain improved data transfer speeds and increased transmission lengths.

One major benefit of using MBT for network improvement is the use of existing fiber infrastructure, which leads to a substantial reduction in Capital Expenditure (CAPEX) compared to other upgrade options [10, 11]. However, managing several spectral bands presents challenges for the telecom sector. This is because it requires integrating extra optical devices for each band, and each device has its own distinct operational characteristics across different bands and frequencies.

The objective of this thesis is to do a thorough examination of MBT in optical transport networks. This study analyzes the physical layer to the network layer in disaggregated optical networks, with focus on the network capacity enhancements for various network elements.

1.2 Outline of the thesis

This thesis presents a comprehensive analysis at the networking level to evaluate multi-band transmission systems, focusing on detailed modeling of propagation impairments and the capabilities of multi-band switching devices. These elements are crucial for understanding the capacity limitations and the options available for expanding network capabilities.

Chapter 2 delves into the optical network architecture, discusses multi-band systems, and explores physical layer propagation modeling. This provides the foundational knowledge needed to assess the impact of multi-band technologies on network design and performance.

In Chapter 3, we explore a machine learning framework designed to predict control states and the quality of transmission within switching architectures. This chapter highlights how machine learning can enhance the management and efficiency of optical networks.

Chapter 4 details the simulation tools used and provides a comprehensive networking-level performance analysis under various network conditions. It includes a thorough comparison of network capacities enabled by multi-band technologies, offering insights into the benefits and limitations of these systems.

Chapter 5 concludes the thesis and discusses potential avenues for future research. This final chapter summarizes the findings and underscores the implications for future developments in optical network technologies.

Chapter 2

Optical network architecture and modelling

2.1 Optical network structure

Figure 2.1 visually represents the complete hierarchical structure of communication networks. The highest tier encompasses the long-haul or backbone optical networks, which typically span hundreds to thousands of kilometers [12]. These networks are tasked with transmitting high-capacity optical communications over extensive distances (in some cases between countries or continents). Long-haul networks employ Dense Wavelength Division Multiplexing (DWDM) to concurrently transport multiple data streams over a single fiber optic cable. Each data stream is allocated a unique wavelength within the DWDM system. As a result, long-haul networks have achieved remarkable capacity, with certain networks capable of transmitting terabits of data per second over a single fiber.

The second tier is the regional optical networks. Regional optical networks are the foundation of modern communication infrastructure, enabling the smooth transfer of data between metropolitan areas and rural communities in a certain geographic region. These networks serve as crucial connections that link long-haul networks covering large distances with metropolitan networks catering to heavily populated regions. Regional networks efficiently handle data transfer using advanced optical transport technologies including optical amplifiers and wavelength selective switches to provide maximum performance and reliability. Utilizing advanced optical technology in regional networks allows them to attain unparalleled efficiency and capacity. Optical amplifiers increase signal strength to extend data transmission lengths without degradation, while wavelength selective switches provide accurate routing of data streams to their designated destinations. These networks are crucial for facilitating smooth communication and promoting economic

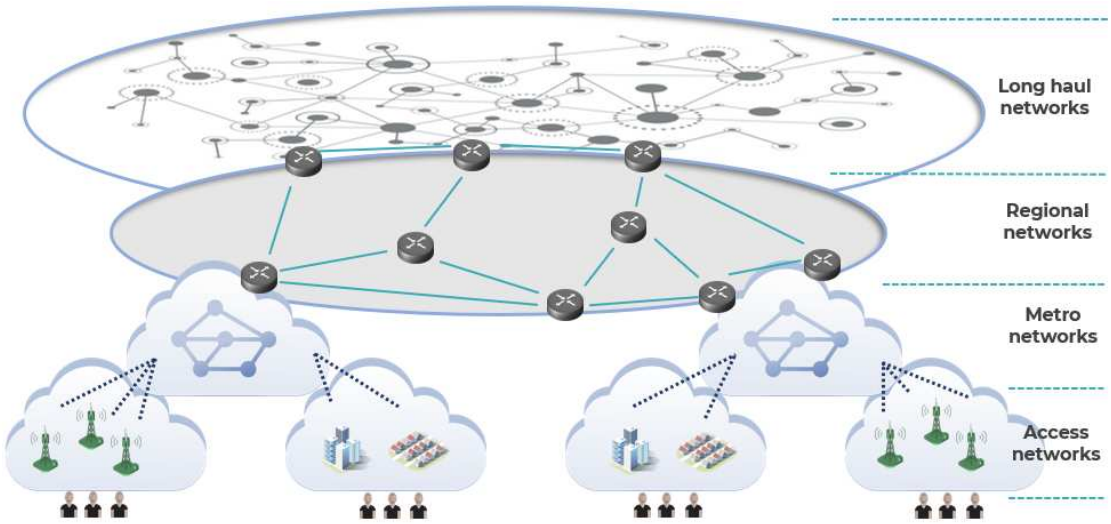

Figure 2.1: Communication network structure

growth within different areas by reducing delays, maximizing capacity, and maintaining reliable connectivity across regional centers. The third tier, Metro optical networks, also known as metropolitan area networks, play a crucial role in facilitating communication across densely populated urban areas. Located in urban areas, these networks serve as crucial connections linking regional networks to access networks, thereby playing a key role in the overall communication infrastructure. Metro networks utilize advanced optical technology such as Reconfigurable Optical Add-Drop Multiplexers (ROADMs) to facilitate adaptable and dynamic traffic routing. This flexibility enables the optimum use of network resources, providing optimal reliability and performance even in dynamic metropolitan settings. Metro optical networks are designed to prioritize low latency, high scalability, and effective traffic grooming to satisfy the increasing demand for high-bandwidth services in metropolitan settings. Low latency is crucial for applications like video conferencing and online gaming that need real-time engagement by minimizing delays in data transfer. Metro networks can successfully handle growing data traffic because to their high scalability. Efficient traffic grooming helps optimize network resources, resulting in enhanced performance and cost-effectiveness. Metro optical networks are the fundamental framework of urban communication infrastructure, facilitating continuous connectivity and meeting the varied requirements of contemporary metropolitan communities [13].

Access optical networks are essential as the last stage in the optical network architecture, acting as the gateway point for end-users, enterprises, and residential areas. The networks serve as the final link in providing high-speed internet access, video streaming services, and other communication solutions directly to individual buildings. Access networks utilize passive optical networks (PONs) [14, 15]

and Ethernet-based solutions to cater to customers' different demands and provide efficient and reliable access [16]. Access optical networks play a crucial function but encounter distinct challenges that demand creative resolutions. The hurdles are deploying fiber optics to individual premises, power budget constraints, and the continuous requirement for cost-effective solutions. To overcome these issues, strategic planning, infrastructure investment, and the deployment of sophisticated technologies are necessary to improve network performance and provide access to high-speed broadband services. Optical networks are crucial for reducing the digital gap and providing broad access to the advantages of current communication technology.

2.2 Advancements in Software-Defined Networking and Open Optical Networks

The emergence of Software-Defined Networking (SDN) addresses these challenges by introducing programmable network architectures that enable dynamic and centralized control over network resources. SDN separates the control plane from the data plane, allowing network administrators to centrally manage and configure network behavior through software-based controllers. This paradigm shift empowers optical communication systems to achieve greater flexibility, transparency, and adaptability. By decoupling control functions from hardware, SDN facilitates more efficient traffic engineering, enables on-demand network reconfiguration, and supports the seamless integration of new technologies. In essence, SDN revolutionizes optical communication systems by providing the foundation for agile, scalable, and programmable network infrastructures capable of meeting the evolving demands of modern communication networks. SDN architecture consists of data plane, control plane and management plane, illustrated in Fig. 2.2

2.2.1 SDN layers

- **Dataplane:** In the architecture of Software-Defined Networking (SDN), the data plane comprises two distinct sublayers: the network infrastructure and the southbound interface. The network infrastructure handles the actual forwarding of packets within the network, while the southbound interface specifies the instructions for packet forwarding and defines the network protocol utilized to facilitate communication between the control plane and the data plane.
  - **Network infrastructure:** SDN design includes conventional network components like routers and switches. In SDN, the traditional capability to independently program various network components is relinquished.

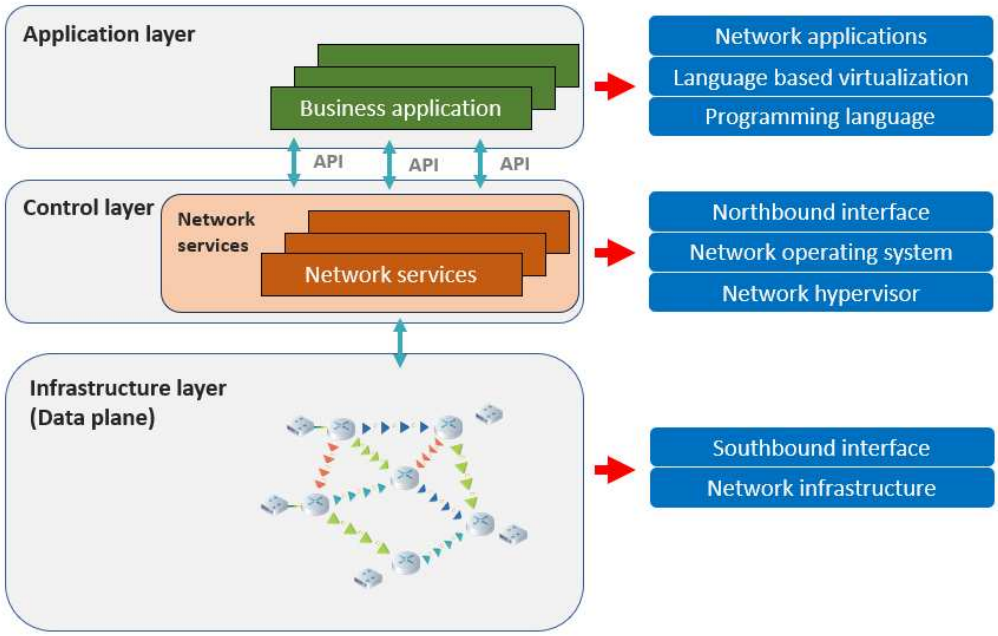

Figure 2.2: SDN schematic diagram

Flow control is centralized and overseen by a unified logical entity instead. This centralization simplifies network components into basic data-forwarding parts that function according to predefined principles. SDN data forwarding mechanism utilizes a sequence of flow tables. Flow tables store rules that are compared to incoming packets and determine the actions to be executed when a match is found.

- **Southbound interface:** The southbound interface in the architecture of SDN serves as the conduit for communication between the control plane and the data plane. It plays a pivotal role in promoting interoperability among forwarding devices sourced from diverse vendors within the SDN ecosystem.

- **Control plane:** The control plane has been designed specifically for the administration of network traffic. The centralized software component is responsible for managing network traffic. Centralizing logical control instead of physical control is based on the efficiency and resilience it provides. Centralized physical control poses a risk of a single point of failure that might compromise the entire network, while centralized logical control guarantees resilience and fault tolerance. SDN includes backup controllers to reduce the chance of failures by allowing them to take over control efficiently in case of a breakdown [17]. Following are the sublayers of control plane.

  - **Network hypervisor:** Network hypervisors play a crucial role in facilitating the sharing of hardware resources among multiple virtual machines within a shared cloud infrastructure. By leveraging network hypervisors, SDN enables efficient resource utilization and cost reduction by abstracting physical network infrastructure into virtualized entities. This virtualization concept, originally derived from the software industry, has been adapted to networking through SDN, enabling the creation of virtualized network environments that operate independently of the underlying physical hardware.
  - **NOS:** The network operating system (NOS) serves as a centralized control plane, orchestrating network-wide traffic management and control. This innovative concept introduces a novel approach to networking by providing abstractions and a unified development environment for network engineers. The primary functions of NOS include abstracting underlying network infrastructure, providing a common programming interface, and facilitating centralized logical control over network resources. By centralizing control and management functions, NOS enhances network agility, simplifies management tasks, and enables seamless integration of diverse network services and applications.
  - **Northbound interface:** The northbound interface serves as a crucial communication link between the underlying network infrastructure and the applications and business requirements in the upper layers. While the southbound interface handles communication with the data plane, the northbound interface is responsible for facilitating communication with external applications and services. Although northbound APIs are not yet standardized, they are expected to provide a software environment distinct from the hardware-focused southbound interface

- **Management plane:** The management layer in network architecture consists of three sub-layers: language-based virtualization, programming languages, and network applications.
  - Language-based virtualization abstracts network modules to preserve structural integrity and protection, ensuring efficient resource utilization and network security.
  - Programming languages facilitate defining network abstractions, emphasizing portability and enabling dynamic implementation of user-defined requirements for flexible network configurations.
  - Network applications define logic executed by underlying layers, aligning network operations with business objectives and serving as an interface between management layer and network infrastructure.

2.2.2 Enabling technology of SDN

DSP-based transceivers revolutionized optical communication systems by significantly enhancing their operating capabilities, especially in enabling multilevel modulation formats using coherent technology [18, 19]. Before DSP-based transceivers became prevalent, optical communication systems mostly used direct-detection (DD) transceivers, which had limited flexibility. DD transceiver implementations limited optical network links to rigid data pipelines, lacking the flexibility needed to support different configurations [20, 21]. As a result, the inflexibility caused major constraints on the ability to carry out transparent lightpath (LP) routing, requiring fixed setups to be established at the network design stage. Moreover, due to the inherent technological limitations of DD transceivers, optical-electrooptical (OEO) traffic regeneration was necessary in nodes. This hindered the achievement of desired transparency and elasticity at the logical network layer, presenting significant challenges to network scalability and adaptability.

Advancements in dynamic digital-to-analog (DAC) and analog-to-digital (ADC) converters, as well as improvements in DSP modules, have greatly improved the flexibility of optical transmission systems in the past ten years [22]. By utilizing electronic dispersion correction (EDC) [23, 24] and DSP-enabled equalization [25], receivers are able to reduce linear propagation effects like chromatic dispersion (CD) and polarization mode dispersion (PMD). The progress made has established the groundwork for the design of DSP-based transceivers, signaling the beginning of a new era in optical transceiver technology [26, 27]. The transceivers are capable of handling different modulation formats and eliminating Dispersion compensating units (DCUs) from optical lines without incurring any additional penalty [28]. The removal of DCUs has significantly improved flexibility, enabling transparent wavelength routing and resulting in significant improvements in the design of Reconfigurable optical add-drop multiplexers (ROADMs) [29]. The integration of DSP-based transceivers into optical networks has initiated a substantial revolution in the architecture of ROADMs, allowing them to offer flexible and transparent optical networking. By eliminating DCUs from optical connections, ROADMs can now offer seamless and efficient wavelength routing, revolutionizing the flexibility and adaptability of optical networks. This transformative attribute enhances the efficiency of the network and simplifies administration by allowing real-time adjustments to meet evolving bandwidth requirements. The implementation of Digital signal processing-based transceivers resulted in a new era of flexibility and efficiency in optical communication systems, facilitating the creation of enhanced network architectures capable of addressing the evolving demands of modern telecommunications and the concept of software-defined networking.

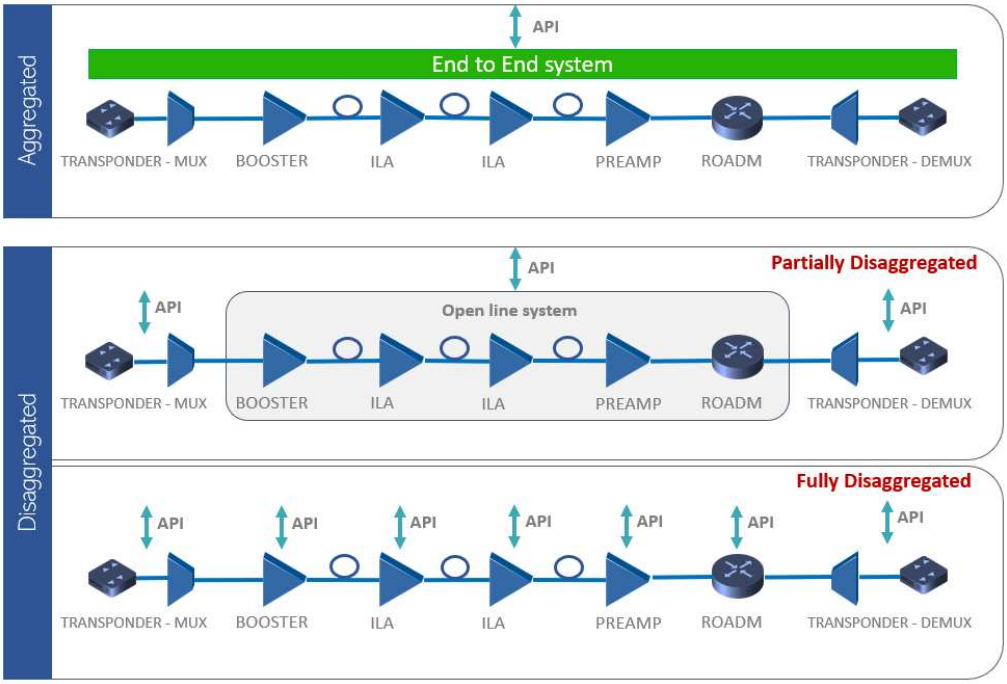

Figure 2.3: Optical networks structure

2.2.3 Open optical networks

Disaggregated optical networks in the field of SDN revolutionize the administration and control of optical communication infrastructure. These networks adopt the concept of disaggregation, which allows for independent management of distinct network elements (NEs) from different vendors, such as amplifiers, ROADMs, and transceivers. The disaggregation can take place at two levels: complete disaggregation, where each individual network element is managed individually, or partial disaggregation, where whole OLSs are controlled independently. This technique enables enhanced flexibility and interoperability inside the network, since it allows for the smooth integration and management of equipment from several suppliers utilizing protocols that are not exclusive to any particular vendor. Vendor-agnostic protocols in disaggregated optical networks provide for centralized control and management of various system implementations from numerous suppliers. Interoperability guarantees that the central optical network control can effectively manage and regulate both hardware devices and the whole network. This includes tasks like configuration, performance monitoring, and alert management. Fig. 2.3 demonstrates the operational concepts of both partially and fully-disaggregated networks, providing a practical representation of how these networks function. By utilizing the interoperability of these technologies, the central optical network control may offer full management and control capabilities, ultimately resulting in more effective

resource use and easier network administration.

In this study, we assume a fully-disaggregated optical network, where all the configurations of the OLS are set and maintained by a unified control plane. This method provides a multitude of benefits, such as increased adaptability, expandability, and impartiality towards vendors. Organizations may enhance their optical communication infrastructure and easily react to changing network requirements by adopting the notion of disaggregated optical networks within the context of SDN.

2.3 Multi-band transmission systems

The growing adoption of technologies like the Internet of Things (IoT) and Machine-to-Machine (M2M) communication, along with progress in fixed and wireless access technologies, is putting considerable pressure on optical transport networks [30]. The increasing need for bandwidth among end-users and the concentration of traffic in backbone networks provide unique issues such as capacity constraints and system congestion. Innovative solutions are necessary to improve the scalability and efficiency of optical transport networks in order to address these difficulties.

The implementation of Elastic Optical Networks (EONs) has greatly improved the efficiency of spectrum usage in the C-band. EONs strive to achieve transportation rates beyond 100G, with the ultimate objective of attaining single-wavelength 1 Tb/s line rates. Nevertheless, these progressions come with inherent limitations. EONs mainly aim to increase the capability of direct connections while optimizing spectral efficiency. Two main techniques to increase line-rates to 200G/400G or 800G within EONs are using higher baud-rates or implementing higher modulation formats. Operating at faster speeds requires more optical bandwidth by using more spectral slots. This reduces the number of spectral slots available for connecting nodes, requiring a decision between node connection and channel capacity [30]. Despite improvements DSP enhancing QoT performance, reaching greater single channel rates results in lower reach, which further limits inter-node connection. Accommodating fluctuating traffic patterns and optimizing the cost-effective use of high-capacity connections presents obstacles. The problems highlight the necessity for creative solutions to meet the changing requirements of optical transport networks [31].

This work examines Multi-Band Transmission (MBT) options, which have been extensively researched for many years and provide different alternatives as well as issues [32, 33, 34]. The primary objective of MBT is to broaden the spectrum use of fiber transmission beyond the conventional C-band systems prevalent during the past two decades [35]. C-band systems usually span a range of 35 nanometers (nm), as shown in Fig. 2.4. Recent improvements have enabled the creation of systems that use a broader spectral range, incorporating transmission in both the

Figure 2.4: Optical spectral bands (ITU-T)

C-band , L-band (60 nm) and S-band (≈ 70 nm). This method can span a spectral range of up to 165 nm, greatly increasing the bandwidth for optical communication. MBT solutions offer a spectrum scenario that includes both C-band and L-band transmission (95 nm) [36, 37], and it is currently available for commercial use and has been deployed in recent years [38]. The extended spectral range provides more flexibility and capacity in optical transmission systems to meet the rising need for higher data rates and to support a wider variety of applications and services.

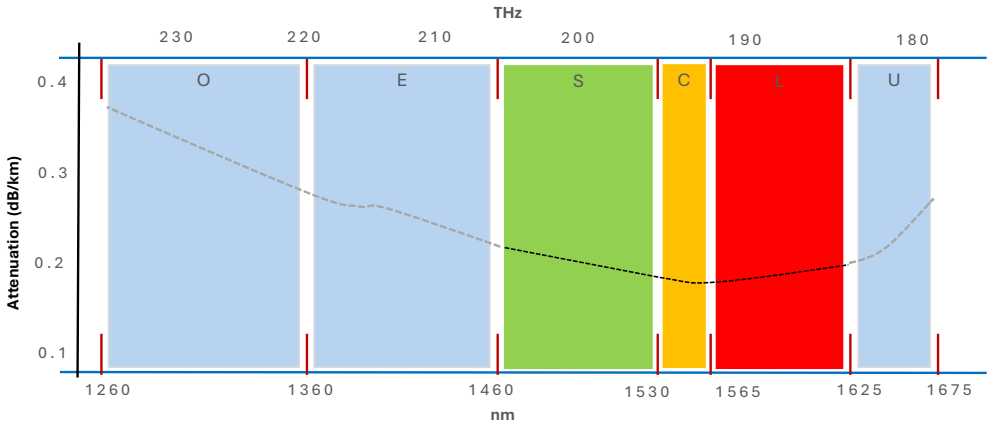

Figure 2.5: Loss profile of SSMF

Fig. 2.5 depicts the low-loss spectral range of standard single-mode fiber (SSMF), which extends from the U-band to the O-band with a loss of approximately less than 0.4 dB/km, and L- to S-bands with a loss of around 0.2 db/km. This spectral range spans over 16 THz in total, showcasing substantial capacity potential without requiring the installation of new fiber [39, 40].

Since optical fibers currently experience the least amount of signal loss in the C-band, they are often utilized in metro, long-haul, ultra-long-haul, and submarine optical transmission systems. They are frequently combined with WDM and erbium-doped fiber amplifier (EDFA) technologies. The L-band is a suitable alternative when the C-band lacks sufficient bandwidth. WDM and EDFA technologies are also suitable for use in the L-band. Optical fibers in the S-band show lower loss than those in the O-band. The S-band is commonly utilized as the downstream

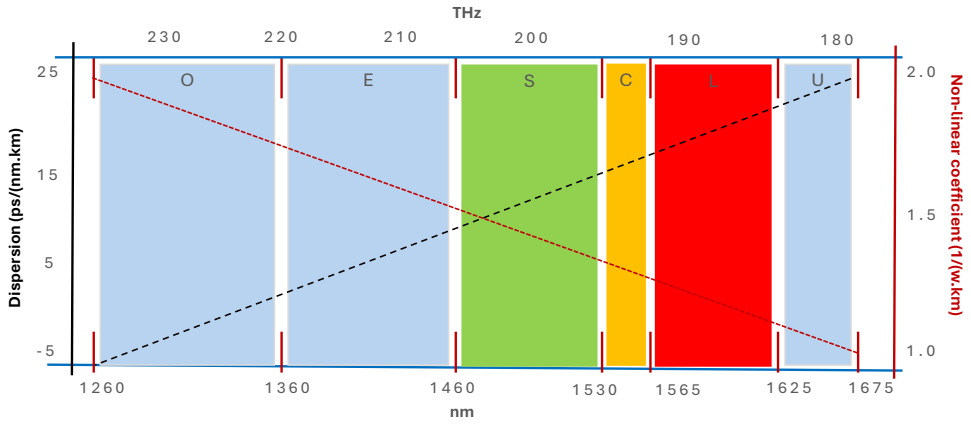

Figure 2.6: Dispersion and non-linear co-efficient profile of SSMF

wavelength in several PONs technologies. Expanding capacity beyond the C+L-band with DWDM transmission in terrestrial optical networks is another area of growing interest. [41]

Effectively predicting optical fiber properties across the entire spectrum utilized poses a fundamental challenge in MBT systems. Parameters such as the attenuation profile (α), chromatic dispersion (D), and nonlinear coefficient (γ), depicted in Fig. 2.5 and Fig. 2.6, must be accurately defined to forecast the performance of MBT systems reliably.

Modeling the propagation in MBT systems necessitates consideration of Stimulated Raman Scattering SRS, the primary nonlinear effect in these systems [42, 43]. SRS significantly influences signal propagation and must be precisely incorporated into the modeling framework. Furthermore, precise simulation of MBT systems relies on appropriately scaling the Raman gain across the frequency spectrum. This ensures an accurate representation of the Raman effect across the entire bandwidth utilized in MBT systems.

Finally, it is essential to include the influence of SRS while calculating NLI in MBT situations. The degradation of signal quality in optical communication systems is significantly influenced by NLI, and correctly assessing its impact necessitates considering the SRS effect. In order to tackle these modeling difficulties, we have utilized the Generalized Gaussian Noise (GGN) model [44] in our simulations. This model has exhibited outstanding precision in estimating NLI, even in diverse situations, making it an excellent option for modeling MBT systems and reliably predicting their performance [42].

An important challenge for MBT systems is the limited availability of components that can operate well across several spectral bands. There are two methods for transceivers. An effective approach is to develop dedicated transceivers designed for certain bands or frequency ranges. This approach entails the development of

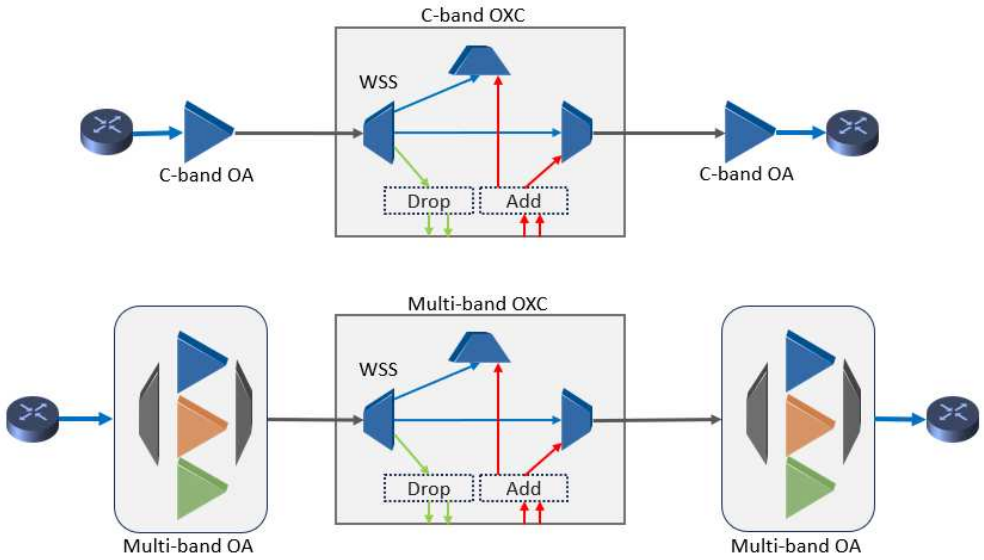

Figure 2.7: Optical node architecture for single and multiband WDM system

several elements such as tunable lasers, dual-polarization IQ modulators, and coherent receiver front end [45]. These customized transceivers are not currently on the market. Some researchers have investigated employing C-band transceivers in other spectral bands as a temporary solution [46, 47, 48]. These findings are intriguing, but more research is required to comprehend any extra performance limitations.

The wavelength-selective switch (WSS) is a vital component for MBT systems since it is necessary for the construction of ROADM nodes. Researchers are now creating broader devices to enhance the flexibility of multi-band network nodes [49], but C+L-band WSS are already on the market. In this work, we have used the photonic WSS device which is capable of handling three bands (C, L, and S), explained in [50].

EDFAs are commonly utilized for C- and L-bands in amplification applications because of their dependable performance and effectiveness and can acheive 6 Thz of spectral range [51]. Thulium-Doped Fiber Amplifiers (TDFA) have been studied as alternative amplifiers for the S-band [52]. The amplifiers are designed for certain spectral ranges, providing possible solutions for MBT systems.

Fig. 2.7 demonstrates the node architecture from a C-band to an MBT system, incorporating C, L, and S bands. It is crucial to take into account extra consequences for band separation needed for particular amplification. We analyze the performance and effects of MBT on the network level by considering elements such as fiber transmission impairments and device characteristics in the upcoming chapters.

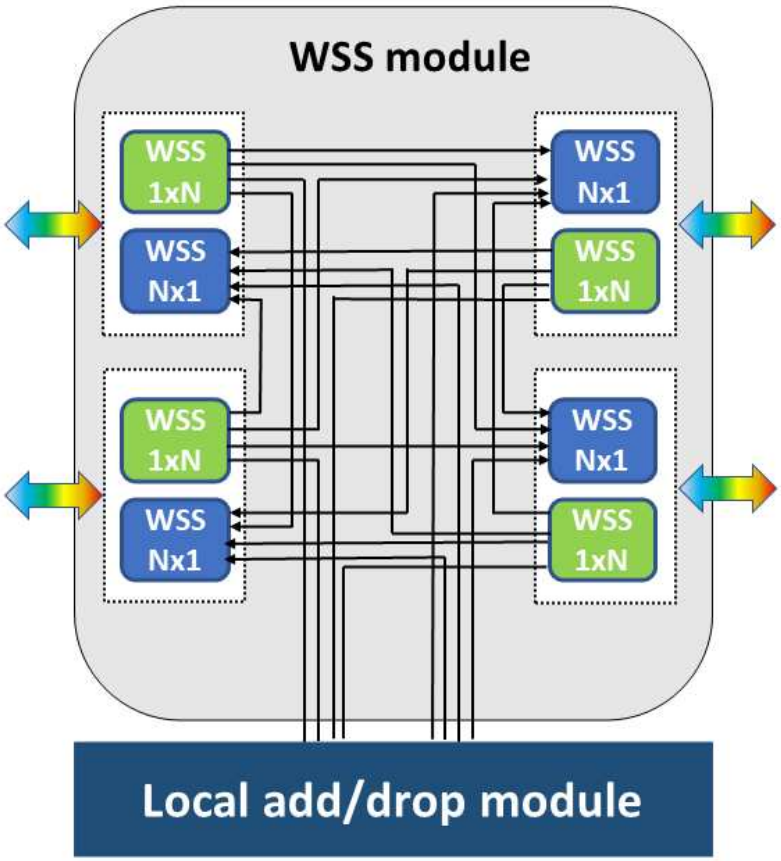

Figure 2.8: ROADM architecture enabled by multiple WSS modules

2.3.1 Multi-band enabled WSS device

The network component, such as Wavelength selective switch (WSS), is crucial since it provides independent management and routing of each input channel to a fiber output of the WDM comb. WSS systems are often built utilizing sophisticated and large-scale technologies such as Liquid Crystal on Silicon (LCoS) and Microelectromechanical Systems (MEMS) [53]. This thesis use the multi-band WSS implementationusing Photonic integrated circuit (PIC) technology, originally explained in [50] and [54]. This method differs from current large and cumbersome WSS systems that rely on MEMS and LCoS technologies. The WSS features a modular architecture, as seen in Figure 2.8, enabling operation throughout a wide optical spectrum encompassing the C, L, and S bands. It provides the capacity to handle more output fibers and channels while taking up less space compared to conventional MEMS-based solutions.

The underlying design principles of the PIC have been chosen to allow modularity and scalability of the structure, allowing the architecture to be adapted and

simulated for various applications, envisioning different amounts of ports, channels, and spectral characteristics. This is achieved through a "divide and conquer" approach, splitting the demultiplexing and switching operations into separate sections while implementing the required functionalities through cascades of simpler integrated components. The device architecture is depicted in Fig. 2.9, which highlights both the general structure, the filtering cascade, and the switching network structures [55].

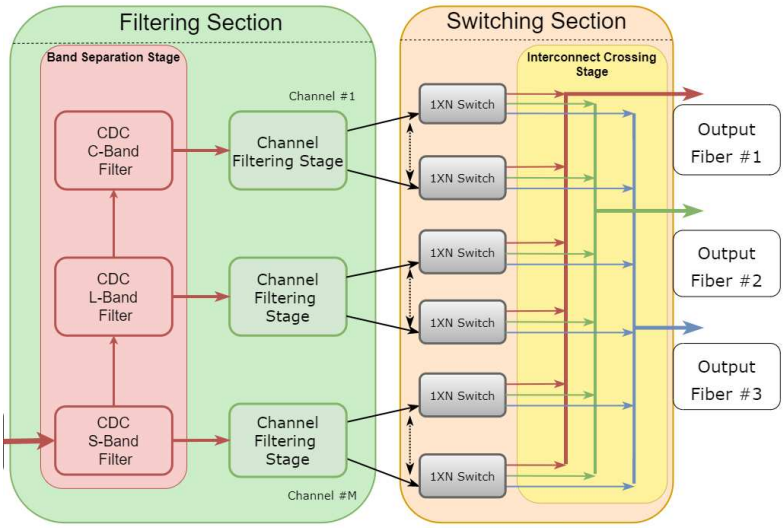

Figure 2.9: WSS architecture

2.3.1.1 Filtering section

In this first step, the input signal is split into its individual channels and guided into separate pathways while keeping losses and interference to a minimum. This is done using a series of filters arranged in stages. The process begins by separating the main bands of operation (C+L+S in this case) before moving to finer filtering. This initial stage is crucial for reducing losses and interference between bands, which helps optimize the design of subsequent components. Each spectral sub-region is then further separated using a cascade of filtering elements. There are two main devices used for this: Contra-Directional Couplers (CDCs) for band separation and Micro-Ring Resonator (MRRs) based filters for channel separation, shown in Fig. 2.10. CDCs work by engineering their gratings to allow coupling between the forward and backward propagating modes of different waveguides.

The primary design parameters, as illustrated in Fig. 2.11, revolve around the geometry of the waveguides and gratings. Tuning the waveguide's unperturbed effective index, determined by its width ($W_{1,2}$ and height, along with the perturbed effective index ($\Delta W_{1,2}$), in conjunction with adjusting the gap G between

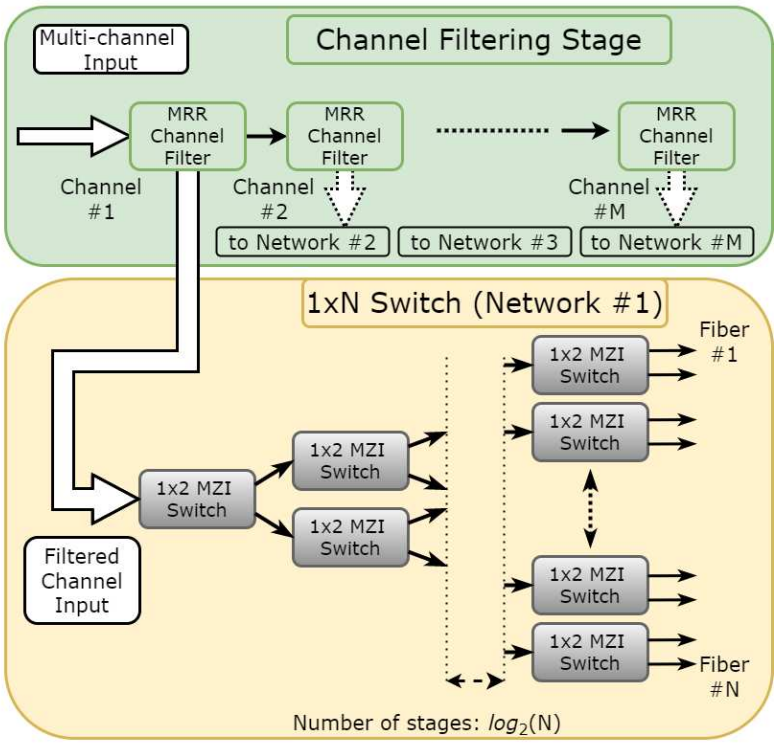

Figure 2.10: Operational stages of WSS

the waveguides, enables the suppression of direct coupling and the maximization of the contra-directional effect. Additionally, through meticulous engineering of the grating periodicity ($\Lambda_{1,n}$), it is possible to finely adjust the effect to target specific bandwidths and central frequencies, thereby optimizing the performance of

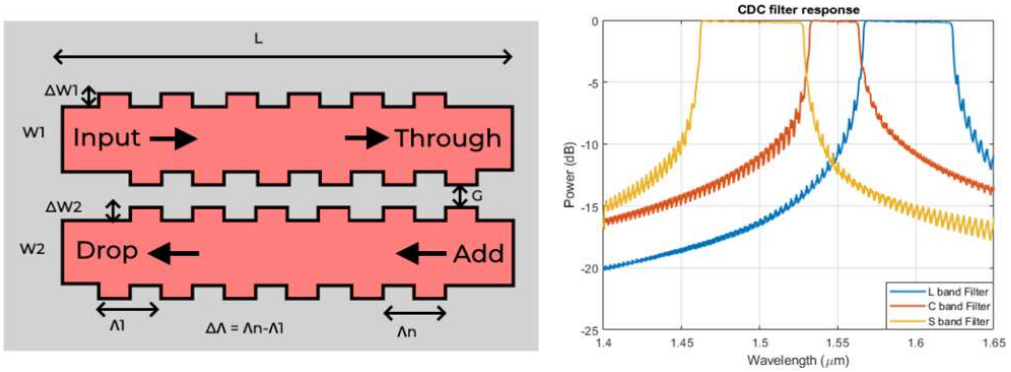

Figure 2.11: Contra-Directional Coupler filter: (a) schematic and (b) frequency response. [56, 55]

the system.

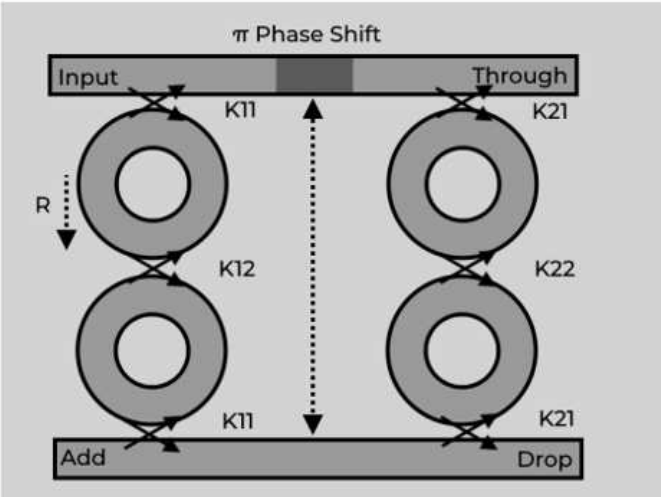

Figure 2.12: Device schematic for the two-stage ladder MRR filter [56, 55]

MRRs function based on the interference principle where certain frequencies experience constructive interference as light circulates within the ring structure. MRRs may selectively transfer specific wavelengths to a second waveguide while without impacting the remaining spectrum. Single-ring structures have limitations in terms of spectral flatness and stop-band attenuation, but these may be improved by using multiple rings in more intricate structures, as shown in Fig. 2.12. MRRs structure are mainly designed based on two key parameters: the coupling coefficients ($K_{11,12,21,22}$ and the radius (R) of the rings. Adjusting the radii allows for choosing the desired channel, whilst the coupling coefficients determine the overall frequency response.

CDCs and MRRs have different operating principles, leading them to fulfill slightly different objectives. CDC structures are effective in isolating the central operating region due to their broad flat-top characteristics and abrupt stop-band transitions. Although CDCs have a bigger footprint than other filtering systems, they are crucial parts of multi-band applications because they can be tailored to cover extremely wide operating bands. MRRs are commonly used for channel separation in add-drop filtering systems. They are more appropriate for channel filtering but are unable to attain extremely wide filtering bandwidths.

Each channel in the design in is filtered using a two-stage ladder MRRs filter. This setup guarantees a flat-top response, a quick stop-band transition, and a high extinction ratio, which helps minimize inter-channel crosstalk and decrease transmission penalties. To overcome aliasing problems in MRR-based solutions, devices have been created and tested using intricate grating-assisted coupling architectures. These couplers help decrease the necessary number of filtering elements, removing

the requirement for extra anti-aliasing components used in prior versions. This enhancement allows for more accurate tuning of the coupling value based on the specific wavelength, to counteract the inherent periodic behavior of the MRR-based device. This method results in an element that is free from free spectral range (FSR) and does not cause channel aliasing. After demultiplexing, the next step is to direct signals to the desired output port.

2.3.1.2 Switching section

Following the filtering stage, each channel is directed through a specialized switching network to be routed to the proper output fiber. The network depicted in Fig. 2.10 omprises a cascade array of 1×2 programmable Optical Switching Elements (OSEs). The switching network is designed for a certain number of target output fibers (N) and consists of $N-1$ optical switch elements OSEs organized in $\log_2 N$ phases.

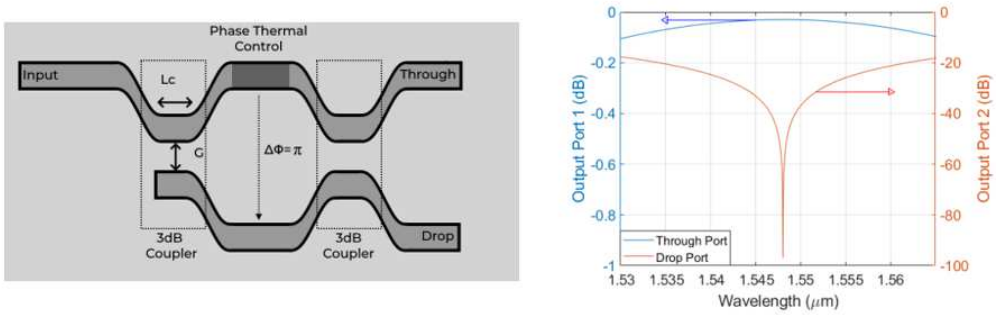

Figure 2.13: 1×2 Mach-Zehnder Interferometer Switch - schematic and frequency response [56, 55]

The benefit of obtaining a large, flat response is provided by the Mach-Zehnder Interferometer (MZI) switch in the OSE used in these sub-networks. Their essentially frequency-independent switching function makes them ideal for MBT applications [56, 57, 58, 59]. Fig. 2.13 illustrates the overall structure of the MZI, emphasizing the essential physical design parameters and the switching control section. The device may switch between two routing states (UP or DOWN) by adjusting the temperature of the specified arm of the MZI using a suitable electrical control signal. The electrical control system and pads are designed to fulfill the necessary switching performance and technological requirements [56, 60]. Fig. 2.13 illustrates the frequency response for the off state (UP) in the C-band, highlighting the area where the target 8 channels are located. The device shows a consistent response at the central frequency of the design, allowing for frequency-independent switching operation, with comparable results in the L- and S-bands. After switching, the next step is to cross and multiplex the outputs from the previous switching network to

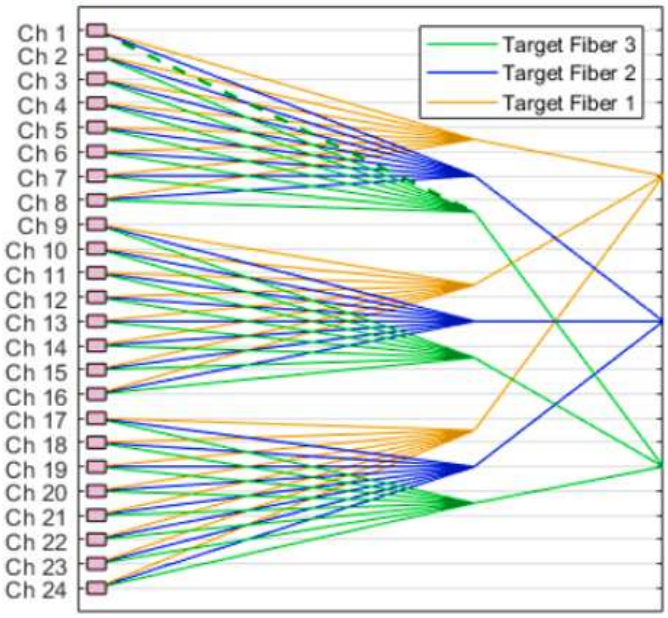

Figure 2.14: Crossing stage circuit topology [56, 55]

link and integrate them into the egress waveguide of each output port. In the final segment of the structure, passive waveguide crossings and wavelength combiners are utilized to consolidate all connections to the target output port. These structures, depicted in Fig. 2.14, serve as passive lossy elements in the model. Reference values for these components are sourced from literature documenting experimental and state-of-the-art devices for crossings [61, 62, 63], as well as integrated wavelength combiners [64, 65]. The active routing section culminates with the switches.

2.3.2 Multi-band enabled WBSS device model

In today's telecommunications industry, ROADMs and OXCs primarily function utilizing a wavelength-path level of detail and are equipped with WSS that can handle up to 35 ports. In anticipation of future networks embracing extensive spatial parallelism, which requires increased port counts, it is imperative to connect numerous WSSs in a cascading manner to fulfill these requirements. The number of these cascaded WSSs in a node is approximately equal to the square of the degree of the ROADMs / OXCs [66]. This configuration results in higher transmission losses at each step, necessitating the use of extra amplifiers to offset these losses, thereby leading to the introduction of more noise into the system. The administration of dynamic network services in SDN, which include capabilities such as dynamic optical path allocation, switched optical paths/circuits, and optical burst/packet services, becomes more complicated as their range and complexity develop. The

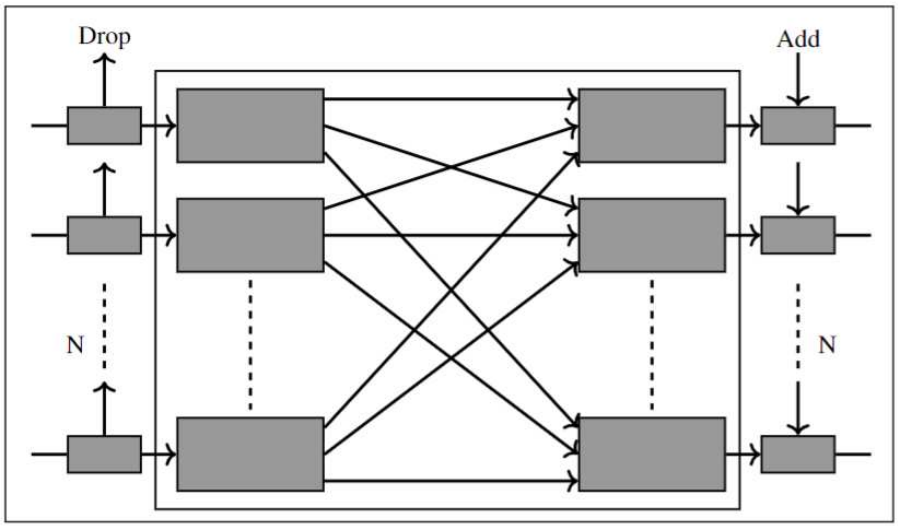

Figure 2.15: Wavelength enabled node architecture

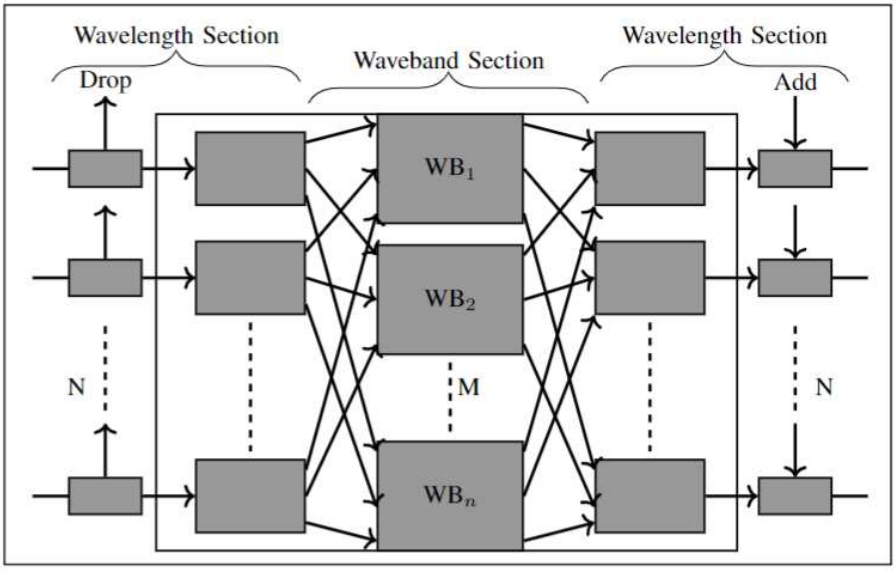

Figure 2.16: Waveband enabled node architecture

increase in complexity and the resulting expenses are substantial as the optical transmission systems progress towards MBT and greater SDM systems in preparation for 6G communications [67]. In order to tackle these difficulties, there has been a thorough investigation on the deployment of an extra optical layer, known as the waveband (WB) path layer [68, 69, 70, 71]. The purpose of this layer is to combine numerous wavelength lines into groups and route them together as a single unit. This architectural approach minimizes the requirement for individual optical control of each node, which is commonly found in single-layer systems.

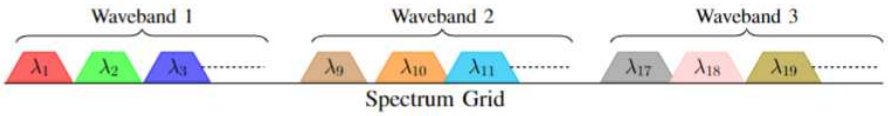

Figure 2.17: Wavelengths arrangement to form waveband

Within a multi-layer design, only WB ending nodes require signaling to build or release wavelength pathways. This greatly simplifies the signaling and control operations, resulting in reduced delays and costs associated with path management and signaling. Moreover, implementing a multilayer design can greatly decrease the amount of hardware needed for constructing OXC. In the era of extensive SDM, where OXCs need to support multiple multicore fibers and parallel single mode fiber links, the current architecture based on wavelength granularity would require the use of multiple expensive WSSs to remain feasible. This is because commercial WSSs can only handle a capacity of slightly more than 35 ports. WB switching is a practical and economical alternative to this method. It has been shown in recent research to streamline the network structure. The conventional wavelength-based (WL-based) switching system utilizes granular wavelength routing methods and consists of a major component called WSSs, which is responsible for both switching and add/drop features, as shown in Fig. 2.15. On the other hand, the WB routing system, shown in Fig. 2.16 utilizes a coarse granular approach that consists of many essential steps: Initially, the optical routes of the incoming fibers are organized into a certain number of WBs based on the requirements of maintaining continuity and contiguity shown in Fig. 2.17. Subsequently, these wavelength bands are individually directed to their assigned fiber ports for transmission. Finally, the incoming WBs at a specific fiber port are connected together to enable their transmission to other outgoing fibers, making the whole process more efficient and improving the system's effectiveness.

2.4 Physical layer modeling

Fig. 2.18 depicts an Optical Line System (OLS) comprising several key components. Initially, N transmitters convert electrical signals into optical signals for transmission via optical fibers, with each signal at a unique frequency for multiplexing. The multiplexed signals then traverse a ROADM node for fiber interconnection. Subsequently, the transmission path incorporates optical amplifiers, EDFA or TDFA, to mitigate signal attenuation, and fiber segments to facilitate signal transmission over specific distances. In the final stages, the signals are either directed through additional fibers connected to the main ROADM node or demultiplexed and dispatched to N receivers, where they are converted back into digital signals.

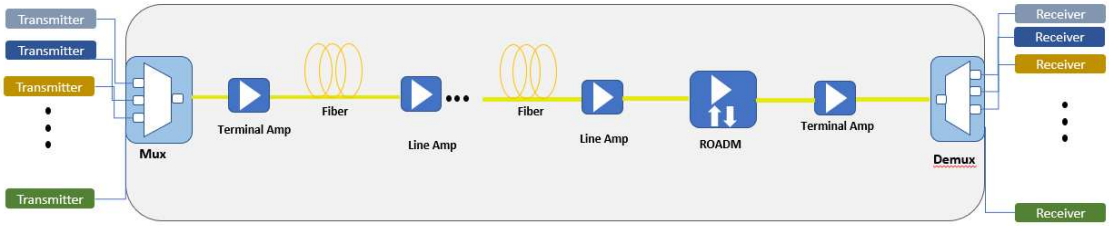

Figure 2.18: Optical line system (OLS) and its key components

2.4.1 Coherent transceiver technology

Coherent transmitters and receivers in modern optical communication systems allow for the use of multi-level modulation schemes, improving the efficiency and capacity of optical networks. These devices increase data throughput by encoding information into several dimensions of the light wave by modulation of in-phase (I) and quadrature (Q) components across two orthogonal polarizations (X and Y) of an optical carrier.

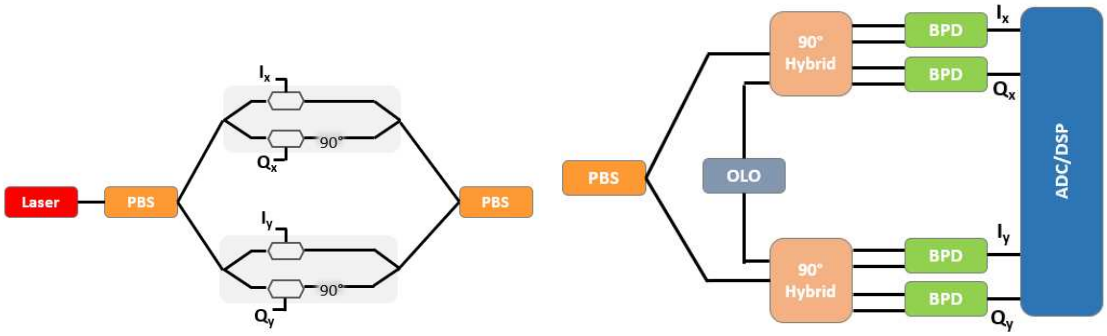

(a) Transmitter (b) Receiver

Figure 2.19: Coherent transceiver structure

- **Coherent transmitter**
  Fig. 2.19a depicts the structure of a coherent optical transmitter, which consists of a laser source, polarization beam splitters (PBSs), and Mach-Zehnder modulators (MZMs). The initial stage involves the generation of a coherent laser beam, which acts as the optical carrier for the transmitted information. The beam is split into two separate polarized directions, vertical and horizontal, by PBSs. This distinction is essential for the dual-polarization approach, enabling the separate control of the in-phase and quadrature components for each polarization. The polarized beams are then modified using MZMs to encode the I/Q components of the signal onto the light. This is achieved

through the precise control of the optical phase and amplitude of the carrier wave, corresponding to the encoded digital data. After modulation, the polarized beams are combined using another PBSs, merging the separately modulated signals into a unified composite optical signal. The laser frequency is adjusted to allow for the centered transmission of the signal at a certain frequency (f), which makes it easier to use WDM methods [72]. This approach enables the concurrent transmission of many channels using a single optical fiber, greatly increasing the system's capacity.

- **Coherent receiver** The coherent receiver, shown in Fig. 2.19b, is responsible for precisely demodulating the incoming optical signal in the transmission system. The receiving procedure starts by subjecting the incoming signal to a PBSs, which separates the signal into its individual polarizations [73]. Each polarization component is combined with a reference signal from an optical local oscillator (OLO) using a 90-degree optical hybrid. The optical hybrid, a passive device consisting of 3 dB couplers and a 90-degree phase rotator, combines the incoming optical signal with the local oscillator reference to enable the extraction of the I/Q components of each polarization. The process involves sending the combined optical signals to balanced photodetectors (BPDs), which then transform the optical signals into electrical signals representing the in-phase and quadrature components. Electrical signals are converted into a digital format by analog-to-digital converters (ADCs) for processing by DSP units [72]. The DSP stages are precisely crafted to extract the phase and amplitude details from the received signals, as well as to correct for different transmission issues including chromatic dispersion and polarization-mode dispersion [74]. This advanced processing guarantees the precise reconstruction of the sent data, highlighting the effectiveness and dependability of coherent transmission systems in contemporary optical communications.

2.4.2 Modeling of propagation impairments

2.4.2.1 Attenuation in optical fibers

Attenuation, which refers to the decrease in signal intensity as it travels through an optical fiber, is an important factor to consider when designing optical transmission systems. This phenomenon is caused by several reasons, including as Rayleigh scattering, absorption in the ultraviolet and infrared ranges, peaks in hydroxyl (OH^-) ion absorption at wavelengths approximately 1.25 µm and 1.39 µm, and absorption due to the presence of phosphorous in the fiber core [75]. The fiber's attenuation properties are determined by these factors. These qualities are represented by the attenuation coefficient (α), which is often measured in dB/km [76].

When using WDM technology in applications that cover a wide frequency range, it is very important to comprehend the attenuation dynamics of the fiber. The frequency dependency of the attenuation coefficient, denoted as $\alpha(f)$, emphasizes the need of modeling attenuation as a function of frequency in order to precisely understand its effect on signal transmission.

The mathematical framework to assess optical power output, taking into account the frequency-specific attenuation, is formulated as:

$$P_{\text{out}}(f) = P_{\text{in}}(f)e^{-2\alpha(f)Ls} \tag{2.1}$$

Here, P_{in} and P_{out} denote the optical power at the input and output, respectively, for a signal at frequency f, while L_s indicates the fiber's length. This equation elucidates the exponential decrease in optical power as influenced by the fiber's length and the attenuation coefficient's frequency dependence, serving as a fundamental tool for evaluating the optical transmission system's efficiency in mitigating fiber attenuation. Incorporating a detailed understanding of fiber attenuation into the design and analysis of optical networks is indispensable for the accurate prediction of system performance.

2.4.2.2 Polarization mode dispersion

Polarization-Mode Dispersion (PMD) is a significant issue that affects the quality of signals in optical transmission systems. It is mainly caused by the natural birefringence present in optical fibers. This phenomenon is seen as a difference in temporal delay between two light modes that have orthogonal polarization as they pass through the fiber. This condition is present even in single-mode fibers [77]. PMD is mostly caused by little deviations from perfect cylindrical symmetry in the fiber, usually resulting from random variations in the geometric form of the core along its length. The irregularities cause disturbances in the uniform propagation circumstances, resulting in the differentiation between the two polarization modes and initiating their interaction and blending [76].

The effects of PMD are significant in high-speed, long-haul optical networks, where even small variations in the arrival timings of polarization states can cause signal distortion and a decrease in the bit-error rate (BER). Nevertheless, in the domain of coherent optical communication systems, the obstacle presented by PMD is greatly reduced by implementing advanced digital signal processing (DSP) techniques at the receiver. When advanced DSP techniques are used with adaptive equalization approaches, they create a strong and effective strategy to counteract PMD. These methods enable the realignment of orthogonally polarized light components into a coherent signal form by dynamically correcting temporal dispersion effects caused by PMD. The effectiveness of DSP in counteracting PMD depends on its ability to adapt in real-time to the changing dispersion properties of the fiber, which can be influenced by ambient circumstances and physical factors.

The operational threshold for PMD tolerance in optical transceivers is a crucial design parameter. It is carefully determined by manufacturers via thorough system assessments and performance criteria. The PMD criteria are crucial for the system's design, since they guarantee that the transmission quality remains within acceptable limits under expected operational situations. Therefore, it is extremely important to follow these requirements closely while deploying the system. This will enable the establishment of reliable communication lines that can handle the specified data rates and transmission lengths without any compromise.

2.4.2.3 Chromatic dispersion

Chromatic dispersion is a critical factor affecting the performance of optical transmission systems, characterized by the temporal spreading of optical pulses as they travel through a fiber [76]. This phenomenon occurs because the fiber's refractive index varies with wavelength, causing components of a pulse at different wavelengths to propagate at slightly different speeds. Such dispersion results in pulse broadening, which can constrain the system's maximum data transmission rates and reduce the effective transmission distance [78].

Mathematically, the influence of chromatic dispersion on an optical signal can be quantified through the Taylor series expansion of the propagation constant (β), which is fundamentally related to the phase velocity of light in the fiber and varies with the angular frequency (ω). For a signal of frequency (f), where $\omega = 2\pi f$, the propagation constant can be expressed as follows:

$$\beta(f) = \beta_0 + 2\pi\beta_1(f - f_0) + 2\pi^2\beta_2(f - f_0)^2 + \frac{4}{3}\pi^3\beta_3(f - f_0)^3 \tag{2.2}$$

Here, f_0 is the reference frequency chosen for the Taylor series expansion. The coefficients in this expansion (β_0, β_1, β_2, and β_3) serve different roles in the propagation of the signal. β_0 and β_1 and correspond to phase offset and linear propagation delay, respectively, which generally do not impact the QoT directly. However, the coefficients β_2 and β_3 , which are responsible for the second and third-order effects of group-velocity dispersion (GVD), significantly affect pulse broadening and hence, the QoT. The second-order dispersion coefficient β_2, quantified in ps^2/km, is directly linked to the dispersion parameter D, also expressed in $\text{ps}/(\text{nm} \cdot \text{km})$, through the relationship:

$$\beta_2(f) = -\frac{c}{2\pi f^2}D(f) \tag{2.3}$$

In this equation, c denotes the speed of light in a vacuum. The sign and magnitude of D indicate the nature of chromatic dispersion within the fiber; positive values of D cause longer wavelengths to propagate more slowly than shorter wavelengths, leading to pulse broadening. Conversely, negative values result in pulse compression due to shorter wavelengths moving slower.

Furthermore, the third-order dispersion coefficient β_3 is associated with the dispersion slope S, which indicates how the dispersion parameter D changes with frequency. It is given by:

$$\beta_3(f) = \frac{c}{2\pi f^2} S(f) - \frac{2cf}{\beta_2(f)} \tag{2.4}$$

Optical fiber manufacturers typically specify the zero-dispersion slope S_0 in their datasheets, providing essential information for designing systems with minimal dispersion impacts [42].

In high-performance coherent optical systems, chromatic dispersion, including its higher-order effects, can be effectively compensated using DSP techniques at the receiver. This compensation is crucial for maintaining signal integrity over long distances and high data rates, ensuring that the system operates within the maximum tolerable chromatic dispersion limits specified by the transceiver design [79].

2.4.2.4 Stimulated Raman scattering

Stimulated Raman Scattering (SRS) is a non-linear optical process wherein an incident photon with frequency ω_p interacts with a medium's molecular vibrations, leading to the generation of a new photon at a shifted, lower frequency ω_s, known as the Stokes frequency. This process can be mathematically represented and understood through its impact on light propagation in optical fibers, particularly within the framework of WDM systems. The frequency shift ($\Delta\omega$) between the pump (ω_p) and the Stokes (ω_s) waves is defined by the vibrational frequency of the medium's molecules, expressed as $\Delta\omega = \omega_p - \omega_s$.

The Raman gain spectrum, $G_R(\Delta\omega)$, dictates the efficiency of this frequency shift, typically extending around 40THz below the pump wave frequency in optical fibers like SSMF The peak gain occurs at a shift $\Delta\omega_{\max}$, typically around 13.2 THz for silica fibers, where the Stokes wave experiences the maximum amplification. Fig. 2.20 illustrates the Raman gain spectrum for a SSMF. The power transfer from the pump to the Stokes wave can be described by the coupled differential equations governing the evolution of the pump ($P_p(z)$) and Stokes ($P_s(z)$) powers along the fiber length z.

$$\frac{dP_p(z)}{dz} = -g_R(\Delta\omega) P_p(z) P_s(z) \tag{2.5}$$

$$\frac{dP_s(z)}{dz} = g_R(\Delta\omega) P_p(z) P_s(z) \tag{2.6}$$

where $g_R(\Delta\omega)$ is the Raman gain coefficient, which is a function of the frequency shift $\Delta\omega$ and represents the efficiency of power transfer from the pump to the Stokes wave.

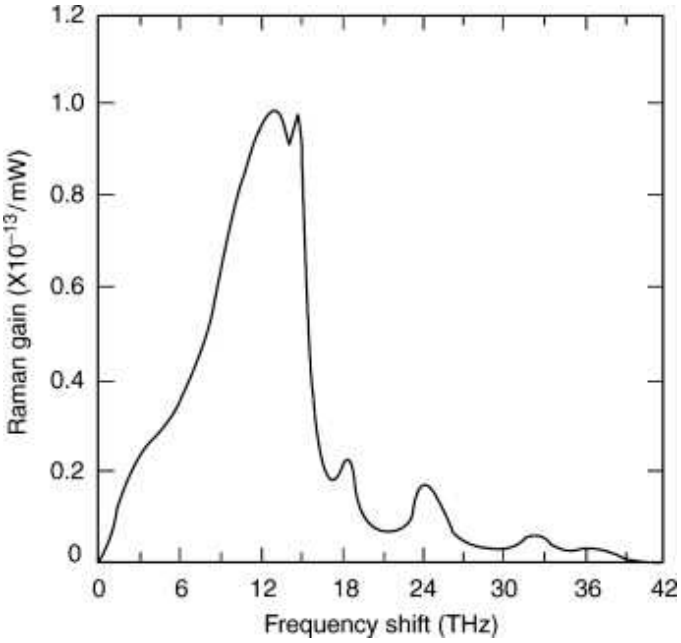

Figure 2.20: Normalized Raman efficiency vs the frequency shift for SSMF. [80]

In high-power situations, the efficiency of power transfer to the Stokes wave increases significantly, which can be quantified by the exponential growth of the Stokes power as a function of the fiber length and the input pump power. Under such conditions, nearly all of the pump power can be transferred to the Stokes wave, leading to a significant alteration in the signal propagation characteristics within the fiber. In MBT systems, SRS effects can lead to power imbalances across different wavelength channels. Shorter-wavelength channels (higher frequency) may lose power to longer-wavelength (lower frequency) channels within the Raman gain spectrum, necessitating careful power management across channels to minimize losses and ensure system performance [81, 82]. This involves maintaining channel powers below a critical level to prevent excessive power transfer via SRS, described as $P_{\text{ch}} < P_{\text{critical}}$, where P_{ch} is the power on each channel and P_{critical} is the threshold power above which SRS-induced losses become significant.

2.4.2.5 Amplified spontaneous emission (ASE) noise

ASE noise is a critical source of signal degradation in optical communication systems, primarily resulting from the inherent properties of optical amplifiers. In the context of EDFA, ASE noise originates from the spontaneous emission occurring within the gain medium as it amplifies an optical signal. This noise can be precisely modeled as additive White Gaussian Noise (AWGN) with a bilateral PSD, encompassing effects from both polarization modes due to the amplifier's operation

[83, 84]. The ASE noise power, denoted as G_{ASE}, is quantified using the formula:

$$G_{\text{ASE}} = 2hf_0 n_{\text{sp}}(G-1) \tag{2.7}$$

where, h is the Planck's constant, f_0 is the carrier frequency of the optical signal being amplified, G denotes the amplifier gain expressed in linear terms, n_{sp} is the spontaneous emission factor or inversion factor, with $n_{\text{sp}} > 1$, indicating the ratio between populations in the excited and ground states of the Erbium ions within the amplifier [83]. This factor is crucial as it directly influences the amplifier's noise performance by indicating the efficiency of the spontaneous emission process relative to the stimulated emission. The noise figure (NF), F, a parameter indicative of the noise performance of an amplifier, is mathematically linked to the spontaneous emission factor as follows:

$$F = 2n_{\text{sp}} \tag{2.8}$$

Substituting n_{sp} in the expression for G_{ASE} with $F/2$ yields a reformulated equation for ASE noise power:

$$G_{\text{ASE}} = hf_0 F(G-1) \tag{2.9}$$

This relationship underscores the interplay between the noise figure, the gain, and the carrier frequency in determining the ASE noise output of an amplifier.

For TDFA, which operate effectively in the 2 µm wavelength region, ASE noise is a significant consideration as well. The ASE noise generation mechanism in TDFAs is analogous to that in EDFAs, with the spontaneous emission factor n_{sp} indicating the ratio of populations in excited and ground states specific to the Thulium ions. However, the specific atomic transitions and energy level schemes of Thulium ions necessitate tailored-modeling to accurately describe ASE noise in TDFAs. The optimization of TDFAs for minimal ASE noise involves careful management of the dopant concentration, pump wavelength, and optical cavity design, among other factors, to enhance the SNR and overall system performance in the 2 µm band, a region of growing interest for next-generation optical communications due to its lower loss and scattering characteristics compared to traditional bands.

2.4.2.6 Non-linear Kerr effect

The Kerr effect is a fundamental nonlinear optical phenomenon characterized by a change in the refractive index of a material proportional to the intensity of the light traversing it [85, 86]. In the context of WDM optical communications, particularly within MBT configurations where signal power varies across different bands, the Kerr effect plays a critical role in determining the QoT of the transmitted signals. A key parameter for quantifying the Kerr effect in optical fibers is the nonlinear coefficient, denoted as γ, which is typically measured in units of $W^{-1} \cdot km^{-1}$. This coefficient is instrumental in calculating the extent to which the Kerr effect influences signal propagation through an optical fiber. The magnitude of γ

directly correlates with the intensity of the Kerr effect: a higher γ value signifies a stronger influence of the Kerr effect on the optical signal.

The Manakov equation is a crucial tool for fully comprehending the distortions caused by the Kerr effect in WDM systems. This equation represents the progression of WDM signals in optical fibers, assuming that the propagation constant is not affected by polarization, which means that the analysis may disregard the impact of birefringence. The Manakov equation is expressed as follows:

$$\frac{\partial E(z,t)}{\partial z} = -\alpha E(z,t) - j\frac{\beta_2}{2}\frac{\partial^2 E(z,t)}{\partial t^2} - j\gamma\frac{8}{9}E^{\dagger}(z,t)E(z,t)E(z,t) \tag{2.10}$$

In this equation, the β_0 and β_1 coefficients are omitted as they represent constant phase shifts and propagation delays, respectively, which are typically considered negligible for the analysis of Kerr effect-induced distortions. Similarly, the dispersion slope term β_3 is excluded for simplification. The equation comprises three main terms: the first represents field loss, the second accounts for chromatic dispersion, and the third, crucially, denotes the Kerr effect term, which is a function of the WDM signal power.

The WDM signal field, $E(z,t)$, can be represented as a Jones vector, $\begin{bmatrix} E_x(z,t) \\ E_y(z,t) \end{bmatrix}$, encapsulating the signal's polarization components, with $|E(z,t)|^2$ indicating the signal power where $\dagger$ symbolizes the Jones vector conjugate transpose. In WDM systems, the Kerr effect manifests through phenomena such as Self-Phase Modulation (SPM), Cross-Phase Modulation (XPM), and Four-Wave Mixing (FWM), each contributing to signal distortion and degradation:

- Self-Phase Modulation: This effect results in pulse broadening due to a self-induced phase shift proportional to the instantaneous power of the pulse itself, altering the pulse's phase spectrum and leading to temporal spreading.
- Cross-Phase Modulation: XPM induces a phase shift in a signal caused by the intensity of another co-propagating signal, leading to interaction between channels that can distort signal integrity.
- Four-Wave Mixing (FWM): FWM is a phenomenon in which interactions among two or more different wavelengths generate new frequencies. This can lead to unwanted spectral components, causing crosstalk and signal degradation in WDM systems.

2.4.3 Amplification modelling

Optical Amplifiers (OAs) are important components in modern optical transmission systems, serving to amplify light signals directly in the optical domain, thus eliminating the need for conversion to electrical signals. These amplifiers are

strategically positioned within the OLS to optimize performance and mitigate signal degradation over long distances. Their deployment is categorized based on their operational location and function within the network:

- Booster Amplifiers: Positioned immediately after the ROADM, booster amplifiers are designed to compensate for signal losses incurred through ROADM processing. By boosting the signal power at the outset of transmission, these amplifiers help to maintain optimal signal levels as the light propagates through the fiber.
- Inline Amplifiers (ILAs): These amplifiers are deployed at regular intervals along the fiber link to counteract the gradual attenuation of the optical signal during its journey through the fiber. By restoring signal power, ILAs extend the reach of the transmission without compromising signal integrity.
- Pre-amplifiers: Located just before the signal reaches the receivers, pre-amplifiers play a crucial role in enhancing the SNR and detection sensitivity of the receiving devices. This enhancement is vital for ensuring the accurate and reliable detection of the incoming optical signals, particularly after traversing long distances.

In this context, three primary types of amplifiers are employed to address power loss and signal degradation:

- Semiconductor Optical Amplifiers (SOAs): SOAs are active devices fabricated from semiconductor materials. They amplify optical signals through current injection, leveraging the gain medium's properties to boost signal strength [87]. SOAs are valued for their versatility and wide applicability in various optical networking functions, including switching and signal regeneration.
- Doped Fiber Amplifiers (DFAs): The most prevalent amplifiers in long-haul optical transmission, DFAs utilize a length of optical fiber doped with rare-earth elements (e.g., Erbium or Thulium) as the gain medium [88]. Amplification is achieved via stimulated emission, where an external pump laser excites the dopant ions, which then release their stored energy as additional photons coherent with the signal light, thereby amplifying it.
- Raman Amplifiers: Raman amplification harnesses the SRS effect, where power from a high-intensity pump laser is transferred to the signal light within the transmission fiber itself, effectively amplifying the signal [89]. This technique is especially beneficial for extending the effective transmission distance and improving the overall system performance by leveraging the fiber's nonlinear properties.

A critical aspect of modeling and understanding the performance of these optical amplifiers involves the consideration of ASE noise. ASE noise is generated due to spontaneous emission in the amplifier's gain medium, contributing to the noise background and potentially degrading the SNR of the system [42]. The ASE power for a channel centered at frequency f is a function of the amplifier's gain $G(f)$ and noise figure $NF(f)$, and can be expressed mathematically as:

$$P_{\text{ASE}}(f) = hf(G(f) - 1)NF(f)B_{\text{ref}} \tag{2.11}$$

Here, h is Planck's constant, and B_{ref} represents the reference noise bandwidth, which typically corresponds to the channel's symbol rate $R_s(f)$ or a predetermined value. Accurate modeling of ASE power is essential for assessing the SNR and, by extension, the overall performance of optical transmission systems, enabling the design of networks that maximize signal integrity and capacity over extended distances.

2.4.4 Quality of Transmission (QoT) metric

The precise modeling of signal propagation within an optical fiber, particularly in MBT configurations, necessitates a thorough understanding of how fiber parameters such as attenuation and chromatic dispersion vary with frequency. For instance, in SSMF, the attenuation coefficient typically remains below 0.2 dB/km within the C- and L-bands but can escalate to approximately 0.22 dB/km in the S-band, as depicted in Fig. 2.5. Furthermore, SRS as described in Sec. 2.4.2.4, a nonlinear optical effect facilitating power transfer from higher to lower frequency signals [90], becomes a critical factor in MBT systems due to their expansive transmission spectrum. While SRS might be negligible in systems confined to the C-band, its influence is pronounced in MBT configurations, exacerbating the inherent higher fiber loss in the S-band and consequently diminishing the QoT across this band.

The QoT for each channel in an optical fiber span, indexed by i, is quantitatively assessed by computing the Generalized Signal-to-Noise Ratio (GSNR), represented as:

$$\text{GSNR}_i = \frac{P_{\text{S},i}}{P_{\text{ASE},i} + P_{\text{NLI},i}} = (\text{OSNR}_i{}^{-1} + \text{SNR}_{\text{NLI},i}{}^{-1})^{-1} \tag{2.12}$$

where $P_{S,i}$ denotes the span input power, OSNR_i is the optical signal-to-noise ratio, and $\text{SNR}_{NLI,i}$ is the nonlinear signal-to-noise ratio. This model presupposes that the primary factors degrading optical performance are ASE noise and NLI noise—emanating from optical amplifiers and fiber propagation, respectively. Both types of noise are approximated as Gaussian disturbances for a broad range of transmission scenarios. The ASE noise power $P_{ASE,i}$ is derived from the established equation, while the NLI power contribution $P_{NLI,i}$ is calculated using the Generalized Gaussian Noise (GGN) model [91]. This model accounts for the effects

of spectral and spatial variations in fiber loss and SRS-induced inter-channel power crosstalk.

In a disaggregated view of the physical layer [92, 93], the total QoT for a LP l is determined by aggregating the inverse of the GSNR values for each fiber span s traversed by the LP:

$$\mathrm{GSNR}_{i,l} = \frac{1}{\sum_{s \in l} (\mathrm{GSNR}_{i,s})^{-1}} \tag{2.13}$$

This methodology, implemented in the open source GNPy [94] library, allows for an accurate estimation of QoT in MBT systems, which necessitates a tailored approach to optical amplification due to the limited bandwidth and maximum output power of existing amplifiers. Specifically, EDFAs are employed for the C- and L-bands, while TDFA is proposed for amplification in the S-band. The choice of amplifier technology is driven by performance considerations across different bands, with average NFs of 4.3 dB, 4.7 dB, and 6.5 dB assumed for the C-, L-, and S-band amplifiers, respectively. The higher NF in TDFAs is attributed to the relatively nascent state of this technology.

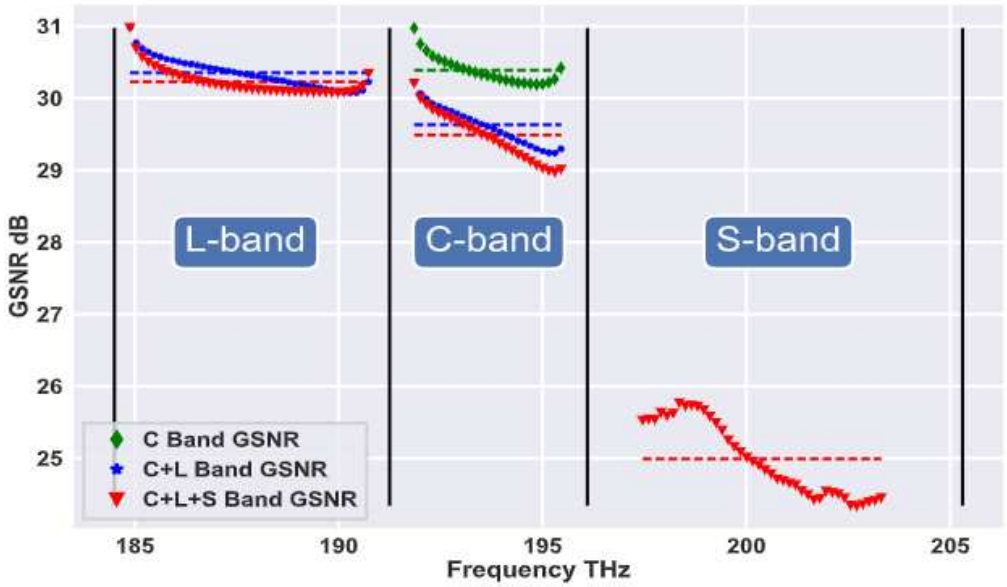

Figure 2.21: GSNR profile of MBT system

Moreover, MBT configurations necessitate the separation and combination of transmission bands before and after amplification, introducing additional insertion losses. These losses, which are not present in single-band systems, are estimated to be 1 dB for each multiplexing and demultiplexing operation. The cumulative effect of these parameters and system configurations on the GSNR and, by extension, the QoT, is exemplified through a simulated transmission over a 75 km span of ITU-T G.652D optical fiber, shown in Fig. 2.21. This simulation, which

incorporates modeled attenuation (Fig.2.5) and chromatic dispersion (Fig. 2.6) characteristics highlights the intricate balance required to optimize MBT systems for high-performance optical transmission.

2.5 Network layer abstraction

The integration of DSP-based coherent transmission technologies, alongside advancements in optical amplifiers and ROADM, has ushered in a paradigm shift in the field of optical networking. These technological advancements facilitate the realization of elastic and transparent optical networks, particularly within unified network domains, thereby significantly transforming operational dynamics. This evolution towards an all-optical network architecture is marked by enhanced flexibility, scalability, and efficiency in handling optical signals directly in the optical domain without necessitating conversion to electrical signals for amplification or switching purposes. An essential advancement facilitating this change is the introduction of transceivers that can handle hybrid modulation formats and provide adaptable rate modifications. These transceivers enable networks to dynamically create and change optical channels. The capacity to adapt is essential for adapting changing traffic patterns in real-time, guaranteeing that the network can effectively manage bandwidth and optimize resource allocation according to current demands.

When considering WDM transport layers, it is crucial to comprehend the constraints of the physical layer in order to construct LPs between network nodes. To guarantee optimal performance, it is necessary to thoroughly evaluate the physical parameters of the network due to the dynamic nature of optical channel design, which is made possible by the transceivers discussed earlier. After obtaining the specific information about the GSNR for each wavelength in single-band or MBT situations over different bands, the network topology is simplified and represented as a weighted graph. In this abstraction, the weight assigned to each link corresponds to the GSNR value for the relevant wavelengths, which serves as a measurable indicator of QoT throughout the network. This model reduces the inherent complexity of optical network topologies to a more understandable form by representing them as a set of light routes, each with a distinct GSNR value. A greater GSNR leads to better signal integrity and lower noise levels, resulting in increased transmission quality and the possibility for higher data throughput. One method of RWA in this framework involves using waveplanes. Waveplanes function as virtual representations of the wavelengths that can be used for transmission, providing a visual depiction of possible routing choices. This visualization assists network engineers in choosing the most optimal routes for building light lines, considering characteristics such as latency, throughput, and network dependability.

The utilization of optical network abstraction, which includes the assessment of

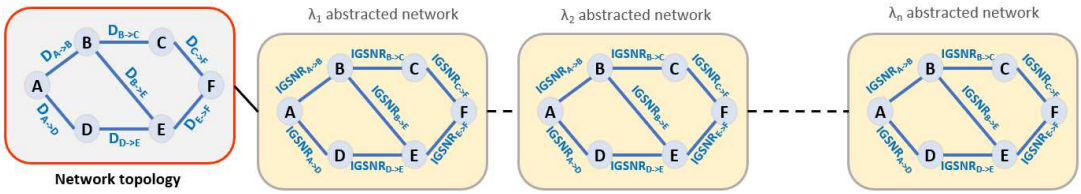

Figure 2.22: Network abstraction model

light path quality using GSNR values and the strategic implementation of waveplanes for RWA, offers a strong approach for constructing, analyzing, and improving the performance of high-speed optical networks. An example that demonstrates this method may be observed in the simplification of an optical network structure, depicted in Fig. 2.22. The diagram visually represents the network, with Optical Line Systems (OLS) indicating the distance between the source and destination nodes, such as $D_{A\to B}$ measured in kilometers. By assessing the GSNR for each channel and subsequently for all LPs between source and destination nodes, a comprehensive collection of waveplanes is generated for each wavelength/channel (λ_1, ..., λ_n). This set of waveplanes provides a detailed plan for optimizing network configurations based on current and expected traffic requirements.

2.5.1 Lightpath establishment

In optical networks, a Light Path (LP) represents a dedicated optical channel established between two ROADMs or network nodes. Functionally analogous to a circuit in electronic networks, LPs play a pivotal role in managing optical communication by providing a specified path for light to travel between nodes. This dedicated connectivity ensures the absence of bandwidth contention, a critical aspect for maintaining high network performance and reliability.

LPs are instantiated over specific wavelengths, leveraging the WDM technology to multiplex multiple optical carrier signals on a single optical fiber by using different wavelengths (colors) of laser light. This technique enables the simultaneous transmission of various signals over the same medium, significantly enhancing the network's capacity. In scenarios where the network's spectral resources are heavily utilized, and no single wavelength is free across the entire desired path, the RWA algorithm is challenged to leverage the existing spectral capacity more creatively. Under such circumstances, it may opt to utilize the residual capacity of already established LPs sharing the same source and destination nodes.

2.5.2 Routing and wavelength assignment (RWA)

Routing and Wavelength Assignment (RWA) [95, 96] is a vital procedure in the administration of optical networks, especially when it comes to establishing data connections between two nodes. This procedure entails choosing a suitable LP for transmitting data by assigning spectral resources along a predetermined path for an optical signal. The RWA process consists of two primary stages: the calculation of routing space and the assignment of wavelengths.

- **Routing space computation:**

  The routing space refers to the set of possible routes that can be taken between the source and destination nodes. The k-shortest path approach is used in this study to identify the routing space [97]. This algorithm produces a collection of k possible pathways sorted by length, from shortest to longest. The process of selecting a path is carried out on a graph that has assigned weights to its edges. These weights might change depending on different metrics.

  - Uniform Weight: Assigns a uniform weight (e.g., weight = 1) to every link, aiming to distribute the network traffic evenly. This approach tends to minimize wavelength contention by reducing the number of traversed ROADM nodes.
  - Link Length: Utilizes the physical length of the links as the weight. This method prioritizes minimizing the total distance traveled by the signal, thereby reducing latency.
  - GSNR Degradation: Focuses on the degradation of GSNR as the weight. An impairment-aware RWA strategy employs this metric to maximize the GSNR along the paths, enhancing the capacity and quality of each LP [98, 99].

- **Wavelength assignment strategies:** Once the routing space is established, the next step is to assign a specific wavelength for the connection. Various strategies exist for this purpose [95], with the most notable being:

  - First-Fit Strategy: Wavelengths are considered in ascending order from lowest to highest frequency. This method is favored for its simplicity and does not require comprehensive knowledge of the network's current state.
  - Most-Used Strategy: Prioritizes wavelengths based on their usage frequency within the network, from most to least utilized. Although this can optimize the use of network resources, it contrasts with the first-fit strategy by necessitating a global overview of the network's wavelength usage.

Despite the various strategies available, they tend to offer comparable performance outcomes. However, the first-fit strategy retains a notable advantage in operational simplicity and the lack of requirement for global network state information [95].

- **Wavelength assignment constraints**
  - Wavelength continuity, a critical feature of the RWA algorithm in optical networks, mandates the uniform use of a specific wavelength for the entire length of a connection between two nodes. This principle is primarily applied to avoid the need for wavelength converters, which would indeed improve RWA flexibility at the cost of additional equipment. The RWA algorithm simplifies network construction and operational administration by maintaining a consistent wavelength over all segments of a light route. In order to maintain this consistency, the RWA algorithm searches for an available wavelength within the specified spectral range that matches the wavelength used in previous segments. In situations where all available wavelengths are being used, the algorithm identifies the wavelengths that are presently in use and ensures that their selection does not cause any interference with the existing connections. This strategy not only simplifies network administration but also enhances the efficiency of using bandwidth, hence improving the performance and scalability of optical communication systems.
  - Wavelength contiguity refers to the arrangement of multiple wavelength channels in a way that they are closely spaced without significant gaps in the spectrum. This ensures efficient use of the optical spectrum, allowing for high data transmission rates and improved network performance. Contiguous wavelengths help to maximize the data-carrying capacity of optical fibers and facilitate easier wavelength management and allocation in the network.

The implementation of the RWA algorithm within this work is structured as follows:

- Pre-Computation of Routing Space: Initially, the network's routing space is calculated and established, as described in section 2.5.2.
- Dynamic LP Allocation: Upon receiving a new connection request, the algorithm attempts to allocate an LP, starting from the shortest path and progressing to longer ones based on the first-fit wavelength availability strategy.
- LP Allocation Decision: If the required network resources are available (availability of wavelengths keeping the constraints explained in check) and the chosen path is deemed feasible based on the signal quality (GSNR), the LP is allocated. If not, the connection request is blocked.

2.5.3 Traffic distribution and grooming

In analyzing network traffic distributions, two distinct models—uniform and nonuniform—are employed to progressively simulate network load scenarios. In a uniform traffic distribution, the Joint Probability Distribution Function (JPDF) for all node pairs is identical, reflecting an even distribution of traffic across the network. Conversely, the nonuniform distribution tailors the JPDF based on the population sizes of the nodes (cities) within the network, introducing a realistic variability in traffic patterns.

For uniform traffic distribution, the probability $P(s, d)$ that a specific source-destination pair is selected is uniformly distributed, calculated as:

$$P(s, d) = \frac{1}{N(N-1)} \tag{2.14}$$

where N represents the total number of nodes in the network. The equation 2.14 assumes that lightpath requests are directional.

In the case of nonuniform traffic distribution, $P(s, d)$ is determined by the relative populations of the source and destination nodes, formalized as:

$$P(s, d) = \frac{\text{pop}_s \cdot \text{pop}_d}{\sum_{(i,j)\in A} \text{pop}_i \cdot \text{pop}_j} \tag{2.15}$$

Here, pop_x denotes the population associated with node x, and the summation in the denominator accounts for all possible source-destination node pairs (i, j) in the network, encapsulated by A.

Traffic grooming in optical networks is a process aimed at enhancing bandwidth utilization by aggregating multiple lower-rate traffic streams into fewer high-capacity wavelengths. This technique is pivotal in optimizing the use of network resources, significantly reducing the necessity for multiple wavelengths and, consequently, diminishing the infrastructure costs associated with deploying additional network capacity. Within the framework of RWA, traffic grooming plays a critical role in determining the most efficient path and wavelength allocation for diverse traffic streams, with the overarching objective of minimizing the wavelength count while fully accommodating the traffic demands [100].

In a typical optical core network scenario, various independent traffic streams coexist, each with distinct bandwidth requirements that can be expressed as fractions of a full wavelength's capacity (denoted as λ). For instance, traffic streams may necessitate bandwidth allocations equivalent to $x\lambda$, where x can be from 0 to 1. In networks without traffic grooming functionalities, this would necessitate allocating entire or multiple wavelengths to each traffic stream, potentially leading to underutilization of link capacities due to the granular nature of demand versus wavelength capacity. The introduction of traffic grooming capabilities transforms this scenario by allowing for the consolidation of several smaller traffic streams into

a composite signal that occupies a single wavelength or a minimal set of wavelengths. This consolidation process is facilitated by traffic grooming nodes within the network, which aggregate traffic streams in such a manner that maximizes the payload of each wavelength, thereby achieving substantial bandwidth savings [101]. As a result, the network can transport the same aggregate volume of traffic using fewer wavelengths, enhancing efficiency and reducing operational costs.

Traffic grooming optimizes the distribution of routes and wavelengths in order to meet high traffic needs and improve the efficiency and cost-effectiveness of optical network infrastructure. This technique highlights the significance of traffic grooming in optical networks, especially in situations that need high data throughput and effective bandwidth control.

Chapter 3

Machine Learning for photonic devices

This chapter focuses on the utilization of machine learning methods to create switching structures and evaluate their controlling states and QoT. This research has been conducted in collaboration with Synopsys, Inc. and the research team associated at Politecnico di Torino, Italy. The findings have been reported in [102, 103]. Through this collaboration, we explore innovative approaches to enhancing the efficiency and reliability of optical network switching structures, leveraging the predictive and analytical capabilities of machine learning to optimize performance and QoT.

3.1 Introduction

Artificial Intelligence (AI) is a crucial tool that allows us to create computer devices or systems that can imitate human cognitive processes and behaviors. This emulation involves the ability of computers to perform a wide range of logical operations that require complex cognitive processes, including perception, learning, and deductive reasoning. AI systems function using a three-phase approach: gathering and organizing knowledge, applying this knowledge to tackle complex problems, and continuously improving its knowledge base through experiential learning over time. AI-driven applications cover a wide range of specialized sub-disciplines, such as Machine Learning (ML), computer vision and natural language processing (NLP). Machine learning (ML), which is a crucial component of AI, allows computer systems to improve their performance on specific tasks by autonomously learning from data, rather than relying on explicit instructions. This process of inductive learning allows these systems to apply the garnered insights for the purposes of classification, prediction, and executing various decision-making protocols based on previously unseen data [104].

Currently, ML is experiencing rapid expansion and is being integrated into a multitude of applications across various sectors, significantly impacting both everyday consumer experiences and specialized industry practices. ML algorithms are at the core of several ubiquitous platforms and services such as Google Maps for route optimization, Google Assistant for natural language processing and task execution, Facebook's content recommendation engines, Amazon's personalized shopping experiences, Netflix's predictive analytics for viewer preferences, YouTube's video suggestion algorithms, and many more. Beyond these consumer-oriented applications, ML's deployment extends to critical real-world domains, offering advanced solutions and enhancing efficiency and accuracy. In healthcare, ML algorithms assist in diagnosing diseases by analyzing medical images and patient data, thereby aiding in early detection and tailored treatment plans [105, 106]. Traffic management systems leverage ML for predicting congestion patterns, optimizing traffic flow, and improving safety in automated driving technologies [107]. In the financial sector, ML algorithms are utilized for predictive analysis in stock market trading, enabling informed decision-making based on historical data trends. Email services employ ML for spam detection, filtering out unwanted communications with high precision. Furthermore, ML plays a pivotal role in developing speech recognition systems, facilitating user interaction with technology through voice commands, and in computer vision, enabling machines to interpret and understand visual information from the world around them. These applications underscore ML's versatility and its capacity to revolutionize various aspects of both daily life and specialized professional fields.

3.2 Machine Learning Techniques for Photonic Device Optimization

In the field of optical networking, the increasing growth in internet traffic, driven by bandwidth-intensive applications and the emerging Internet of Things (IoT) ecosystem, requires higher degrees of adaptability across all network levels. SDN integration is a crucial approach for efficiently addressing these objectives. The use of the SDN framework enables the complete virtualization of network architecture and operational activities under a single network operating system. This shift in paradigm allows for an unparalleled degree of programmability and control over network resources. Furthermore, the introduction of sophisticated coherent optical transmission methods in WDM networks, together with the implementation of ROADMs, brings about substantial improvements in optical transport capabilities. These advancements establish the foundation for expanding the scope of SDN to the physical layer, enabling the real-time dynamic routing of wavelengths and the optimization of optical pathways.

In order to smoothly integrate SDN down to the optical physical layer [108], it is

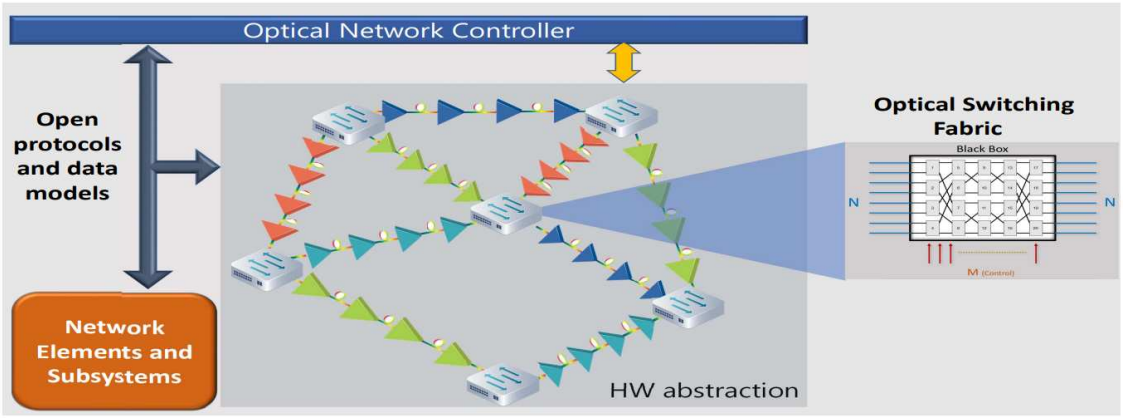

Figure 3.1: Software-defined Open Optical Networks [110]

essential to abstract important network aspects and transmission operations. The process of abstraction entails defining the attributes of optical signals, network devices, and their operating statuses in a format that can be programmatically modified. The use of abstraction is crucial in accurately measuring and reducing the impact of QoT impairments, such as signal weakening, dispersion, and non-linearities, by employing intelligent control mechanisms. To achieve a high degree of SDN implementation, a complex optical network controller is required. This controller must be capable of coordinating all network elements and transmission operations [109]. This controller must have the capability to intelligently allocate resources in response to real-time network conditions, demand predictions, and QoT needs. By utilizing extensive network data, the controller may employ predictive algorithms and ML models to enhance network performance, guarantee stability, and enable quick scaling in accordance with changing traffic patterns and service requirements. The sophisticated SDN design highlights the promise of software-defined optical networking to handle the rapid increase in data traffic and the complexity of next-generation internet applications. Photonic Integrated Circuits (PICs) play a crucial role in performing complex tasks in modern smart optical networks and data centers. Large-scale photonic switches and WSS are now essential components because of their wide bandwidth capabilities, low latency, and energy-efficient operation. These characteristics greatly improve the practicality and implementation of PIC-based network components, especially photonic switches, which in turn drives the requirement for a standardized software-driven architecture to manage control states and measure degradation in QoT. This criterion enables thorough governance through a centralized network control unit, as seen in Fig. 3.1.

This thesis introduces a model that utilizes ML to build photonic devices in optical networks, based on the framework of SDN. This approach allows for the software-based management of any N×N photonic switching system, regardless of

its physical arrangement or level of complexity. The proposed model utilizes an ML-based inverse design technique to derive control parameters that maximize the operational states of photonic switches, even without previous knowledge of their physical design features. Furthermore, we introduce a direct design method within the same ML framework to accurately predict the QoT degradation attributable to the intrinsic and extrinsic switching elements. Predictive capability is essential for preserving optimal signal integrity throughout the network and guaranteeing the strength of communication links. This optimization process improves performance and reduces penalties in quality of transmission across large and complex photonic switching structures.

3.2.1 Routing states

The study aims to assess a management model that utilizes ML and is applied to advanced switching networks. Specifically, the focus is on multistage crossover switches that share structural similarities with Banyan and Clos networks. These networks are constructed using a collection of basic 2×2 crossbar switches, systematically arranged over numerous layers to enable the routing of a certain number N of input signals to a predetermined output configuration. The dynamic reconfiguration capabilities of these networks are controlled by modulating control signals that are aimed at each of the M optical switching elements (OSEs), which together decide the network's output configuration, shown in Fig. 3.2.

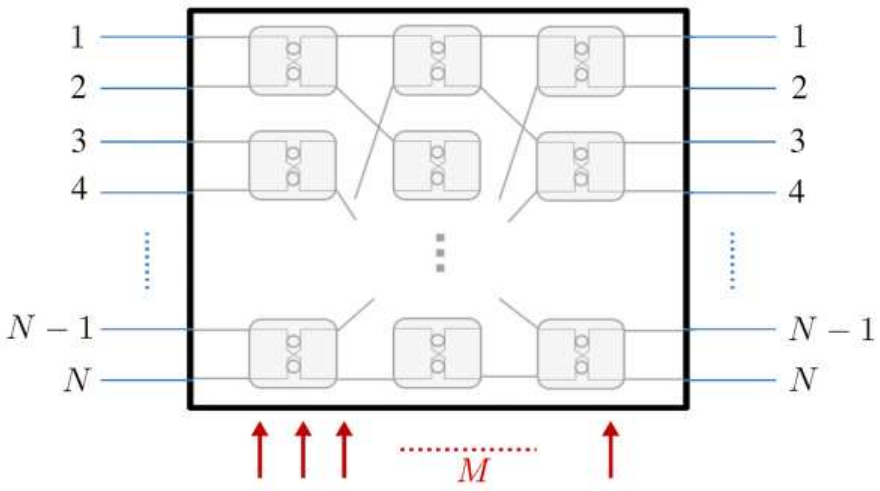

Figure 3.2: Generic N × N optical switch fabric [111]

An essential topological characteristic of these optical switching networks is their innate ability to handle any possible output arrangement required by the input signals without causing internal routing conflicts. This feature divides the

networks into two main categories: non-blocking and blocking networks. Non-blocking networks are characterized by their capacity to allow the routing of any possible input combinations to their corresponding outputs without any obstacles, ensuring a continuous flow of data. On the other hand, networks that are being blocked may experience internal disputes in how they route data, which can result in delays in transmitting data or need the implementation of alternative routing algorithms. This analysis focuses specifically on non-blocking networks due to their greater operational efficiency and the extensive topological complexity they possess in comparison to blocking networks. Non-blocking networks are a more relevant area of research for implementing management models based on machine learning. This is because they include intricate routing mechanisms and a greater need for efficient and conflict-free paths for transmitting data. This focus is in line with the main goal of improving the performance of optical networks by using intelligent control strategies driven by machine learning. These strategies take advantage of the advanced routing capabilities and flexible configurations of non-blocking multistage crossover switch architectures.

Non-blocking switching structures

The foundational element in constructing these networks is the 2×2 CrossBar switch, a two-state device controlled by a signal M, toggling between bar and cross states. In the bar state (M = 0), inputs are propagated straightforwardly (λ_1 to λ_1 and λ_2 to λ_2), and in the cross state (M = 1), the outputs are swapped (λ_1 to λ_2 and λ_2 to λ_1). This switch serves as the core component in network designs and can be realized through technologies such as MRRs or MZI, each offering distinct advantages for either wavelength-agnostic or wavelength-specific applications. The control of these switches, typically achieved via electrical signals in OSEs, adheres to a binary model that, despite physical implementation differences, provides a universally applicable framework for evaluating routing paths in a device-independent manner.

The arrangement of crossbar elements into a certain topology is crucial in the design of a N×N switch architecture. It has a basic impact on the switch's routing efficiency and the amount of components needed. The analysis focuses exclusively on a certain subset of switching networks, specifically Rearrangeable Non-Blocking networks. These networks have the intrinsic capability to enable any combination of input signals to be sent to their corresponding output ports without causing any internal conflicts, even while taking into account existing input-output (I/O) connections. Reconfigurable Non-Blocking networks have the ability to efficiently direct any combination of inputs to the required outputs. Nevertheless, this capacity is subject to the condition that current I/O connections may require reconfiguration in order to support new routing demands. The need for dynamic reconfiguration emerges due to the network's structure, which does not guarantee path availability

in situations where the network is already handling traffic. This feature highlights a major disadvantage when compared to non-blocking architectures, which provide path availability without requiring any changes to established I/O linkages.

3.2.2 Quality of Transmission

In this section, we expand on the previous section that explained how to determine control states for a Photonic Integrated Circuit PIC N×N photonic switching system. We use a ML inverse design methodology, which is described in [112]. This approach is completely independent of the circuit's topology. This first model, although robust, requires more refining to completely capture the consequences of switch operations on the physical layer of the photonic network. In order to fill this void, we propose the implementation of an additional machine learning network. This network will be designed using a straightforward approach and will be specially tailored to accurately forecast the deterioration of QoT caused by the operational changes of the switching element. It is vital to have this predictive capacity in order to comprehend and alleviate the negative impacts that the switch may have on signal integrity and overall network performance.

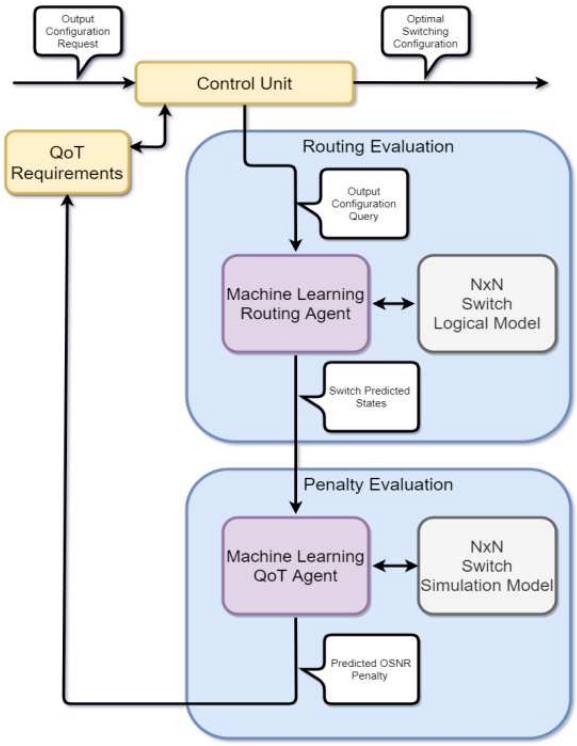

Figure 3.3: Routing states and QoT evaluation model [112]

This synergistic operational framework is made possible by the integration of

these two ML networks, shown in Fig. 3.3, which specialize in different areas of switch design and performance evaluation. This framework not only enhances the control and administration capabilities of N×N optical switches but also incorporates QoT awareness into the system. This comprehensive management system is essentially driven by software, providing a versatile and dynamic approach to optimizing optical networks. Moreover, the suggested model is conceptualized in a way that facilitates easy expansion and adjustment, hence enabling the assessment of the N×N optical switch's influence on more comprehensive network layer measurements. The ability to extend this capacity is crucial for expanding the model to support different network topologies and operating circumstances, therefore offering a complete set of tools for analyzing and optimizing photonic networks.

3.3 Machine learning for predicting routing control states

The current framework in ML enables the interpretation of complex characteristics of systems that are intrinsically difficult to assess directly. Machine learning models develop a deep understanding of complex data patterns by using advanced algorithms. These sophisticated algorithms condense the subtle data characteristics into decision-making frameworks that are mostly active during the testing phase. Thoroughly trained advanced cognitive models improve the real-time operation of systems by enabling them to make intelligent inferences and respond autonomously.

The development of the suggested machine learning architecture consists of three main parts: pre-processing, training, and testing modules, shown in Fig. 3.4. The primary function of the pre-processing module is to normalize the dataset, preparing it for further actions. The training module utilizes the improved dataset to impart information to the machine learning models. After the training process is finished, the models is evaluated in the testing module using a specific subset of the total dataset. The usage of high-level Python Application Programming

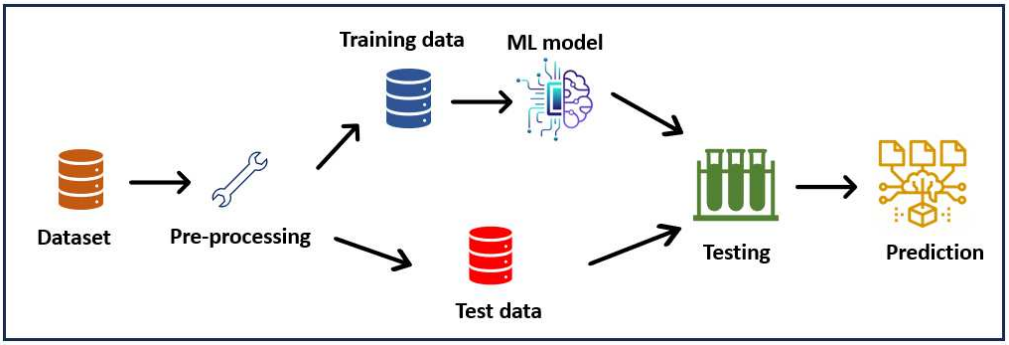

Figure 3.4: Machine learning model

Interfaces (APIs) supplied by two well-known open-source libraries—TensorFlow (TF)[113] and Scikit-Learn [114]—enables the development of ML engines. Both libraries are well-known for their extensive range of features that are essential for building data-driven models. Those features encompass a wide range of advanced tools for data preparation and noise filtration, which are crucial preliminary stages before feeding the data into the machine learning models. In this work, we have used DNN model, depicted in Fig. 3.5.

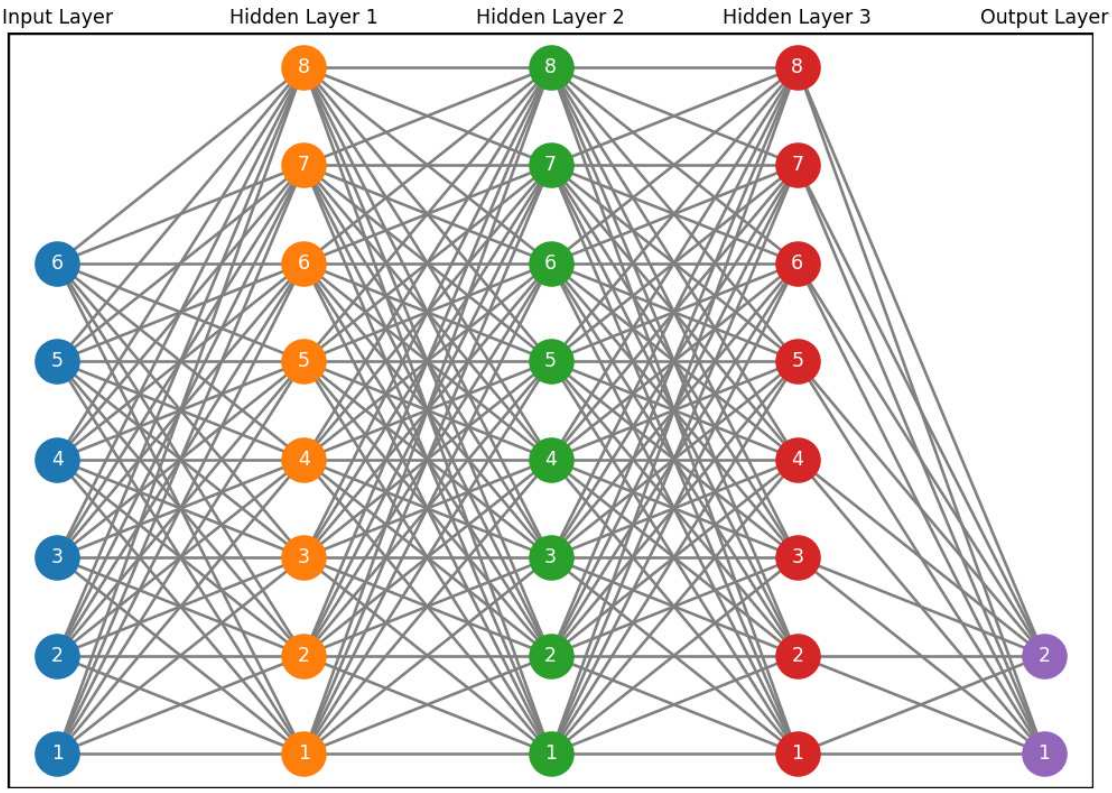

Figure 3.5: DNN model

DNNs are advanced machine learning models that replicate the structure and functionality of the human brain for data processing. They are made up of numerous layers of artificial neurons, which include an output layer, multiple hidden layers, and an input layer. Each layer in the network processes the incoming data to create a more abstract and composite representation, allowing the network to understand intricate patterns in extensive datasets. DNNs are employed in several domains, including picture and speech recognition, natural language processing, and autonomous vehicle systems, since they possess the capability to comprehend and represent complex connections within data. The effectiveness and precision of DNN rely on their structure, which includes the number of layers (depth), the number of neurons per layer (width), and the selection of activation functions that

induce non-linearities throughout the learning process.

3.3.1 Beneš switching network

This section provides an explanation of the composition of Beneš networks, which are a specific type of Clos networks distinguished by their use of 2×2 basic switching components. Beneš networks are designed to function with a certain number of inputs, denoted as $N = 2^k$, where k is a positive integer and belongs to the set of natural numbers. Despite this limitation, the Arbitrary Sized Beneš (AS-Beneš) [115] networks expansion allows for the adaptation to unlimited number of inputs (N) while maintaining the network's core characteristics. Beneš networks are characterized by their reconfigurable non-blocking design. Unlike non-blocking networks that need modifications to current paths for establishing new connections, Beneš networks enable any output permutation by reconfiguring paths. This characteristic guarantees that although all necessary input-output links may be established, existing connections may need to be rerouted through different paths to satisfy additional demands.

The analytical foundation for Beneš networks is centered on two crucial parameters: (i) the number of distinct output arrangements, which may be calculated as $N!$, where N denotes the number of inputs. (ii) the number of network configurations in a strict-sense Beneš network may be characterized by the exponential function 2^M, where $M = N\log_2(N) - \frac{2}{N}$. Recursive computation is required for AS-Beneš networks since the parameter depends on the non-fixed nature of N [115].

Beneš topologies typically provide different routing pathways for identical output permutations due to the significant difference in the number of unique output permutations and the total network configurations. The diversity in equivalent routing paths varies based on the specific output permutation sought, averaging $\frac{2M}{N!}$ alternative routes for each permutation.

In order to emphasize the capabilities of our proposed machine learning approach to handle networks of different complexities, we examine two different Beneš network configurations with variable sizes, especially for N=8 (Fig. 3.6) and N=10 (Fig. 3.7). The number of 2×2 switching components in these designs is M=20 and 26, respectively. The figures represent the dimensions of the control vector, which is used as the labeling framework for the machine learning agent. This research seeks to clarify the effectiveness of machine learning approaches in handling the operational dynamics of Beneš networks, thereby providing insights into their potential for enabling more efficient and flexible photonic switching systems.

Model implementation and data collection

For routing evaluation purposes, the implementation utilizes a black-box abstraction for the essential 2×2 switching element. This abstraction suffices for path

analysis, where the input-output relationship is depicted as an edge within a pertinent graph-based model. In terms of assessing the internal routing configurations within the network device, a Benes network architecture is deployed. This is realized via a matrix representation that aggregates the permutation vectors from each individual switching stage. The derivation of the output permutations is contingent upon specified control states, which dictate the BAR and CROSS configurations for each of the M switch elements in the matrix. These configurations are encoded in a binary control vector V, a member of the space $R^{1\times M}$, where a '0' in V_i indicates the BAR state, and a '1' indicates the CROSS state. The resultant network routing configuration for any given control state is captured in a permutation vector of size N. This model is instrumental in the verification phase of network design, where predicted control states are subjected to evaluation on a simulated abstraction of the physical device.

To accurately assess the QoT, a detailed simulation incorporating both the physical component design and the transmission characteristics is essential. The device under investigation has been modeled using a second-order MRR switch, as part of the crossbar architecture. This model was developed following a recursive definition and implemented within the Optsim‖ simulation environment, as referenced. Central to the QoT evaluation is the simulation of the device with realistic ingress and egress stages, which are respectively connected to a transceiver and a receiver module. The entire setup enables the simulation of the transmission system under practical conditions, employing a PM-64-QAM modulation format. The transmission operates over central frequencies defined by $f = (193.1 + 0.1 \times x)$ THz for x in the range $[1, N]$, and a symbol rate R_s of 50 Gbps. For the generation of training and validation datasets, the OSNR penalties are calculated for a variety of unique state configurations. These configurations are randomly generated and tested, aiming for a target BER threshold BER_{th} of 5×10^{-3}. The OSNR penalties are derived from simulations that propagate the signal through the specified component, capturing the impact on the signal quality due to various control states of the device.

The datasets compiled include OSNR penalties recorded at each port for 1000 random realizations of control states. This extensive simulation effort has been executed across two different Benes network configurations, specifically the 8x8 and 10x10 structures, shown in Fig. 3.6 and Fig. 3.7.

3.3.2 Machine learning for predicting control states

In the context of controlling photonic switches in optical networks, the goal is to develop a machine learning (ML) model capable of predicting the control signals required to configure an N×N photonic switch. The specific task of this ML model is to map input wavelengths to correct output ports by accurately configuring the switch's internal states. The inputs to the machine learning model are binary control signals, which represent the state of individual 2×2 optical switching elements

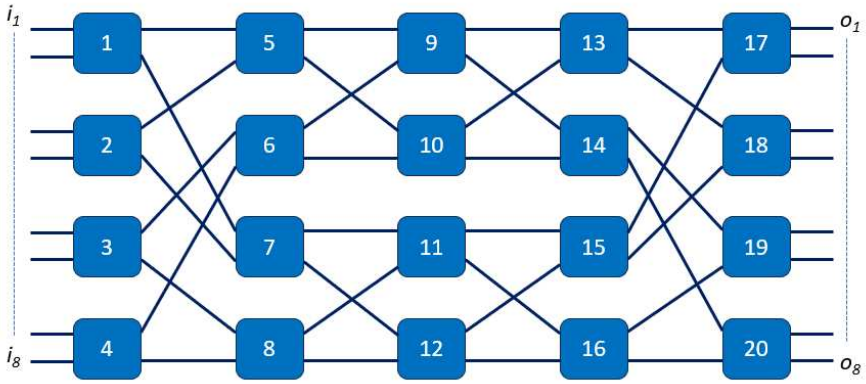

Figure 3.6: Beneš 8x8

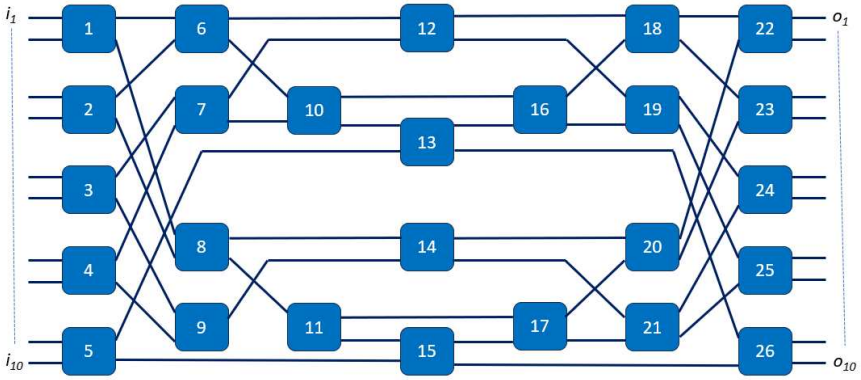

Figure 3.7: Beneš 10x10

(OSEs). These control signals are crucial in determining how input wavelengths (λ) are routed through the switch fabric.

Inputs

- **Control Signals**: These control the state of each 2×2 switch in the network (either bar or cross state). Each element of the vector indicates whether a switch will swap (cross) or directly pass a wavelength through the network.
- **Wavelengths** (λ): The specific wavelengths that are routed from the input to the output ports through the switch fabric. Each input wavelength requires a corresponding control signal configuration to direct it to the correct output.

Outputs

- **Routing Configuration**: The predicted configuration of control signals, which ensures accurate routing of input wavelengths to the desired output ports. The output is a unique combination of M binary control signals that define the path each wavelength will take within the photonic switch.

The machine learning model addresses a non-trivial problem, as the same output can sometimes be achieved by multiple configurations of the M control signals, making it necessary for the model to learn the optimal or correct configuration for each scenario.

This collaborative research details the implementation of ML agents which are tailored to forecast photonic integrated switch control and routing topologies. This methodology utilizes a machine learning framework that employs a black-box approach, hence reducing the requirement for a comprehensive comprehension of the underlying structures of the components involved. The essence of this methodology is around a carefully constructed Deep Neural Network (DNN) model, designed specifically for the TensorFlow© platform. The DNN architecture consists of three hidden layers, each containing a unique number of neurons, which are specifically tailored to improve its cognitive skills. The activation function used in all of these layers is the Rectified Linear Unit (ReLU). The model's performance is evaluated using the Mean Square Error (MSE) measure as the loss function. The training protocol for the DNN consists of 1,000 iterations, with a learning rate established at 0.01. The dataset is divided between training and testing sets in a 70/30 ratio, respectively, based on the N-size (N = 8, 10), shown in Fig. 3.6 and Fig. 3.7, of the Benes˘ topology being studied.

The distinguishing characteristic of this ML model resides in its feature selection, which specifically targets the different combinations of wavelengths that can be seen at the output ports. The target labels are equivalent to the values of the M control signals. The first step in the machine learning process involves creating a synthetic dataset that accurately replicates the operating properties of the switch topology being studied. This technique is very adaptable and can handle different topological configurations, making it suitable for a wide range of black-box applications without requiring special knowledge of the underlying switch topology. The machine learning training and testing dataset was generated using a N × N Benes network. In order to demonstrate the scalability of our suggested strategy, we analyzed two different situations: N = 8 and 10. These scenarios correspond to configurations with 20 and 26 internal switches. As shown in Table 3.1, a subset of the 2^M possible control combinations was chosen to create the dataset.

Fig. 3.8 illustrates the impact of varying training data sizes on prediction accuracy for the control states of both 8x8 and 10x10 Benes networks. The x-axis represents the percentage of training data used, while the y-axis depicts the percentage of correct predictions. At approximately 50% of the training data size,

Network type (NxN)	Beneš 8x8	Beneš 10x10
Permutations ($N!$)	40,320	3,628,800
Switches (M)	20	26
Combinations (2^M)	1,048,576	67,108,864
Dataset	100,000	300,000
Neurons per hidden layer	15	35
Training time (hours)	10	37

Table 3.1: Dataset statistics [111]

Figure 3.8: Correct prediction vs. normalized training size

prediction accuracy nears 80% for the 10x10 Benes and 90% for the 8x8 Benes. When utilizing the full training data set, which constitutes 100% of the selected subset, prediction accuracy escalates to 90% for the 10x10 Benes and reaches 99.9% for the 8x8 Benes. This trend demonstrates that the predictive capability of the machine learning model enhances with larger training data volumes, achieving substantial accuracy with as little as 50% of the training data.

Fig. 3.9 illustrates the precision of forecasts for each of the two Benes network sizes, shown by blue bars. An impressive level of accuracy ($> 89\%$) was obtained, while there is a noticeable decrease in predictive performance as the N values increase: 99.84% for N=8 and 89.39% for N=10. In order to improve the accuracy of the machine learning model's predictions, we integrated an extra heuristic phase. This phase was developed by analyzing patterns seen in incorrect configurations, where it was commonly found that a single switch was in the incorrect state. Our heuristic approach entails systematically rectifying a singular switch

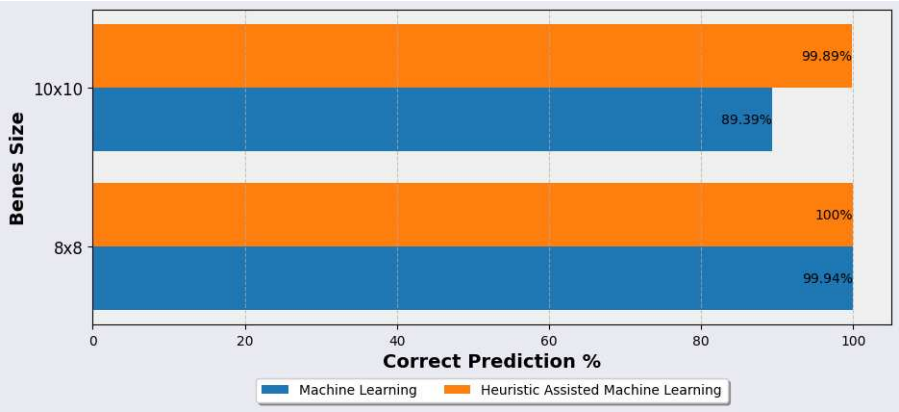

Figure 3.9: Correct predictions with and without heuristics

fault by sequentially toggling individual switches and verifying if the resultant output corresponds to the anticipated output. By combining this rule of thumb with the machine learning method, the precision levels for the Benes networks of size 8x8 and 10x10 significantly increased to 100% and 99.89%, respectively. A simple flowchart of the heuristic is shown in Fig. 3.10.

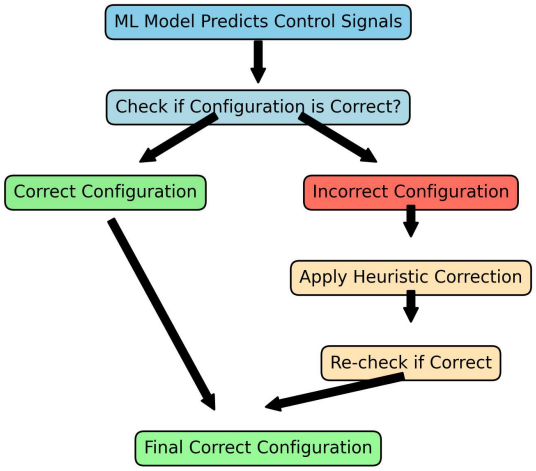

Figure 3.10: ML model configuration validation and correction

This investigation has demonstrated that a machine learning technique can accurately determine the control states of any N × N photonic switch, regardless of the underlying network architecture. The machine learning model demonstrates the capacity to handle greater network sizes (N) while retaining a high level of prediction accuracy, even when trained on a very small dataset. This suggests

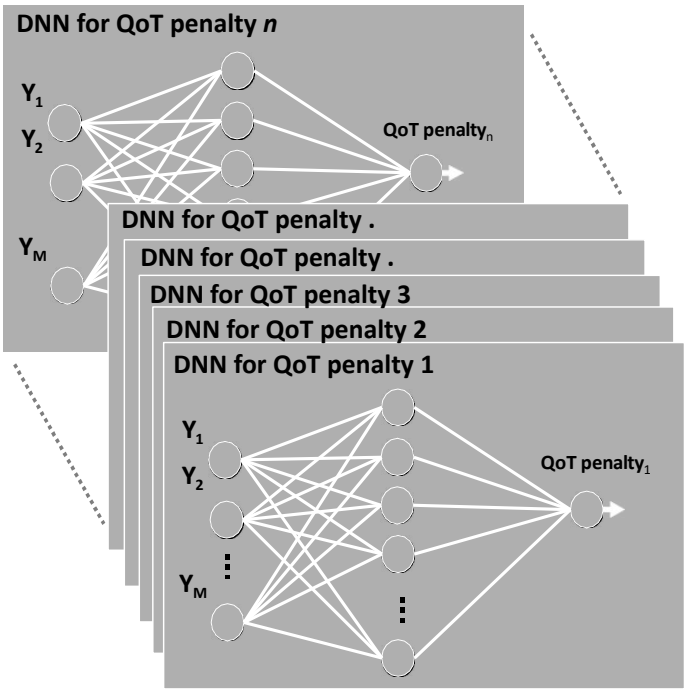

Figure 3.11: Parallel DNN structure

that the method is resilient and has the potential to be used in intricate photonic switching systems with higher N values, providing a viable path for future progress in controlling photonic switches.

3.3.3 Machine learning for QoT

This section examines the architecture and methodology of our ML framework, which includes the configuration of the primary ML engine, as well as the procedures for testing and training. The engine's architecture encompasses the manipulation and choice of features and labels, as well as the fine-tuning of several hyperparameters. Our framework employs a supervised machine learning methodology within a self-contained system, relying on extensive training data to develop a model capable of making decisions without any previous understanding of the internal configuration of the photonic switch. The key part of this approach is the identification of system features and designations, which correspond to the inputs and projected outputs of the model.

The training and validation datasets were created by calculating the OSNR penalty for randomly chosen unique state configurations, with a target BER set at 5×10^{-3}. These OSNR penalties were determined by simulating the signal's propagation through the device under test. Each dataset includes the penalty at

every port of the device for a random selection of 1,000 control state realizations, as detailed in Tab. 3.2. This simulation was conducted on Beneš structure 8x8.

Benes switch	Permutations $N!$	OSE count	Combinations 2^M	Dataset	Train Set	Test Set
8×8	40320	20	1048576	1000	700	300

Table 3.2: QoT evaluation dataset

The features consist of various combinations of control signals that manipulate OSE. The label represents the QoT penalty for the k-th output port of the switch.

The ML engine's cognition is achieved by utilizing a DNN, which takes use of the TensorFlow library's comprehensive capabilities for implementing algorithms and improving datasets. The DNN is carefully configured with optimized hyperparameters. The training iterations are set to 1000. The ADAGRAD optimizer from Keras is used with an initial learning rate of 0.01. Additionally, L1 regularization is set to 0.001 to improve computational efficiency by excluding irrelevant features.

Multiple nonlinear activation functions were assessed, and the Relu function was finally selected because of its superior performance in predicting accuracy and computing efficiency. In order to enhance the accuracy of predictions, a parallel DNN structure is suggested, depicted in Fig. 3.11. The concept of a "parallel DNN structure" refers to an architectural enhancement designed to improve the accuracy of predictions. This structure involves using multiple DNNs in parallel to process different subsets of the data simultaneously. Each DNN is responsible for a specific portion of the data, allowing the main DNN engine to leverage the extensive dataset more effectively. This parallel processing not only boosts the predictive capability of the main DNN engine but also enhances its efficiency by distributing the computational load. This architecture optimally utilizes the extensive dataset for each output port, enhancing the main DNN engine's predictive capability and efficiency. Prior to validating the main DNN engine, it undergoes training using a separate subset of the dataset. The dataset is divided into two halves, following the standard 70/30 split, with 70% of the data used for training and the remaining 30% used for testing. In order to reduce the likelihood of overfitting, the training process is stopped based on the number of iterations, and the loss function used is the MSE, which is determined according to the equation.

$$\text{MSE} = \frac{1}{n}\sum_{i=1}^{n}(\Delta\text{OSNR}_i)^2 = \frac{1}{n}\sum_{i=1}^{n}(\text{predicted OSNR}_i - \text{actual OSNR}_i)^2 \qquad (3.1)$$

where n is the number of test realizations, N is the total number of input/output ports of the specific $N \times N$ switching system, and predicted OSNR − actual OSNR are the predicted and actual OSNR Penalties for the k-th output port of the considered topology. The number of iterations was selected to ensure that the model

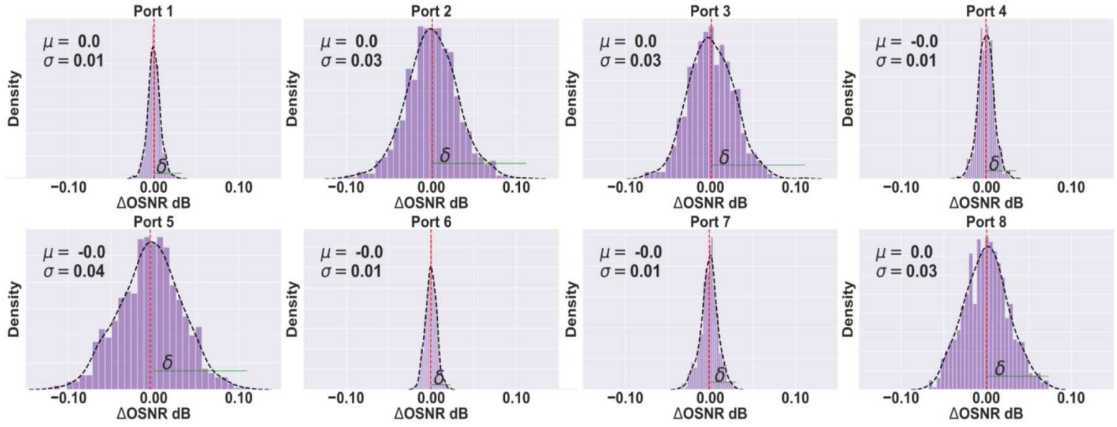

Figure 3.12: Probability density functions of Δ OSNR for each port of the 8×8 Beneš switch

reaches a stable state of learning without overfitting. The convergence was monitored using the MSE, which measures the difference between the predicted and actual QoT penalties. The model's performance was periodically validated using the test set to ensure that the training did not lead to overfitting.

The ML module leverages deterministic switch control states to gauge QoT impairments, delineated as $OSNR\ Penalty_{i,k}$ for each port k of the Beneš switch. A comprehensive case study was conducted to appraise the efficiency of our ML-guided QoT Penalty estimation model within a photonic switching framework. The robustness of the ML-enriched QoT model was substantiated via an evaluation of its performance at each port of the 8x8 Beneš switch. Fig. 3.12 depicts the $\Delta OSNR$ distributions for all the switch's ports, complete with mean (μ) and standard deviation (σ) statistics.

In Fig. 3.12, $\Delta OSNR$ distributions are bisected by a red dotted line at $\Delta OSNR = 0$. The region where $\Delta OSNRs \leq 0$ is deemed non-critical because the predicted $OSNR\ Penalty_{i,k}$ is at most equal to the actual $OSNR\ Penalty_{i,k}$, suggesting that, although some network capacity might be underutilized, the system's operational integrity is maintained. Conversely, instances where $\Delta OSNRs > 0$ are critical, as the predicted $OSNR\ Penalty_{i,k}$ surpasses the actual figure, mandating the addition of a safety margin above the ML prediction to preserve uninterrupted system operation. The essential safety margin (δ_k) for such cases is represented by a green line for each port k of the 8x8 Beneš. Analyzing the necessary margins, we recognized the ML model's notable precision in estimating QoT impairments. Within the 8x8 Beneš construct, the least optimal prediction was observed at port 5, with δ_5 being under 0.12 dB. Considering the attained level of predictive accuracy, it is reasonable to infer that in real-world applications, the safety margin for OSNR Penalty predicated on ML prognostications could potentially be tapered

to a mere 0.12 dB for the 8x8 Beneš switch.

Prediction discrepancies among ports arise from the inherent randomness and limited size of the training dataset, leading to varied efficacy in training and prediction for certain signal paths. Despite these constraints, our study found minimal variation in port predictions, highlighting the potential of our ML approach to significantly improve QoT when deployed.

Chapter 4

Network level performance analysis in multi-band systems

Over the last few years, there have been significant developments in long-haul network technology, specifically in fiber capacity, optical switching, and optical reach [116]. This has led to a noticeable transfer of bandwidth and operational challenges from core networks to metro and access networks. Advancements in wavelength-division multiplexing (WDM) technology have enabled the spread of applications that require high bandwidth and strict performance standards to the network edge. As a result, core networks are expected to experience pressure in terms of both capacity and flexibility as these technologies become more prevalent near the network edge.

Although backbone networks are currently able to handle current levels and types of traffic, the expected increase in capacity at the network edge, along with the rise of on-demand applications, is projected to fuel rapid growth in various services. This expansion will require a substantial transformation of the fundamental network infrastructure. In order to maintain the progress of networking advancements, it is crucial to have a deep understanding of the advantages and constraints of current technologies and architectures. It's essential to determine the required advancements to meet the demands of future core networks in the coming years. Currently, the optical network layer is mostly static. However, the increasing demand for on-demand services requires a much higher level of flexibility in this layer. Moreover, quick reconfiguration is crucial for network restoration as important applications depend more and more on the transfer of large amounts of data. Being able to handle numerous simultaneous failures will be crucial for maintaining continuous service for essential operations [117].

The capacity of optical systems is currently being improved through the use or development of a wide variety of technologies in order to fulfill the ever-increasing demand for information traffic. The use of sophisticated digital signal processing

techniques makes it possible to compensate for a variety of transmission flaws, including chromatic dispersion (CD) and polarization-mode dispersion (PMD) [118]. Moreover, the use of extremely efficient modulation formats that incorporate probabilistic shaping (PS) offers the potential to bring the capacity of fiber transmission closer to the Shannon limit [119, 120], which is the theoretical limit. These technological improvements, in conjunction with variable rate transceivers, have resulted in the development of commercially accessible systems that are capable of transmitting higher rates at each channel [121].

The spatial-division multiplexing (SDM) strategy is another significant development. This method makes use of multi-core, multi-mode, and/or multi-fiber setups in order to enhance the number of network channels that are sent over each connection. While multi-fiber SDM is presently commercially feasible, based on existing C-band systems (4.8THz), SDM based on core or modes is still in the research phase, showing great potential via several field testing [122, 123]. The broad implementation of this technology, on the other hand, would call for upgrades to the fiber infrastructure that is already in place.

Over the past few years, there has been a growing interest in the investigation of transmissions that extend beyond the C-band in both the academic and industrial domain. This technology, which is currently available for commercial use and is known as ultra-wideband (UWB), band-division multiplexing (BDM), or multi-band transmission (MBT) [35], significantly enhances the usage of bandwidth from the C-band to the C+L-bands, thereby doubling the capacity of the fiber to 9.6 THz [124], or even moving towards the C+L+S- bands.

4.1 Optical capacity enhancement

The implementation of advanced technologies (i.e; 5G/6G) represents a substantial advancement in wireless communication, requiring a substantial and rapid expansion of the network's bandwidth capacity. This increase in demand necessitates improvements in all areas of the network, with a specific focus on optimizing the transmission of data through fiber optic infrastructure to handle the growing amount of data more effectively. Network operators are therefore compelled to develop techniques that are both cost-effective and capable of expanding the capacity of their current installations in a scalable and flexible manner. These efforts are crucial to guarantee the dependable and effective operation of the future Internet.

WDM, which is the most advanced optical infrastructure now available, makes use of the 4.8 THz bandwidth in the C band. This band functions as the main channel for transmitting data across different network sizes, ranging from long-distance and underwater networks to urban networks. One often used approach in this context is the application of polarization multiplexed rectangular 16-ary quadrature amplitude modulation (PM-16QAM) schemes. This method enables

data transfer rates of up to 30 Tbps per optical fiber, demonstrating the vast capabilities of modern technologies in managing large amounts of data. It is crucial to acknowledge that increasing the network capacity by installing more fiber is frequently financially unfeasible, particularly in situations when there is a scarcity of fiber resources.

Within this particular situation, the utilization of multi-band transmission arises as a beneficial and advantageous approach. This technology involves transmitting data across a wider range of low-loss spectral bandwidths in optical fibers. This helps to maximize network capacity and make better use of the current fiber infrastructure. Integrating components that are designed to work beyond the usual C-band spectrum has the potential to increase network costs significantly, mainly because specialist amplifiers are quite expensive. In addition, phenomena like SRS present considerable difficulties, which can lead to a decrease in transmission quality across several frequency ranges and negatively impact network capacity, particularly in large-scale network setups.

An essential task is to critically analyze and compare the advantages and drawbacks of integrating multi-band network components in a multi-band transmission system with the conventional single-band transmission. This evaluation will have a pivotal influence in establishing the network's overall performance and capacity augmentation measures.

In order to tackle these difficulties, two main strategies arise: Spatial Division Multiplexing (SDM) and Band Division Multiplexing (BDM). SDM exploits the spatial characteristics of light by employing Multicore (MCF), Multimode (MMF), or Multiparallel (MPF) fibers to increase the data-carrying capacity of the network. This approach, although showing potential for increasing capacity, requires a complete restructuring of the current optical transport system. This includes implementing new fibers and devices specifically designed for this advanced architecture.

In contrast, BDM aims to broaden the range of operations for optical fibers by allowing for low-loss transmission across a wider spectrum, including the 54 THz bandwidth of ITU G.652.D fibers. The advantage of BDM is its potential to enhance network capacity without requiring more optical fibers, making it a more instantly feasible alternative. The main difficulty associated with BDM is related to optical amplification, which is necessary to meet the requirements of the broad spectrum. Currently, there is ongoing progress in creating prototype amplifiers that can function in these expanded spectrum areas. Furthermore, the successful execution of BDM relies on improvements in clear wavelength routing, which necessitates the presence of advanced filtering and switching components specifically designed for this wider range of operations. The initial step in implementing the BDM technique involves the incorporation of filtering and switching components. The network component, such as the Wavelength Selective Switch (described in Chapter 2), is crucial because it provides independent control and routing of each

input channel to a fiber output of the WDM comb.

4.2 Simulation setup

4.2.1 Statistical Network Assessment Process - tool

Following the evaluation of the GSNR (described in section 2.4.4) utilizing GNPy [125] as a physical layer QoT metric, we move on to the network layer. During this phase, we represent the network architecture as a weighted graph, with each link's weight indicating its QoT. This modeling methodology offers an intricate analysis of the network's configuration and its capacity for achieving optimal performance. Subsequently, we present this simulated network to Statistical Network Assessment Process (SNAP), a specialized tool for network analysis. SNAP specializes on evaluating the performance of a network, specifically in terms of its capacity utilization efficiency. The evaluation of network efficiency and dependability is done thoroughly by using exact QoT measurements, such as GSNR.

The operational flowchart of SNAP is depicted in Fig. 4.1. This flowchart outlines the SNAP tool's methodology for conducting a statistical analysis of network performance, utilizing a Monte Carlo (MC) simulation approach.

The initial step involves specifying the input parameters necessary for the tool's operation, which include: a detailed description of the network's physical layer, a traffic model, and the RWA algorithm to be employed. The network's physical structure is delineated as a weighted graph characterized by N_{nodes} and N_{links} edges. Here, nodes symbolize ROADMs, while edges signify the optical links between these nodes. Each edge is assigned a weight $w_{i,j}$, which quantitatively encompasses both the ASE noise and the NLI, computed via GNPy's Quality of Transmission Estimator (QoT-E). The traffic model is articulated as a probability matrix of dimensions $N_{nodes} \times N_{nodes}$, where each element $p_{i,j}$ denotes the likelihood of a connection request arising between nodes i and j. This probabilistic framework allows SNAP to generate a series of connection requests in a stochastic manner, reflective of the matrix-defined probabilities. It's important to note that the probability of connection requests can vary across node pairs, and is designed to be independent of historical request patterns. SNAP's core simulation mechanism executes number of Monte Carlo (MC) (N_{MC}) iterations, starting each iteration with an unallocated network (i.e., no Light Paths (LPs) are initially established). Within each iteration, SNAP selects a connection request based on the traffic model, and attempts resource allocation following the designated RWA algorithm (e.g,; First-fit (FF), min GSNR, max GSNR etc.). Successful allocations result in the acceptance of the connection request, with network resources being earmarked for the corresponding LP for the duration of the network's operational lifespan. The capacity of the

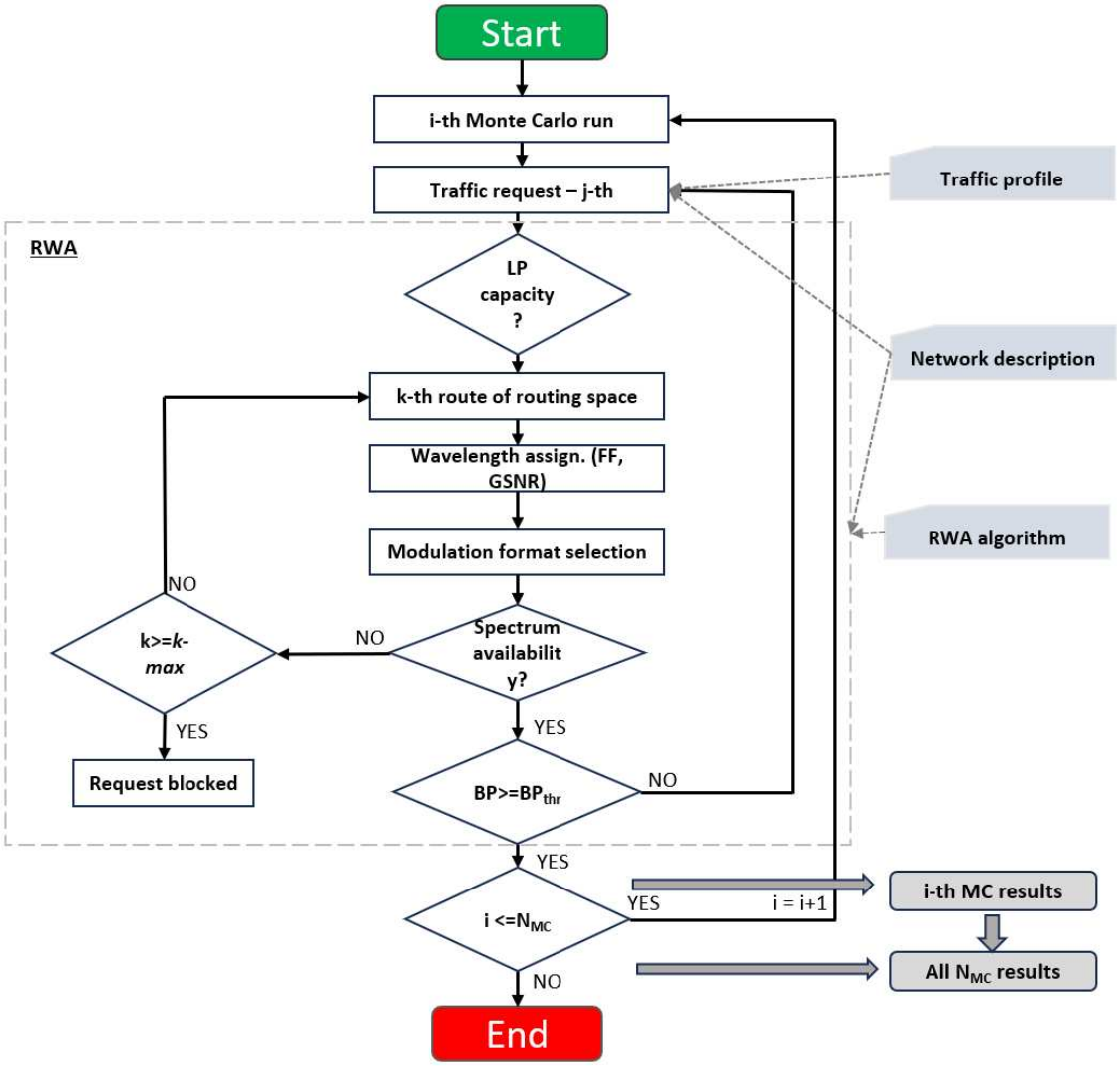

Figure 4.1: SNAP framework.

LP is then calculated based on its GSNR, with this and other relevant data being systematically recorded. Conversely, should the RWA algorithm determine the inability to fulfill a connection request, the request is declined, and the event is cataloged as a blockage. The process continues, generating and attempting to accommodate subsequent connection requests, until the network attains a saturation point—defined by specific thresholds for blocking probability and request quantity. This entire sequence is reiterated across N_{MC} MC iterations, with the outcomes of these iterations being averaged to produce a comprehensive set of performance metrics.

4.2.2 Network topologies

In the subsequent sections, we provide a comprehensive analysis of various network topologies. Specifically, we examine the network structures of Germany (Fig. 4.2a), Italy (Fig. 4.2b), Spain (Fig. 4.2c), the United States (Fig. 4.2d), and a randomly generated Data Center Interconnect (DCI) topology (Fig. 4.3). Detailed descriptions of these topologies are presented in the table.

Table 4.1: Summary of network topologies characteristics.

	German	**Italian**	**Spain-E**	**USA**	**DCI**
Number of nodes	17	21	30	24	20
Number of links	26	36	52	43	32
Average node degree	3.06	3.43	3.46	3.58	3.2
Average link length	207 km	209 km	60 km	660 km	64 km
Reference figure	Fig. 4.2a	Fig. 4.2b	Fig. 4.2c	Fig. 4.2d	Fig. 4.3

4.3 GSNR profile

This study employs a thorough span-by-span method to strategically optimize the input power for the C, L, and S optical bands. The utilization of the Local Optimization Global Optimization (LOGO) algorithm in this context aims to greatly improve the QoT throughout the network. We examine the Gain to Signal-to-Noise Ratio GSNR profiles for each band configuration across a conventional 75 km fiber stretch, analyzing them as functions of frequency. The profiles are assessed using a channel bandwidth of 100 GHz, as depicted in Fig. 4.4. The figure illustrates the GSNR across different channels and bands. The interaction between different bands is evident from the variations in GSNR profiles. This variation arises from the differential gain and noise characteristics of the amplifiers used in each band. An average GSNR of 30.85 dB is achieved when transmission is limited solely to the C-band. Upon activating the L-band alongside the C-band (C+L configuration), the average GSNR slightly decreases with the C-band at 30.43 dB and the L-band at 30.41 dB. Further expansion to include the S-band (C+L+S configuration) results in a small increase in GSNR for the C and L bands, recording values of 30.48 dB and 30.46 dB, respectively. However, the S-band underperforms in comparison, exhibiting a significantly lower average GSNR of 26.69 dB. Balancing the GSNR across bands involves a trade-off between the amplifier gain profiles and the optical power levels. Higher amplifier gain can improve GSNR but may also introduce more ASE noise, degrading overall signal quality.

Furthermore, our study includes detailed analysis of different loading scenarios

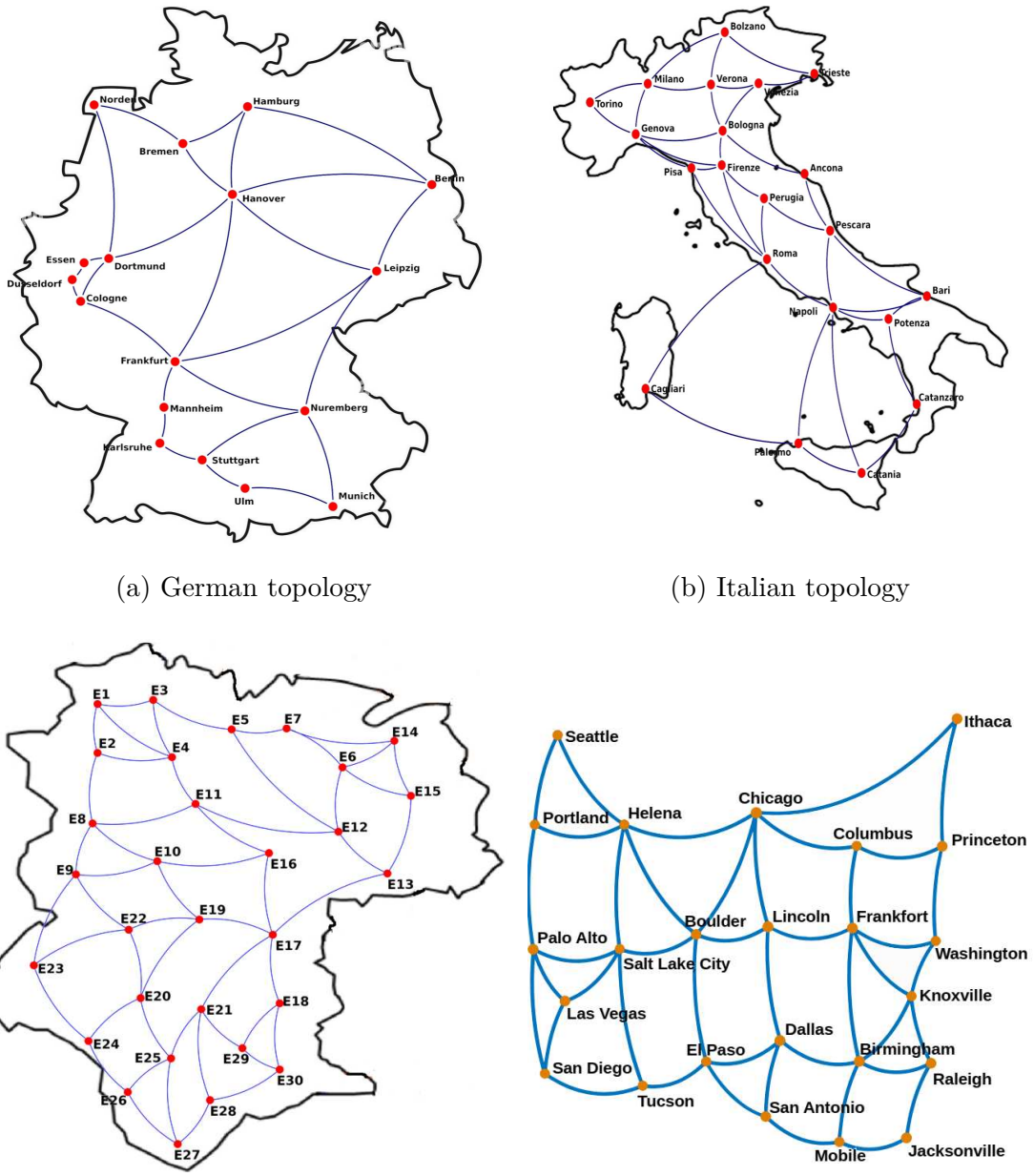

(a) German topology

(b) Italian topology

(c) Spain-E topology

(d) USA topology

Figure 4.2: Network topologies analyzed in the study (A-D)

within these bands at channel bandwidth of 150 GHz. Here, the network configuration comprises a total of 105 channels distributed as follows: 25 channels in the C band, contributing approximately 4 THz; 40 channels in the L band, contributing 6 THz; and 40 channels in the S band, also contributing 6 THz. The graphical representation for GSNR profile of these channel distributions is shown in Fig. 4.5.

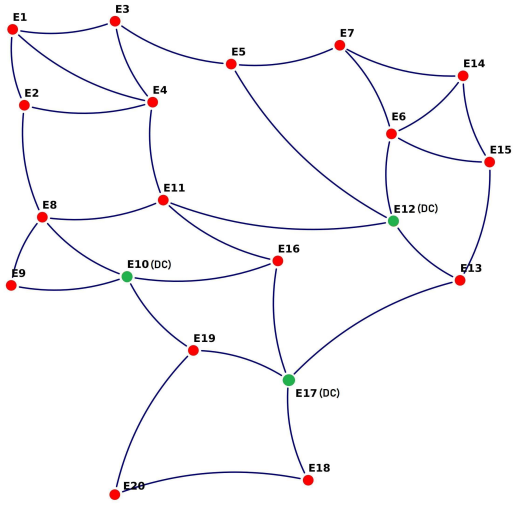

Figure 4.3: E - Random DCI topology (Green dots represent DCs)

Fig. 4.5 depicts the GSNR values across nearly the entire spectrum for the C- and L-bands and partially for the S-band, marked by dotted lines representing the averages. For the standalone C-band configuration, the average GSNR is 30.42 dB. When both C and L bands are activated, the GSNR for the C-band slightly reduces to 29.7 dB, while the L-band achieves an average of 30.3 dB. Engaging all three bands (S+C+L), the average GSNR decreases further for the C-band to 29.5 dB, with the L-band recording 30.15 dB, and the S-band dropping to 25 dB.

Additionally, we investigate the network behavior under a fully loaded C-band scenario (4 THz) while maintaining a consistent channel count across the other bands. In this scenario, each band—C, L, and S—is allocated 25 channels, corresponding to roughly 4 THz per band. This GSNR configuration is depicted in Fig. 4.6, which allows us to compare the impact of different loading strategies on the network's overall performance. In the C-band only scenario, the average GSNR remains steady at 30.4 dB. However, in the combined C+L scenario, the average GSNR for the C-band declines to 29.9 dB, while the L-band averages 30.45 dB. Activation of all three bands (S+C+L) results in a further decrease in the C-band's GSNR to 29.7 dB, whereas the L-band's GSNR is slightly lower at 30.2 dB, and the S-band's average drops to 26 dB.

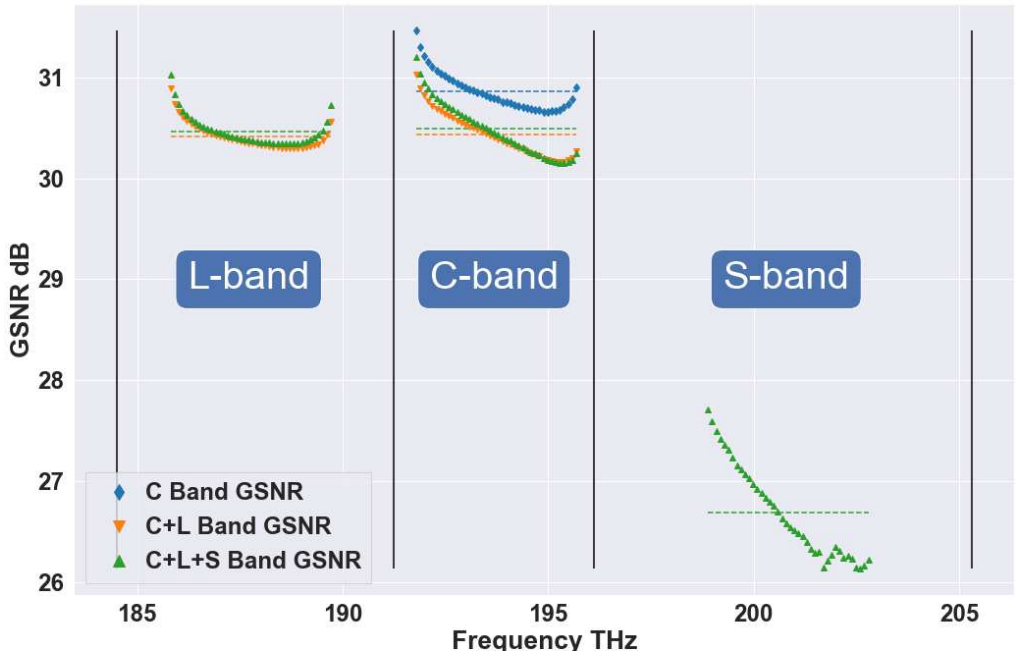

Figure 4.4: GSNR vs. frequency for all channels evaluated in each band for all scenarios (C-band only, C+L and C+L+S).

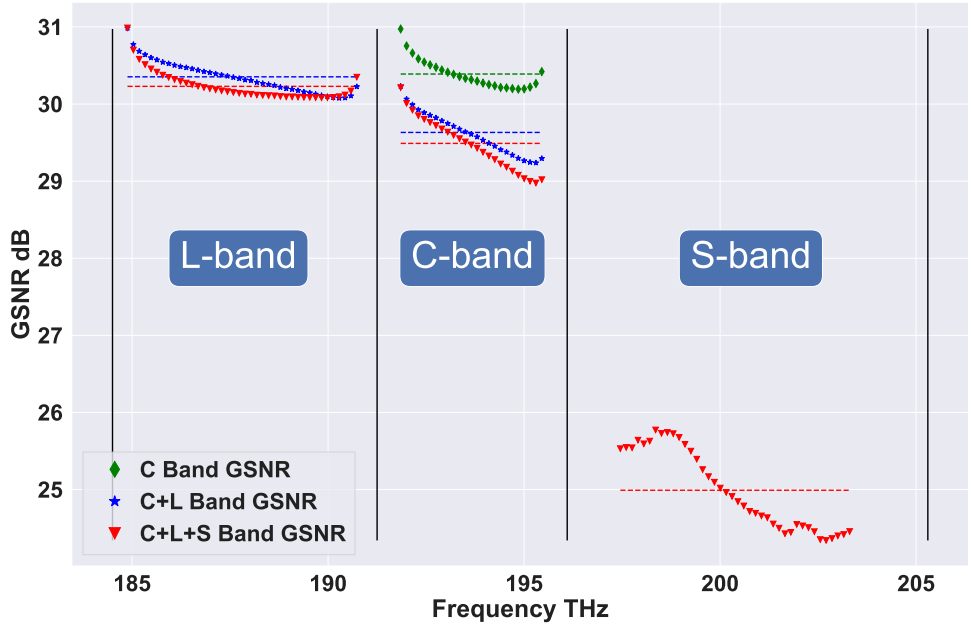

Figure 4.5: GSNR vs. frequency for 105 channels (C+L+S- 25+40+40 channels) for all scenarios (C-band only, C+L and C+L+S).

The observed reduction in GSNR for the C and L bands in the C+L and S+C+L scenarios, relative to the standalone C-band scenario, can be attributed primarily

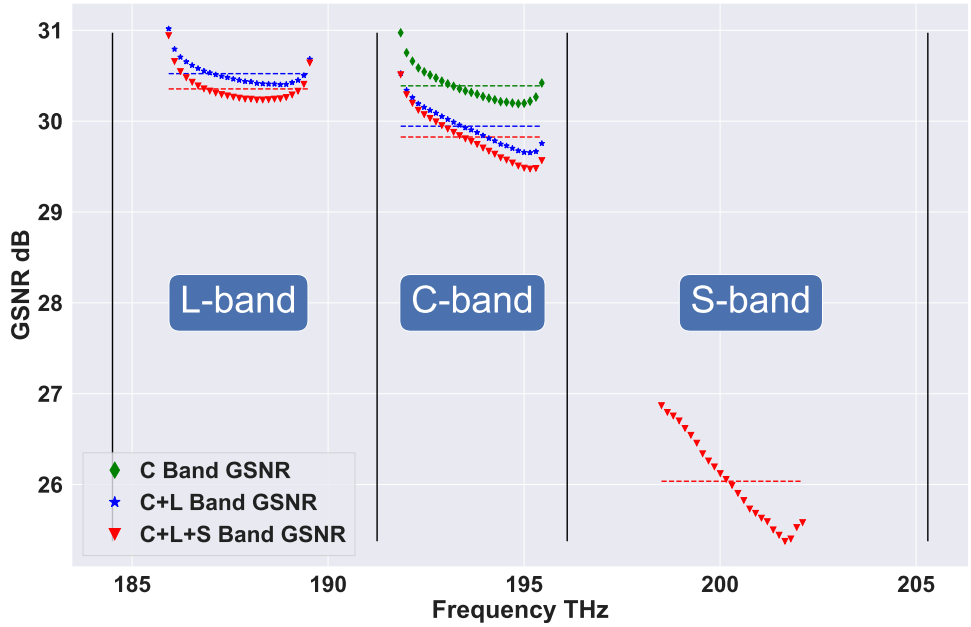

Figure 4.6: GSNR vs. frequency for 25 channels/band for all scenarios (C-band only, C+L and C+L+S).

to the cumulative impact of Stimulated Raman Scattering (SRS) and Non-Linear Interference (NLI), which increasingly affect signal integrity as more bands are engaged in the transmission process. Utilizing multiple bands (C+L+S) introduces more complexity in managing GSNR due to varying amplifier and fiber characteristics. Higher channel density, as shown in Fig. 4.5, leads to more significant variations in GSNR, indicating increased susceptibility to nonlinear impairments and noise. However, a uniform distribution of channels for 150GHz channel width across bands, as shown in Fig. 4.6, results in a more balanced GSNR profile. This approach can reduce nonlinear effects and improve overall network performance. These insights underscore the importance of strategic channel distribution and amplifier optimization to maintain a stable and efficient multi-band optical transmission system.

4.4 Network performance analysis

To assess the impact of the newly deployed WSS architecture on diverse optical transport networks, the Statistical Network Assessment Process (SNAP) is employed, focusing on the physical layer interactions. SNAP evaluates the degradation of the QoT by quantifying the influence of each network component on signal integrity. The methodology adopts a disaggregated approach to the physical layer, simulating each component's influence on the network through specific gains,

losses, and Gaussian noise contributions. This includes quantifying the effects of ASE generated by optical amplifiers and NLI resulting from the Kerr effect in fiber propagation.

The analysis is tailored to a multi-band optical system, considering distinct amplification strategies for different wavelength bands. Specifically, the C-band and L-band utilize EDFAs, each calibrated to optimize performance within their respective spectral regions. Meanwhile, the S-band channels are amplified using a TDFA, which is specially tuned for the lower wavelength range. The amplifiers details are described in Tab. 4.2.

Band	Amplifier Type	Gain (dB)	Noise Figure (dB)	Bandwidth (THz)
C	EDFA [126, 127]	20-25	4.5	4.8
L	EDFA [128]	20-25	5.0	6.0
S	TDFA [129]	20-25	6.0	6.0

Table 4.2: Characteristics of fiber amplifiers

The transmission path consists of 75 km segments of single-mode fiber that meet the ITU-T G.652D standard, which specifies the fiber's attenuation and chromatic dispersion properties, critical for maintaining signal quality over long distances. Each segment's performance is analyzed under these conditions to determine the cumulative impact on the network's overall QoT, ensuring the assessment reflects realistic operational environments. In our comprehensive analysis, alongwith the WSS device, we have evaluated a range of transceivers, including ZR++, 800G, and 1200G models for range of transceiver characteristics, described in Tab. 4.4 and network parameters described in Tab. 4.3.

4.4.1 Optical capacity analysis

SDM and BDM, are crucial technologies that contribute significantly to the progress of optical fiber communications. SDM improves network capacity by using many spatial pathways inside a single fiber, such as MCF and Few-Mode Fibers (FMF), hence increasing the number of transmission channels. However, BDM, specifically using Dense Wavelength Division Multiplexing (DWDM) and Coarse Wavelength Division Multiplexing (CWDM), enhances bandwidth by assigning distinct data streams to various wavelength ranges inside a single fiber. These technologies play a fundamental role in optimizing the efficiency and capacity of optical networks, addressing the increasing need for faster data rates and

Parameter	Value	Description
Channel Spacing	100 GHz, 150 GHz	Depending on the scenario, different spacings were evaluated
Number of Channels	40/40/40 (C/L/S -bands), 25 (C-band) - 40 (L-band) - 40 (S-band), 25/25/25 (C/L/S -bands)	Total number of channels evaluated in multi-band scenarios
Fiber Type	Standard Single-Mode Fiber (SSMF)	Used for all simulations to ensure consistency
Network topology	Italian, German, US, Spain-E, DCI (random)	Real and random topologies are used
Traffic profile	Uniform, Population based	Traffic profiles are considered for different scenarios

Table 4.3: Simulation parameters and their descriptions

wider bandwidth in global communications.

4.4.1.1 SDM vs BDM analysis

To ensure an equitable evaluation of multi-band performance while implementing the ROADM architecture with the proposed WSS structure, we conducted a comparative analysis of BDM versus Space Division Multiplexing SDM in network efficiency. In this comparison, SDM is configured to utilize multiple fibers within the C-band, utilizing the same total available optical spectrum as BDM. For SDM, a core continuity constraint (CCC) is applied, ensuring that each LP maintains the same fiber route from the source to the destination. This constraint aligns with the specific switching technology employed in SDM. This configuration is advantageous as it increases the number of fiber pairs by two to three times relative to the BDM strategy employing S+C+L bands, thereby potentially offering enhanced network robustness and capacity under the SDM framework. In our comparative analysis, we use the single-fiber C-band configuration as a baseline reference to evaluate the performance of different transmission strategies: (i) SDM with dual fibers in the C-band versus BDM with a single fiber in the C+L configuration, and (ii) SDM with triple fibers in the C-band against BDM with a single fiber in the C+L+S configuration. Performance metrics are derived from statistical averages calculated over multiple Monte Carlo simulations, focusing on the BP in relation to the total traffic progressively assigned to each scenario.

Specification	**400G**[130]	**800G**[131]	**1200G**[132]	**Ideal trx.**
Bitrate (Gbps)	400	800	1200	-
Baud Rate (GBd)	60-90	90-120	120-150	60-150
Modulation Formats	QPSK, 16QAM, 64QAM	16QAM, 64QAM	64QAM	-
SNR (dB)				
- QPSK	> 20	N/A	N/A	> 30
- 16QAM	> 18	> 18	N/A	> 28
- 64QAM	> 16	> 16	> 16	> 25
Noise Figure (dB)	5-7	6-8	7-9	3-5
Power Consumption (W)	10-15	15-22	22-30	10-20
Optical SNR (OSNR, dB)	> 24	> 22	> 20	> 30
Receiver GSNR (dB)	> 22	> 20	> 18	> 25
Spectral eff. (bits/s/Hz)	4-6	5-7	6-8	7-10

Table 4.4: Transceiver Specifications

400G transceiver

Traffic allocation

Fig. 4.7 shows the total allocated traffic vs the blocking probability chart for the German network, considering the channel bandwidth = 100 GHz. Uniform traffic profile of 100 Gbps is considered. For our analysis, we set a BP of 10^{-2} as a threshold to assess the traffic handling capacity for each configuration. In this analysis, a single C-band fiber demonstrates a delivery capacity of about 23 Tbps. When exploring scenarios with dual fibers in the C-band and a single fiber in the multi-band C+L configuration, both arrangements exhibit similar performances, capable of handling approximately 45 Tbps of traffic. Further extending the comparison, the use of triple fibers in the C-band significantly enhances capacity, allowing for the allocation of around 73 Tbps. Conversely, employing a single fiber in the multi-band C+L+S configuration results in a slightly lower capacity of approximately 68 Tbps. BDM leverages the broader spectral range by utilizing additional bands. Each band can carry its own set of channels, effectively increasing the network's bandwidth without needing more physical fibers. However, the efficiency of additional bands are not linear due to factors like the inherent limitations of amplification technologies across different bands, and increased complexity in managing cross-band nonlinearities and channel interference. The analysis reveals that BDM configurations perform closely to their corresponding SDM setups, demonstrating the efficacy of BDM in achieving comparable transmission capabilities with fewer

fibers.

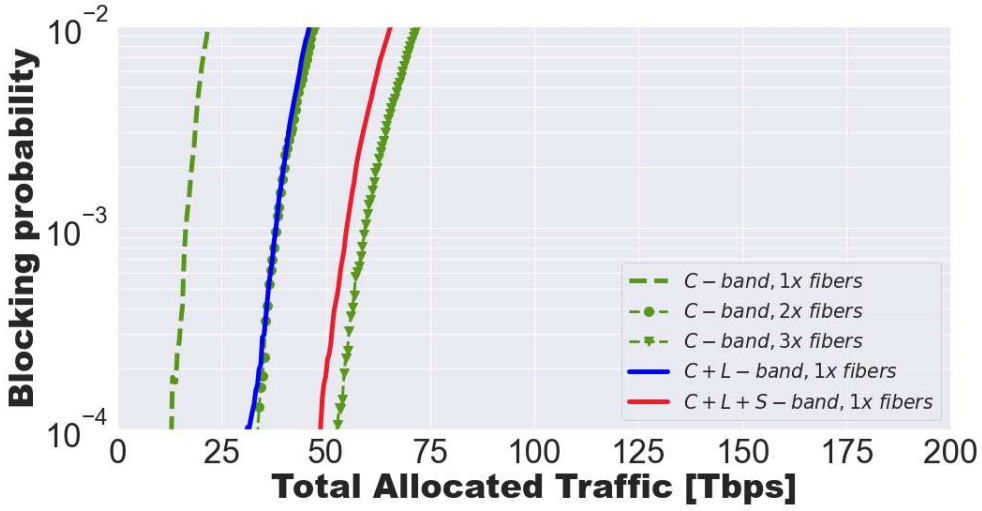

Figure 4.7: Blocking probability evaluated over the German network (≈ 4 THz/band) considering 400G transceivers.

Fig. 4.8 presents the link allocation by traffic volume in the SDM scenario, comparing the outcomes for both uniform and population-based traffic profiles (where the latter aligns with the population sizes of node-cities). In the population-based profile, congestion exceeding 60% is observed in 9 links, whereas in the uniform traffic profile, a lesser number of connections, only 5, exhibit congestion above the 60% threshold. Addressing this disparity in traffic allocation, the implementation of BDM could significantly enhance capacity utilization either on selected high-traffic links or across the entire network. Subsequently, Fig. 4.9 and Fig. 4.10 provide a comparative analysis of SDM and BDM under both traffic scenarios. The results demonstrate close performance metrics between the two multiplexing strategies, with SDM marginally surpassing BDM in terms of efficacy.

By analyzing the Spain-E topology at a BP threshold of 10^{-2}, we determine the amount of traffic that may be allocated as a comparison measure for different transmission systems. In Fig 4.11, two different transceiver cases are used to demarcate the traffic distribution in the figure: the ideal transceiver configuration is represented by the dotted line, and the ZR+ transceiver scenario is represented by the plain lines. After conducting a thorough comparison of BDM and SDM solutions, using both idealized and more practical ZR+ transceiver settings, we have seen a significant similarity: BDM solutions closely resemble their respective SDM benchmarks.

More precisely, a single C-band fiber has the capability to transmit around 31 Tbps when using ZR+ transceivers. The traffic allocation increases significantly to 87 Tbps when ideal transceivers are used, representing a difference of about 180%. When assessing the SDM setup using C-band at double (2x) the fiber count, the

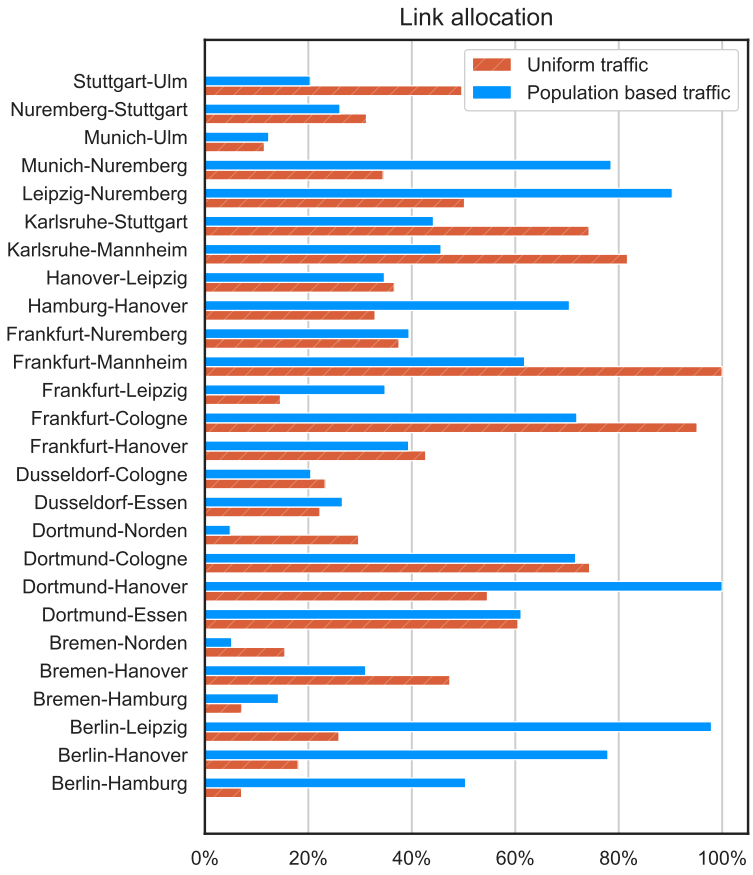

Figure 4.8: SDM (C-band 1x fiber)

ZR+ transceivers enable a traffic allocation of 74 Tbps (≈ 2x of SDM, 1x), which significantly rises to 195 Tbps under ideal transceiver conditions. Simultaneously, the BDM system employs C+L bands and a single fiber to achieve a capacity of 72 Tbps with ZR+ transceivers (≈ same as of SDM, 2x case and 2x of the SDM, 1x case). Under ideal trannsceiver case, this capacity extends to 187 Tbps. Additionally, under the C-band, the SDM technique with a 3x in fiber count distributes traffic at 140 Tbps (≈ 3x of the SDM, 1x case) with ZR+ transceivers, up to 330 Tbps for ideal transceivers. In contrast, the BDM architecture that combines the C+L+S bands on a single fiber allows for a traffic allocation of 105 Tbps slightly less than SDM, 3x case) while using ZR+ transceivers. This capacity is increased to 289 Tbps in the optimal transceiver situation. SDM relies on increasing the number of physical channels (fibers) to scale up capacity. This method is straightforward and effective but involves higher costs associated with fiber deployment. Whereas, BDM increases the spectral efficiency by utilizing additional frequency

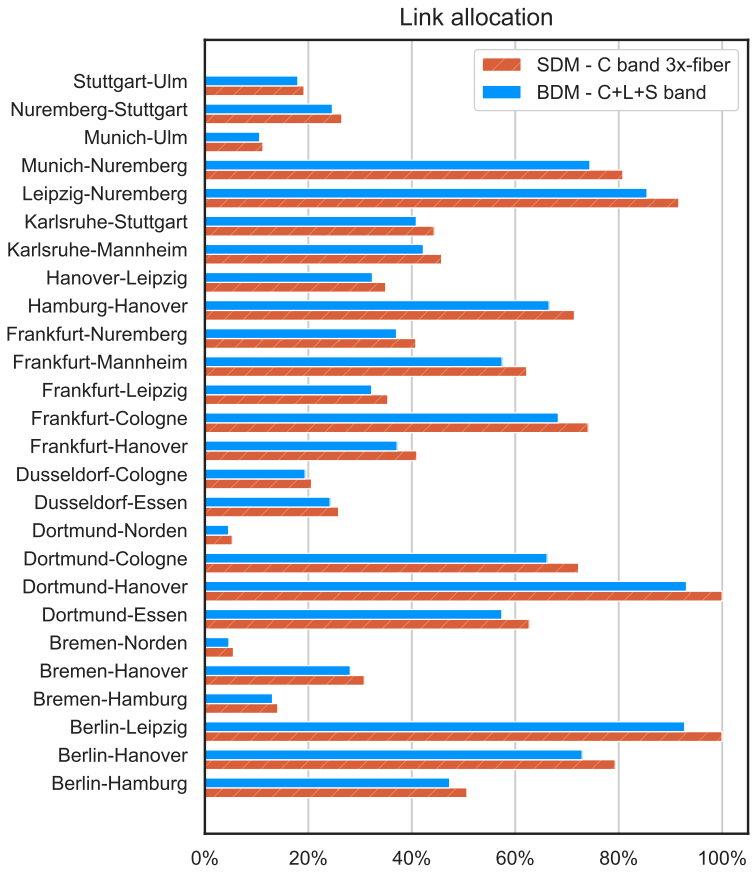

Figure 4.9: Population based traffic (SDM-C-band 3x-fiber vs BDM-C+L+S band 1x-fiber)

bands within the same fiber. While technically complex, BDM can achieve comparable capacities to SDM but with less deployment cost (fibers). BDM with 3 bands perform slightly less than the SDM, 3x fibers case due to the crosstalk and non-linear effects induced across multiple bands. Both SDM and BDM show a capability to scale traffic capacity significantly. The choice between them may depend on specific network requirements, cost considerations, and technological availability. BDM's ability to closely match or approximate the performance of SDM configurations even under practical transceiver conditions (ZR+) highlights its potential for high-capacity networks where physical expansion is limited.

Fig. 4.12 (a) and (b) depicts a comparative analysis of traffic deployment in SDM and BDM setups for Spain-E topology. The graphic displays a side-by-side comparison of SDM using a C-band with double fiber and BDM using a single fiber in the C+L band. Fig. 4.12 (c) and (d) further expand this comparison to compare BDM using a single fiber in the wider C+L+S band with SDM using a 3x fiber

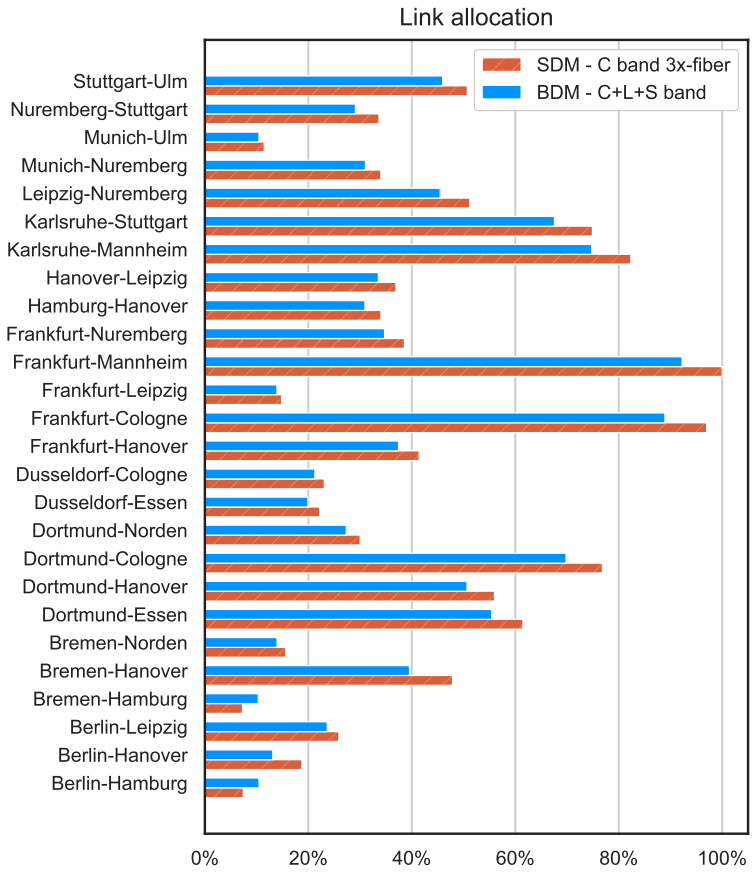

Figure 4.10: Uniform based traffic (SDM-C-band 3x-fiber vs BDM-C+L+S band 1x-fiber)

in the C-band. Figure 4.12 depicts a comparative analysis of traffic deployment in SDM and BDM setups. The graphic displays a side-by-side comparison of SDM using a C-band with double fiber and BDM using a single fiber in the C+L band. Fig. 4.12 (c) and (d) further expand this comparison to compare BDM using a single fiber in the wider C+L+S band with SDM using a 3x fiber in the C-band. The level of deployment is graphically represented using a gradient heat map, with deeper shades of orange indicating higher traffic allocaiton and cooler shades of blue indicating lower traffic allocation. Using this color measure, the graphical analysis shows that the amount of traffic sent per link for BDM, while using fewer fibers, is somewhat lower than that of the SDM setups, which need two to three times more fiber deployment. In particular, in Fig. 4.12(a), the SDM scenario exhibits a 3.3% greater traffic deployment compared to its BDM counterpart, as seen in Fig. 4.12(b). The difference in traffic distribution increases in the shown scenarios of Fig. 4.12(c) and Fig. 4.12(d), with a traffic discrepancy

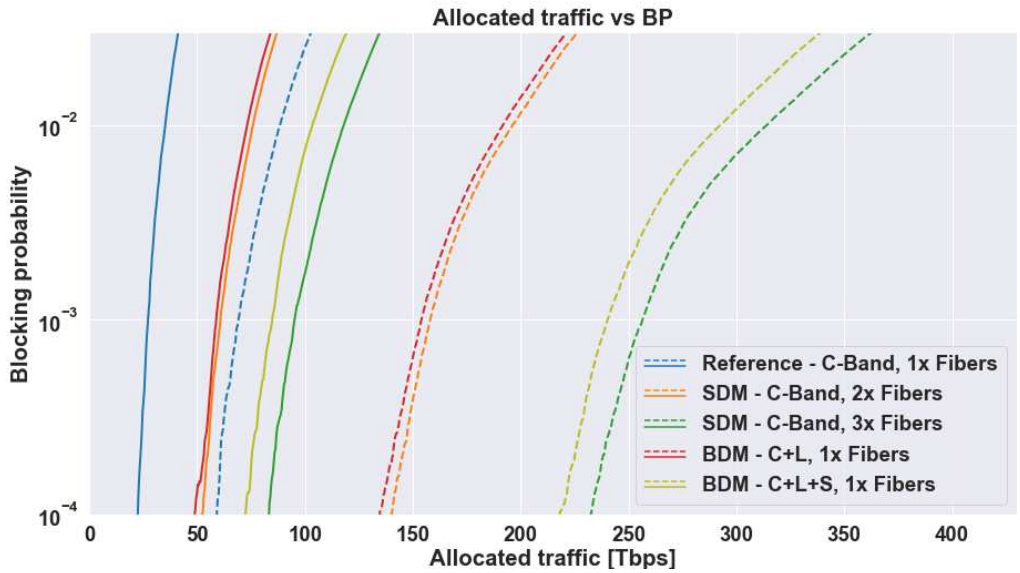

Figure 4.11: Blocking probability evaluated over the Spain-E network considering ideal(....) and ZR+(—) transceivers case.

of around 11.8% between SDM and BDM. The greater difference is due to the non-linear propagation penalties that occur when transmitting over three bands (C+L+S) using a single fiber. This comparative analysis of the two multiplexing systems highlights the inherent efficiency trade-offs involved in selecting between fiber upgrading and bandwidth growth. Having a detailed knowledge of these trade-offs is crucial when considering network design, especially in situations where there are limitations on fiber rollout or when bandwidth is scarce.

Channels allocation

In the previous section, we analyzed the networking performance by examining the traffic allocation of the WSS device equipped with 400G transceivers. In this section, we explore the networking performance further by assessing channel allocation across various network topologies (USA and Spain-E) and characteristics.

The analysis evaluates channel allocation, set at 40 channels per band for the USA topology, in both SDM with multiple fibers and BDM configurations. Fig. 4.13 (a) and (b) compare the SDM setup utilizing two fibers to the BDM setup employing one fiber in the C+L band with 80 channels per fiber. Fig. 4.13 (c) and (d) in the same figure examine the SDM configuration with three fibers against the BDM setup using one fiber in the C+L+S bands, which supports 120 channels per fiber. Channel allocations for each fiber link are depicted through a heatmap, ranging from 0% (blue) to 100% (orange) to represent utilization percentages. In Fig. 4.13 (a), the channel utilization for the SDM scenario (two fibers, C-band only, 40 channels per fiber) is reported at 55.65%, whereas Fig. 4.13 (b) records a

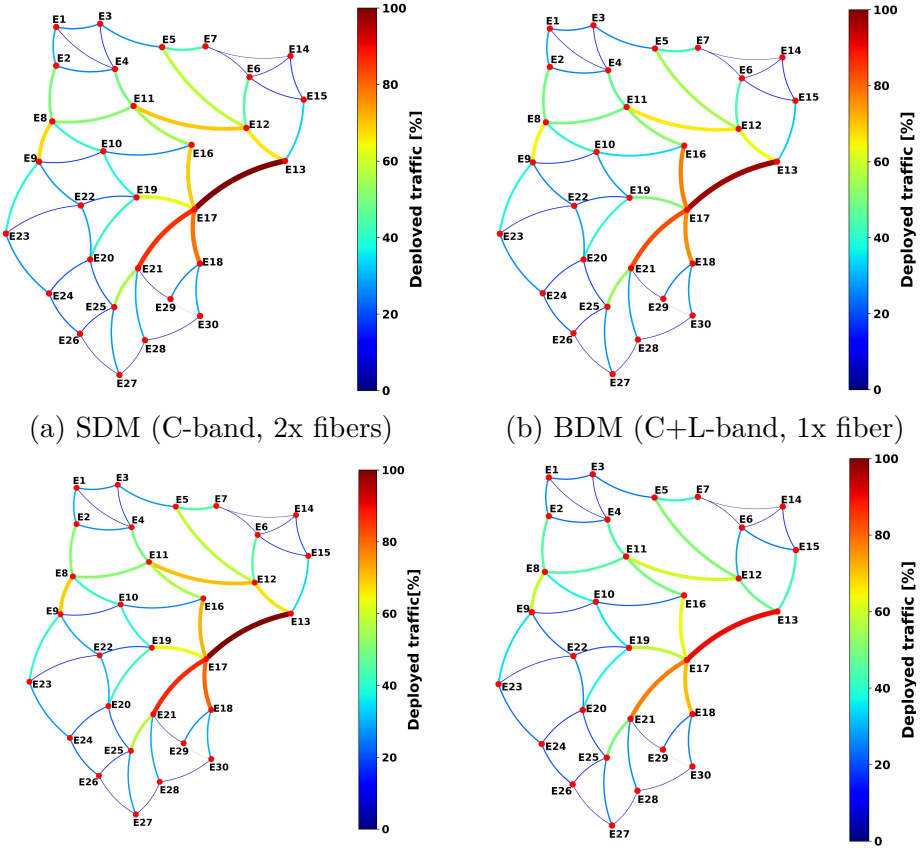

(a) SDM (C-band, 2x fibers)

(b) BDM (C+L-band, 1x fiber)

(c) SDM (C-band, 3x fibers)

(d) BDM (C+L+S-band, 1x fibers)

Figure 4.12: Deployed traffic comparison - ZR+ transceiver.

utilization of 55.46% for the BDM scenario (one fiber, C+L band, 80 channels per link). Fig. 4.13 (c) shows a channel utilization of 56.72% for the SDM setup (three fibers, C-band only, 40 channels per fiber). In contrast, Figure 4.13(d) documents a channel utilization of 54.25% for the BDM configuration (one fiber, C+L+S bands, 120 channels per fiber) across the overall network. The same analysis is shown for the Spain-E topology in Fig. 4.14. In Fig. 4.14 (a), the SDM scenario employing two fibers within the C-band, configured with 40 channels per fiber, exhibits a channel utilization of 41.83%. Conversely, the BDM case using a single fiber in the C+L band with 80 channels per link, as shown in Fig. 4.14 (b), demonstrates a slightly lower channel utilization of 41.67%.

Further analysis in Fig. 4.14 (c) reveals that the SDM setup with three fibers, exclusively in the C-band and maintaining 40 channels per fiber, achieves a channel utilization of 43.59%. Fig. 4.14 (d) illustrates the BDM arrangement, which utilizes a single fiber spanning the S, C, and L bands and can accommodate 120 channels

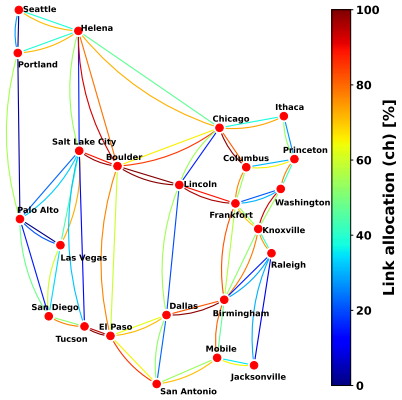

(a) SDM (C-band, 2x fibers, 40 ch/fiber)

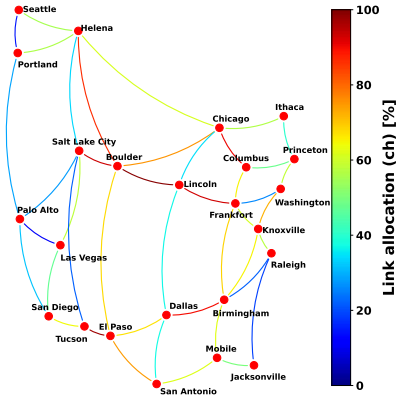

(b) BDM (C+L-band, 1x fiber, 80 ch/fiber)

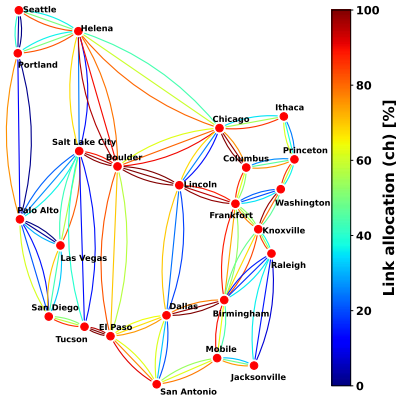

(c) SDM (C-band, 3x fibers, 40 ch/fiber)

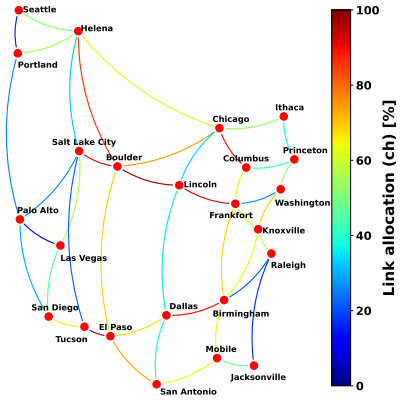

(d) BDM (C+L+S-band, 1x fibers, 120 ch/fiber)

Figure 4.13: Channel allocation comparison - ZR+ transceiver.

per fiber. The network's channel utilization is 42.7%, which demonstrates the interplay between fiber topology, band usage, and channel allocation efficiency in these multiplexing settings. SUmmary of channel allocation is given in Table. 4.5

Configuration	**Fiber Count**	**Bands (GHz)**	**Channel Utilization (%)**- USA	**Channel Utilization (%)**- Spain-E
SDM (C-band)	2x	4×2 THz	55.65%	41.83%
BDM (C+L-band)	1x	$4 + 6$ THz	55.46%	41.67%
SDM (C-band)	3x	4×3 THz	56.72%	43.59%
BDM (C+L+S-band)	1x	$4 + 6 + 6$ THz	54.25%	42.70%

Table 4.5: Channel utilization for different configurations

This analysis underscores the superiority of BDM over SDM, particularly in high-demand scenarios where maximizing data throughput and minimizing loss and

delays are critical. By leveraging multiple spectral bands, BDM not only enhances the total capacity but also efficiently distributes network load, thus reducing the chances of traffic bottlenecks. This strategic use of expanded bandwidth is essential for future-proofing network infrastructures against escalating data demands and for enhancing overall network resilience and performance.

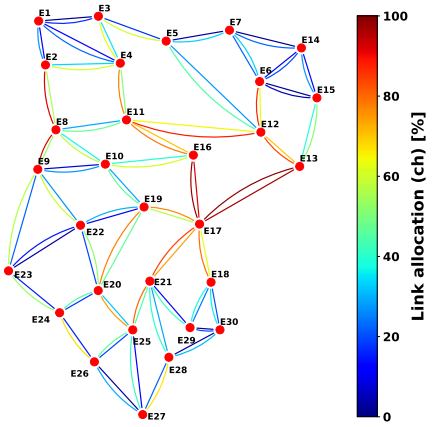

(a) SDM (C-band, 2x fibers, 40 ch/fiber)

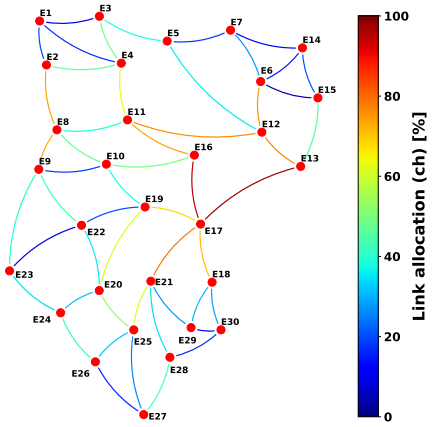

(b) BDM (C+L-band, 1x fiber, 80 ch/fiber)

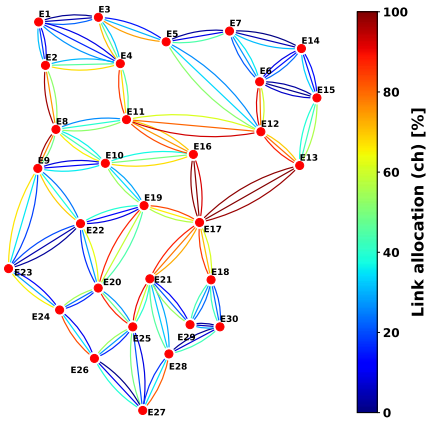

(c) SDM (C-band, 3x fibers, 40 ch/fiber)

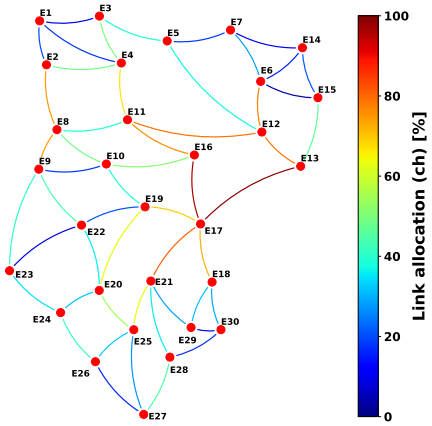

(d) BDM (C+L+S-band, 1x fibers, 120 ch/fiber)

Figure 4.14: Channel allocation comparison - ZR+ transceiver.

800G transceiver

Traffic allocation

For the 800G transceiver shown in Fig. 4.15, starting from the C-band, C+L bands and C+L+S bands, we analyse the total traffic allocation for the USA network topology. In Fig. 4.15, with a blocking probability of 10^{-1}, the C-band only managed to allocate approximately 80 Tbps of traffic. In contrast, the combined C+L-band setup supported a total traffic allocation of around 280 Tbps. When all three bands (C+L+S) were utilized, the traffic allocation for the 800G transceiver case surpassed 500 Tbps.

Figure 4.15: Total traffic allocation vs blocking probability for 800G transceivers

In evaluating the performance of the 800G transceiver for the German network topology, two bandwidth scenarios are considered: one with approximately 4 THz per band across all bands, and the other with extended bandwidth, approximately 6 THz for S and L bands and 4 THz for the C band. The traffic allocation versus blocking probability is illustrated in Fig. 4.16 for the first scenario. For the C-band 1x fiber, the delivery capacity is around 27 Tbps. Introducing C-band 2x fibers and multi-band C+L 1x fiber yields similar performance, capable of allocating approximately 60 Tbps of traffic. Utilizing C-band 3x fiber increases this capacity to around 92 Tbps, while multi-band C+L+S 1x fiber can allocate about 87 Tbps. Notably, in scenarios where both the 400G (Fig. 4.7) and 800G transceivers have similar bandwidth, the traffic allocation slightly favors the 3x fiber over the multi-band scenario.

In the extended bandwidth scenario shown in Fig. 4.17, the C-band 1x fiber has a delivery capacity of approximately 28 Tbps. Traffic allocation for C-band 2x fiber is close to 55 Tbps, while for multi-band C+L 1x fiber, it exceeds 100 Tbps. This substantial difference in allocation is primarily due to the greater spectrum

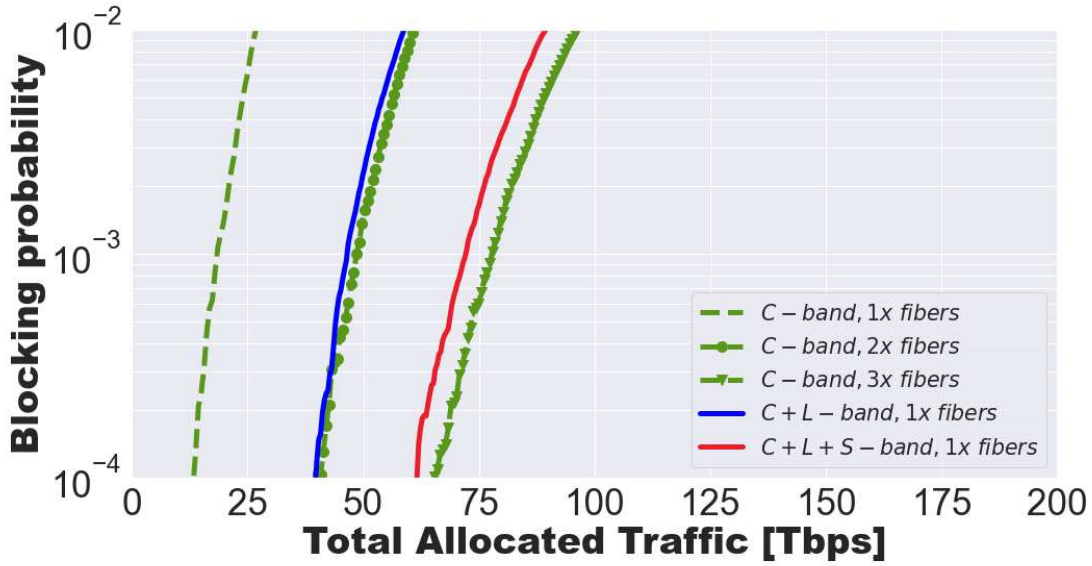

Figure 4.16: Blocking probability evaluated over the German network (≈ 4 THz/band) considering 800G transceivers.

usage in the C+L bands, with nearly 10 THz compared to 7.5 THz in the C-band 2x fiber. With C-band 3x fiber, the allocation reaches around 94 Tbps, whereas with multi-band C+L+S 1x fiber, it climbs to approximately 148 Tbps, largely attributed to the higher spectrum usage in the latter case, approximately 15 THz. It's noteworthy that the C+L+S-band capacity for the 400G transceiver (Fig. 4.7 is 5.67 b/Hz, while for the 800G transceiver, it rises to 14.6 b/Hz. Overall, the 800G transceiver demonstrates superior traffic allocation compared to the 400G transceiver, particularly evident in the multi-band C+L+S scenario due to the increased spectrum usage.

Channels allocation

To ensure a fair comparison, we conducted a comprehensive evaluation of multi-band results utilizing the proposed WSS structure integrated into the ROADM architecture.While the BDM method used multi-bands (C+L and C+L+S), our study used the SNAP network performance analysis, presuming SDM with numerous fibers in the C-band on the same total spectrum. We accounted for different fiber configurations (2x and 3x) for SDM and maintained the channel limit for L- and S-bands at 25, utilizing nearly 4 THz of spectrum per band to ensure an effective comparison of link capabilities.

The evaluation encompassed two network topologies (Italy and Germany), considering the allocation of channels (25 channels per band) in both scenarios of SDM with multiple fibers and BDM for the 800G transceiver. The comparisons between

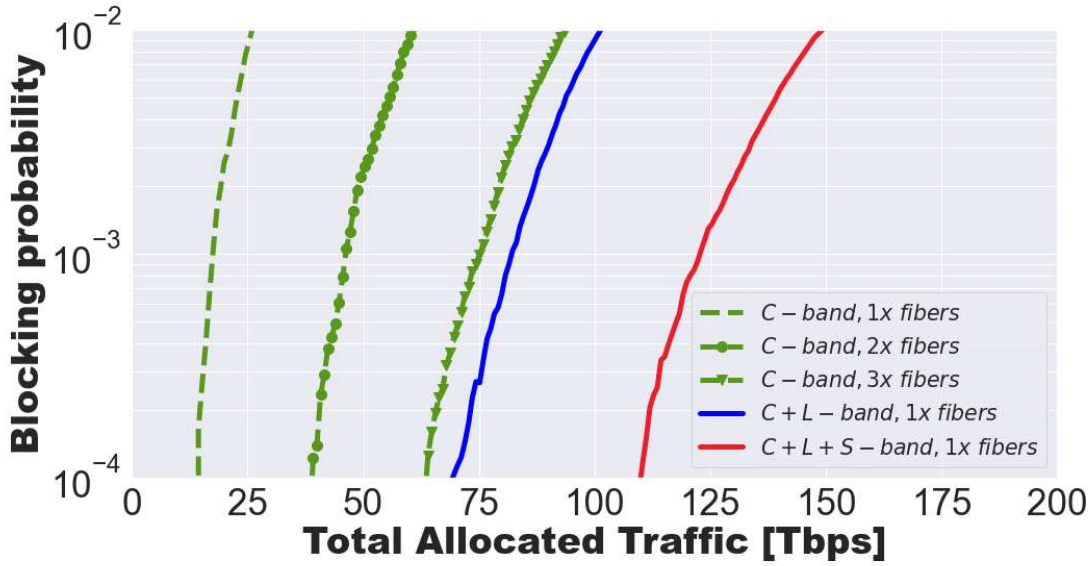

Figure 4.17: Blocking probability evaluated over the German network (C/L/S-band ≈ 4 THz/6 THz/6 THz) considering 800G transceivers.

SDM (2x fibers, 50 channels) and BDM (C+L, 50 channels per fiber) are depicted in Fig. 4.18(a) and (b), while Fig. 4.18(c) and (d) illustrate the comparisons between SDM (3x fibers, 75 channels) and BDM (C+L+S, 75 channels per fiber) for the German topology. Similarly, the comparisons for the Italian topology are presented in the Fig. 4.19. The allocation of links based on channel utilization is visually represented as a heat map, where darker shades of orange indicate a higher percentage of channel allocation, while blue represents a lower percentage of channel allocation.

The link allocation in terms of channels for the SDM and BDM scenarios for both network topologies is summarized in Table 4.6. The multi-band BDM scenario exhibits slightly lower channel allocation in both network scenarios compared to the single-band SDM scenario. However, the difference between SDM and BDM increases marginally in the case of SDM with three fibers and multi-band BDM (C+L+S bands) due to nonlinear propagation resulting from transmitting all three bands on a single fiber.

Transparent vs Translucent network

In the context of a transparent network, our approach involves establishing a new LP that spans end-to-end, utilizing the highest achievable modulation format without intermediate regeneration and adhering to the wavelength continuity

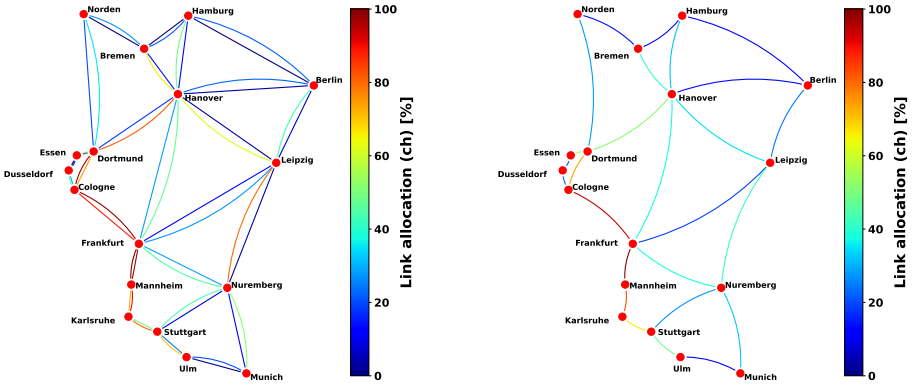

(a) SDM (C-band - 50 channels, 2x fibers)

(b) BDM (C+L-band - 50 channels, 1x fiber)

(c) SDM (C-band - 75 channels, 3x fibers)

(d) BDM (C+L+S-band - 75 channels, 1x fibers)

Figure 4.18: German topology channel allocation comparison - 800G transceiver.

Network Topology	Configuration	Fiber Count	Channels per Fiber	Bands
German	SDM	2x	50	C-band
	BDM	1x	50	C+L-band
	SDM	3x	75	C-band
	BDM	1x	75	C+L+S-band
Italian	SDM	2x	50	C-band
	BDM	1x	50	C+L-band
	SDM	3x	75	C-band
	BDM	1x	75	C+L+S-band

Table 4.6: Channel utilization for different network topologies and configurations

constraint across all links in the path. However, in translucent scenarios, this constraint is eliminated at nodes where regeneration occurs, which involves using a pair

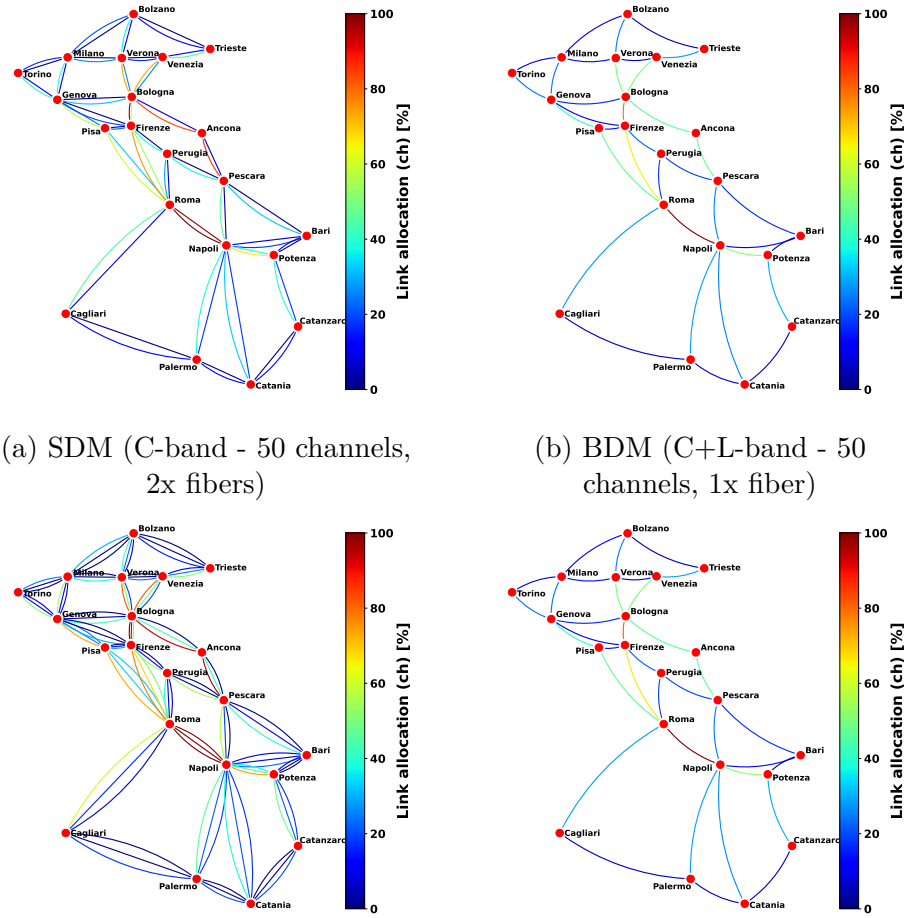

(a) SDM (C-band - 50 channels, 2x fibers)

(b) BDM (C+L-band - 50 channels, 1x fiber)

(c) SDM (C-band - 75 channels, 3x fibers)

(d) BDM (C+L+S-band - 75 channels, 1x fibers)

Figure 4.19: Italian topology channel allocation comparison - 800G transceiver.

of back-to-back transceivers. To ensure that the maximum bit rate of 800 Gbps (16QAM) is maintained for the LP, our controller activates an additional pair of transceivers at intermediate nodes when necessary. We conducted performance evaluations in a multi-band scenario, specifically using the C+L and C+L+S-bands, across network topologies of Italy and Germany, shown in Fig. 4.20 and 4.21. The Italian network, characterized by slightly longer link lengths compared to the German network, demonstrated significant differences in traffic allocation between transparent and translucent scenarios. In the transparent setup, the C+L band supported a total traffic load of 65 Tbps, which increased substantially to 220 Tbps under the translucent setup. For the C+L+S- band, traffic allocation rose from 100 Tbps in the transparent mode to around 350 Tbps in the translucent mode. Similarly, in the German network, the C+L band's traffic allocation

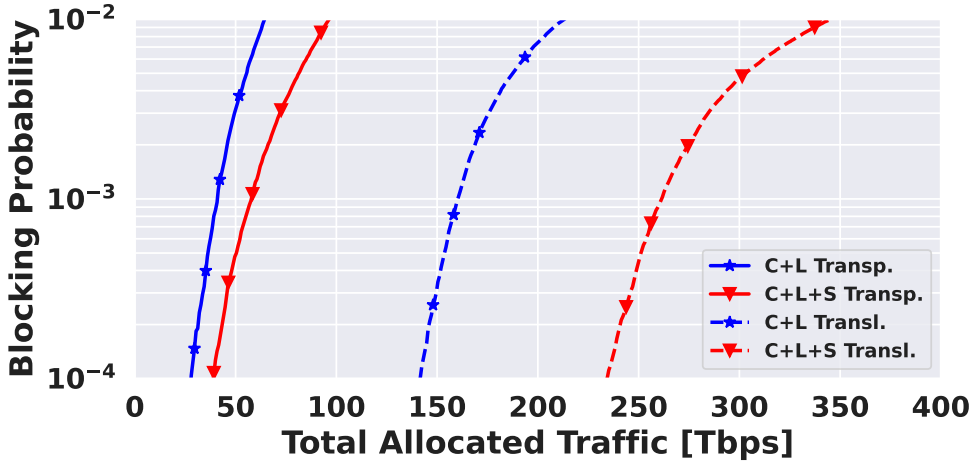

Figure 4.20: Network capacity for transparent and translucent network design for the C-, C+L-, and C+L+S-band with 800 Gb/s traffic request size in the Italian network topology.

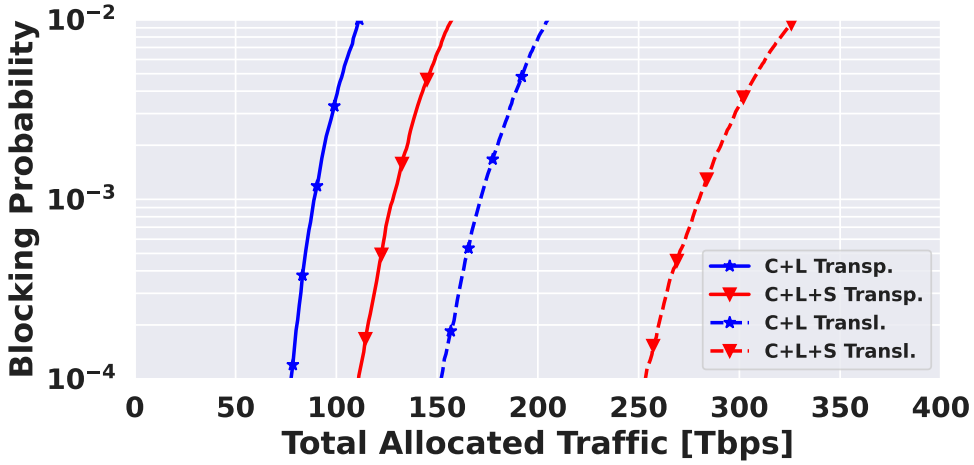

Figure 4.21: Network capacity for transparent and translucent network design for the C-, C+L-, and C+L+S-band with 800 Gb/s traffic request size in the German network topology.

escalated from 120 Tbps in the transparent scenario to 210 Tbps in the translucent configuration. The C+L+S- band exhibited a growth in traffic from 155 Tbps to approximately 330 Tbps when transitioning from transparent to translucent modes.

This marked increase in traffic allocation in translucent scenarios as opposed to transparent ones is primarily attributed to the relaxation of the wavelength continuity constraint at nodes where regeneration is deployed. This adjustment

facilitates greater flexibility in traffic routing and enables the utilization of additional wavelengths, thereby enhancing the overall traffic handling capacity of the network. Furthermore, the activation of supplementary transceiver pairs at critical nodes to sustain the LP's maximum bit rate of 800 Gbps also plays a crucial role in achieving higher traffic capacities in translucent network setups.

1.2T transceiver

Traffic allocation

The network performance evaluation was conducted on a randomly structured DCI network (Fig. 4.3) using two categories of transceivers, specifically the 800 Gbps and 1200 Gbps models. The analysis focused on assessing the relationship between traffic allocation and BP, with a particular emphasis on different transceiver capacities. The results, illustrated in Fig. 4.22, show that at a BP of 10^{-2}, the total traffic allocated using the 800 Gbps transceiver in the C-band was approximately 49 Tbps. Conversely, the 1200 Gbps transceiver facilitated a slightly higher traffic allocation, reaching over 55 Tbps. Expanding the analysis to include the

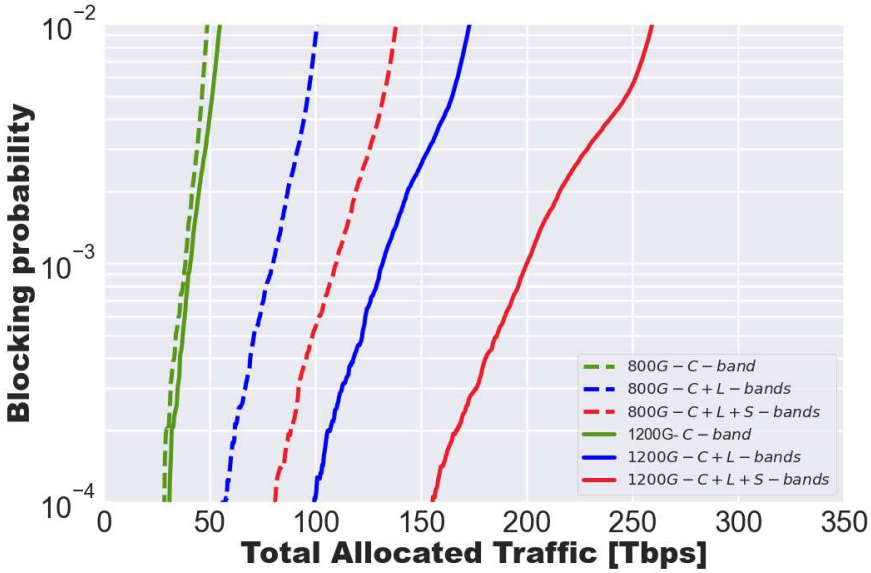

Figure 4.22: BP evaluated considering ideal transceivers.

C+L bands, the traffic allocation for the 800 Gbps transceiver was noted at 102 Tbps. This figure significantly increased to 170 Tbps for the 1200 Gbps transceiver, marking a substantial increment of 66%. The trend continued when considering the C+L+S bands, where the traffic for the 800 Gbps transceiver stood at 140

Tbps, and escalated dramatically to 260 Tbps for the 1200 Gbps transceiver, indicating an 84% increase. This marked improvement in traffic allocation can be largely attributed to the different spectrum/bandwidth allocations between the two transceiver types. For the 800 Gbps transceiver, the total spectrum assigned across the C, L, and S bands was 4 THz. In contrast, the 1200 Gbps transceiver was allocated 6 THz for the L and S bands, with an additional 4 THz for the C-band.

Further insights from the analysis are presented in Fig. 4.23, which details the traffic allocation per link for both transceiver scenarios. Notably, the 'E11-E12' link demonstrated the highest traffic loads, reaching approximately 4100 Gbps for the 800 Gbps case, and 7550 Gbps for the 1200 Gbps case. A horizontal dotted line in the figure indicates 50% of the total traffic allocated, normalized for each transceiver type. The significant traffic allocations observed were predominantly associated with data centers located at nodes E10, E12, and E17, with all links exceeding the 50% threshold primarily linked to these centers. This analysis underscores the substantial benefits of higher capacity transceivers in effectively managing larger volumes of network traffic, particularly in complex DCI environments.

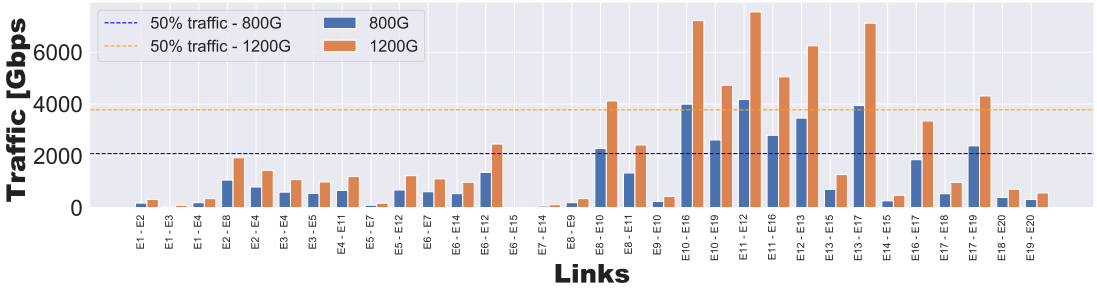

Figure 4.23: Traffic allocation / link

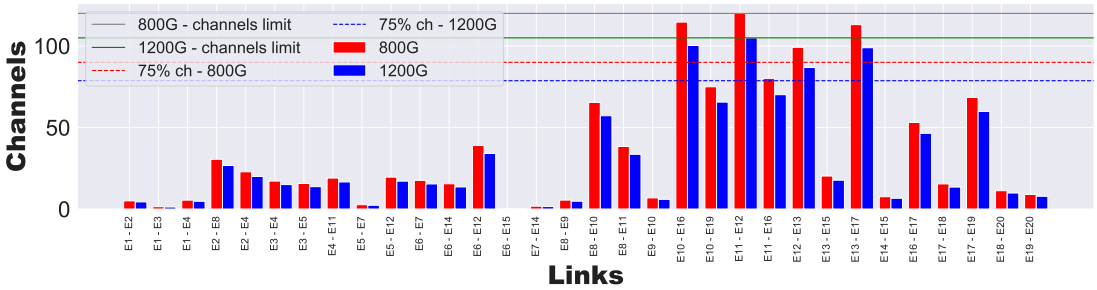

Figure 4.24: Channel allocation / link

Channels allocation

Fig. 4.24 delineates the channel allocations for both the 800 Gbps and 1200 Gbps transceiver scenarios. In the setup with 800 Gbps transceivers, a total of

120 channels are allocated, whereas the 1200 Gbps scenario involves a slightly reduced total of 105 channels. The figure includes dotted lines representing the 75% threshold of total channel allocations for each scenario. Notably, the 'E11-E12' link, which was previously identified in Fig. 4.23 as having the highest traffic allocation, reaches maximum channel capacity under both transceiver conditions. Moreover, all links that exceed the 75% threshold of channel allocations are primarily associated with data centers, highlighting the significant demand for channel resources at these critical network nodes. This observation underscores the pivotal role of channel capacity in supporting high traffic volumes, particularly in scenarios involving advanced, higher-capacity transceivers.

4.4.1.2 Conclusion and future insights

The results examine the performance dynamics inside multi-band optical network systems by comparing SDM and BDM systems using the described WSS device and range of transceivers. Utilizing several fibers or broadening wavelength bands offers clear benefits in various operating situations and limitations. The results of our study demonstrate that SDM, although it necessitates a greater number of fibers, intrinsically provides a slightly improved network allocations, and resilience, particularly when several C-band fibers are employed. Alternatively, BDM techniques offer a cost-effective solution to address the increasing bandwidth demand without the need for major physical infrastructure changes required by SDM. BDM does this by using fewer fibers and expanding operations into the L and S bands.

The performance metrics obtained from Monte Carlo simulations show that SDM can achieve slightly better efficiency in scenarios where dual or triple C-band fibers are used. However, BDM configurations maintain comparable performance with fewer resources in terms of fiber infrastructure, especially in combined C+L and C+L+S band setups. The fact that BDM shows similar performance indicates that it is a feasible approach for expanding networks in situations where deploying fiber is restricted or too expensive. Ultimately, both SDM and BDM play a crucial role in meeting the future requirements for network capacity and efficiency. However, the decision between them should be influenced by unique network needs, budgetary limitations, and physical infrastructure capabilities.

We have done our study with a focus on the future, considering the changing needs of network infrastructure. We assessed the efficiency of several transceivers, namely those with capacities of 400G, 800G, and 1200G, in the context of the German network topology.

Assuming the porjected traffic growth of 25% annually [133], we mapped out network traffic utilization over the next decade. The methodology for projecting network traffic over a 10-year period is based on a systematic increase in traffic demands, reflecting anticipated growth in data consumption. The projection starts

with an initial uniform traffic load of 400 Gbps per request in the baseline year (year 0). This figure is representative of current traffic demands in high-capacity network environments. To model future network traffic, the initial traffic volume is incremented annually by 25% to reflect the compounded growth in data transmission requirements. This rate of increase is aligned with observed trends in data usage and network load, influenced by factors such as increased digital media consumption, expansion of cloud-based services, and broader adoption of high-bandwidth applications like HD streaming and virtual reality. The projection is calculated using the formula:

$$\text{Traffic}_{\text{Year } n} = \text{Traffic}_{\text{Year } 0} \times (1.25)^n$$

where n represents the number of years since the baseline measurement. This method provides a straightforward yet effective way to anticipate future demands on optical transport networks, ensuring that the infrastructure developed can handle upcoming increases in data traffic. It helps in planning for capacity enhancements, strategic investments, and technological upgrades necessary to support the growing needs of network users. The data delineating the usage trends for the C-band alone is illustrated in Fig. 4.25, while Fig. 4.26 and Fig. 4.27 represent the scenarios for the combined C+L and C+L+S bands, respectively. According to Fig. 4.25, in

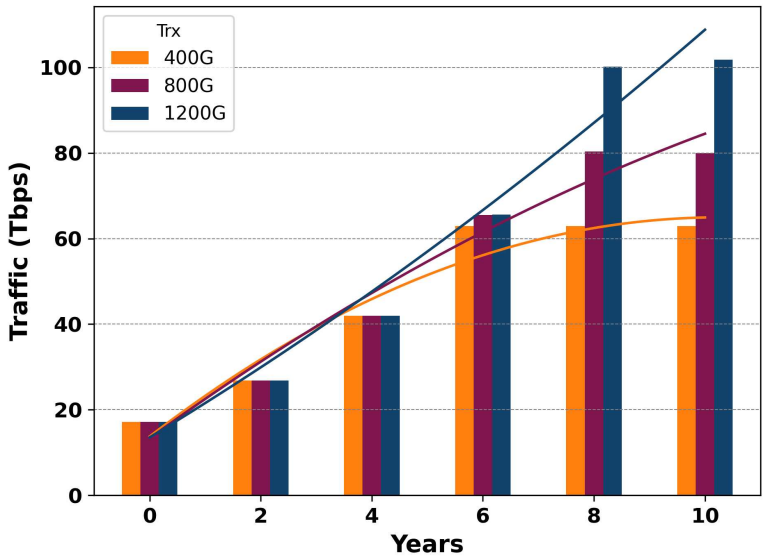

Figure 4.25: C band traffic allocation trend for 10 years

the initial four years, the three transceivers exhibit comparable performance due to the moderate traffic volume. However, as traffic intensifies, the 400G and 800G transceivers begin to reach their limits sooner, leading to earlier blocking and a decline in traffic accommodation capacity. After a decade, it's projected that the 1200G transceiver will handle approximately 105 Tbps, surpassing the 800G by

23.81% and the 400G by 40.9%, which are expected to support 80 Tbps and 62 Tbps, respectively. In the scenario depicted in Fig. 4.26, the traffic can be fully

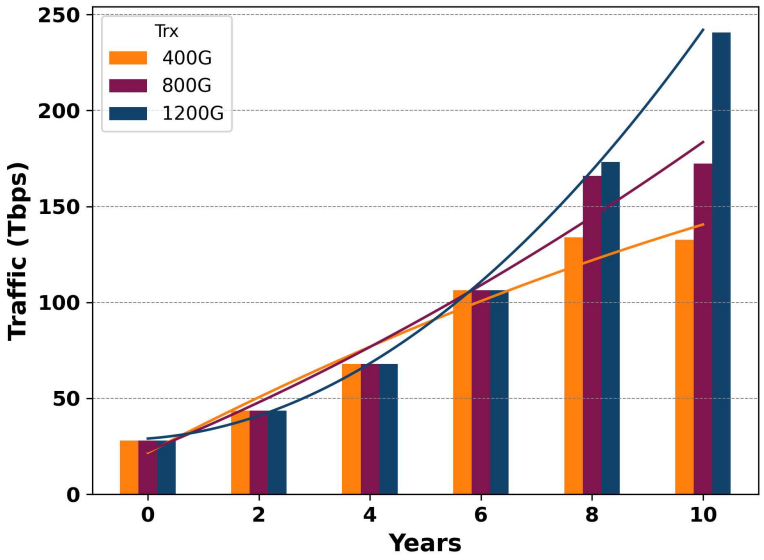

Figure 4.26: C+L band traffic allocation trend for 10 years

accommodated without blocking for up to six years for all transceivers, with an average throughput of around 107 Tbps. Over a span of ten years, the 1200G transceiver is anticipated to accommodate up to 240 Tbps. In comparison, the 800G and 400G transceivers are projected to support 170 Tbps (29.17% less) and 135 Tbps (43.1% less), respectively. Finally, as per the C+L+S bands scenario shown in Figure 4, after ten years, the capacity expected to be facilitated by the 1200G transceiver reaches 365 Tbps, which exceeds the capacity of the 800G and 400G transceivers by 17% and 47.9%, respectively, with the 800G expected to handle 303 Tbps and the 400G around 190 Tbps.

Fig. 4.28 displays a projection for the future of SDM over the next ten years, with the 1200G transceiver serving as the foundation for the analysis. The x-axis of the graph represents the years, while the y-axis measures the number of fiber pairs involved in the German network. The orange line shown illustrates the growth in the number of fiber pairs over a period of years. Starting with one fiber pair per link, we anticipate a yearly growth of 25% in the need for traffic. Initially, the network is comprised of 26 fiber pairs to accommodate high levels of traffic. In the second year, we expect that we will need an average of 36.3 fiber pairs, which is a 1.4-fold increase over the initial 26 fiber pairs. By the conclusion of the projection period, we anticipate that there will be a significant 5.9-fold increase in the number of fiber pairs required, resulting in an average of 153 pairs.

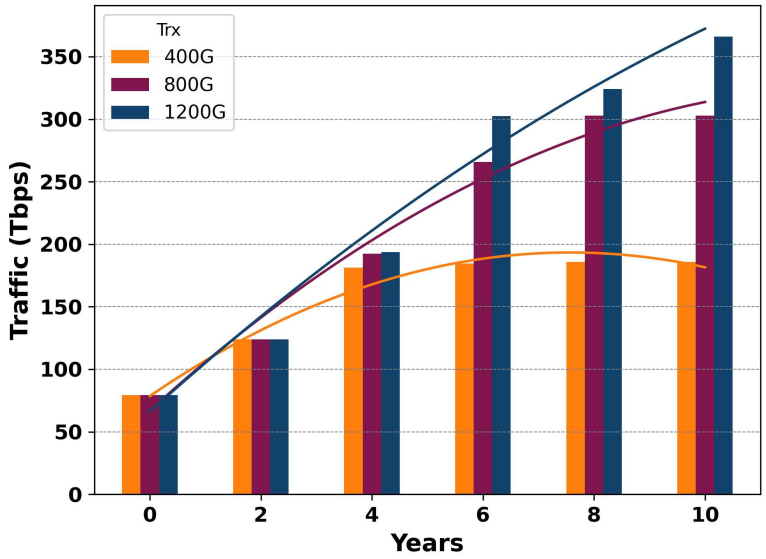

Figure 4.27: C+L+S band traffic allocation trend for 10 years

These analysis highlights the potential for increasing network capacity by upgrading transceivers and expanding the number of fiber pairs to support an architecture based on SDM.

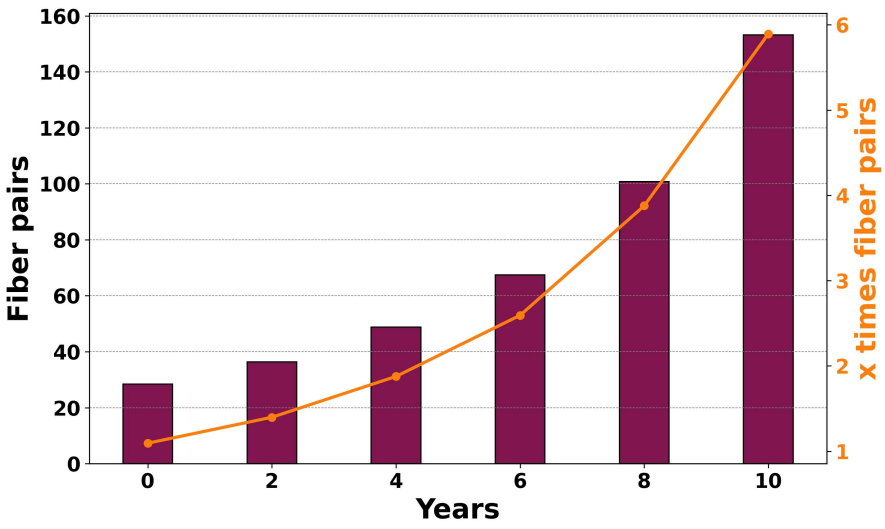

Figure 4.28: SDM trend over years

4.4.1.3 WBSS - Networking performance evaluation

Resource assignment

We propose an algorithm designed for efficient resource allocation in waveband networks, facilitating the deployment of new connection requests in the form of lightpaths (LP). The algorithm is structured as follows:

Initially, the algorithm checks if there is an existing lightpath with the same source (s) and destination (d) nodes that also has enough spare capacity to accommodate the traffic demand (t). This step is shown in line 1 of Alg. 1.

If no suitable existing lightpath is found, the algorithm then considers the establishment of a new lightpath. It sequentially evaluates each of the k possible routes between the node pair (line 4).

For each route (r), the algorithm identifies the available free channels, which are segmented into sets each containing M channels (line 10).

For each channel set, the algorithm calculates the total bit rate, taking into account the modulation format that the Generalized GSNR of these channels can support (line 15). The choice of modulation format is determined based on the required generalized signal-to-noise ratio (RGSNR) for the transceiver.

The algorithm proceeds to check if the capacity of the channels (T) meets or exceeds the requested traffic volume. If so, the connection is established using the selected channels within the identified route (line 18).

This resource assignment algorithm adheres to wavelength continuity and contiguity constraints, which are integral to conventional WL routing where M is set to 1. The same principles apply to waveband WB routing, whether in multiband or multicore fiber/parallel single-mode fiber (SMF) contexts. This method ensures that resources are allocated efficiently, optimizing the utilization of network capacity and supporting the robust deployment of new services.

Traffic allocation

The analysis is performed in two stages; initially, it is sim- ulated for the multiband optical system, and after that, the investigation is further extended to multicore fiber/parallel- SMF. The multiband transmission system is constructed from a series of bands, with components, especially optical amplifiers, optimized for each band. The transceiver of 1200 G transmission with a channel bandwidth of 150 GHz, symbol rate of 130 GBaud is considered. The number of fibers is fixed to five to relax the computation complexity. A single channel is routed at a given time for the conventional single-layer WL switching system. On the other hand, in the WB switching architecture, a continuous WL is grouped up first; the minimum 2WL/WB and maximum 6WL/WB are considered. The grouped WLs

Algorithm 1 Resource Assignment

Require: $RS_{i,j}$: Route space for all network node pairs (i, j), M: number of channels to compose the waveband, $c(s, d, t)$: new connection request (c) containing source (s) and destination (d) nodes, and traffic (t)

Try allocation of c in already deployed LPs
if c is not allocated **then**
    $R \leftarrow RS_{s,d}$
    while $R \neq \emptyset$ & c *not allocated* **do**
        $r \leftarrow$ the first route from R
        $R \leftarrow R \setminus r$
        $c(s, d, t, r) \leftarrow c(s, d, t) \cup r$
        $T \leftarrow 0$
        $n \leftarrow \emptyset$ ▷ Set of channels used to allocate request c
        $H \leftarrow$ list of free channels in route r divided in sets of M channels
        while $H \neq \emptyset$ & T < t **do**
            $h \leftarrow$ first set of M channels from H
            $H \leftarrow H \setminus h$
            $n \leftarrow n \cup h$
            $i \leftarrow$ computation of bit rate of route r using channels in h (GSNR based)
            $T \leftarrow T + i$
        end while
        if $T \geq t$ **then**
            $c(s, d, t, r, n) \leftarrow c(s, d, t, r) \cup n$
            allocate c using channels in n through route r
        end if
    end while
end if

are routed as a single WB at a given time. This work considers the German network topology. In order to evaluate the influence of the WB architecture on networking performance in comparison to the traditional WL architecture, an extensive series of simulations are conducted across various network scenarios. Fig. 4.29 illustrates

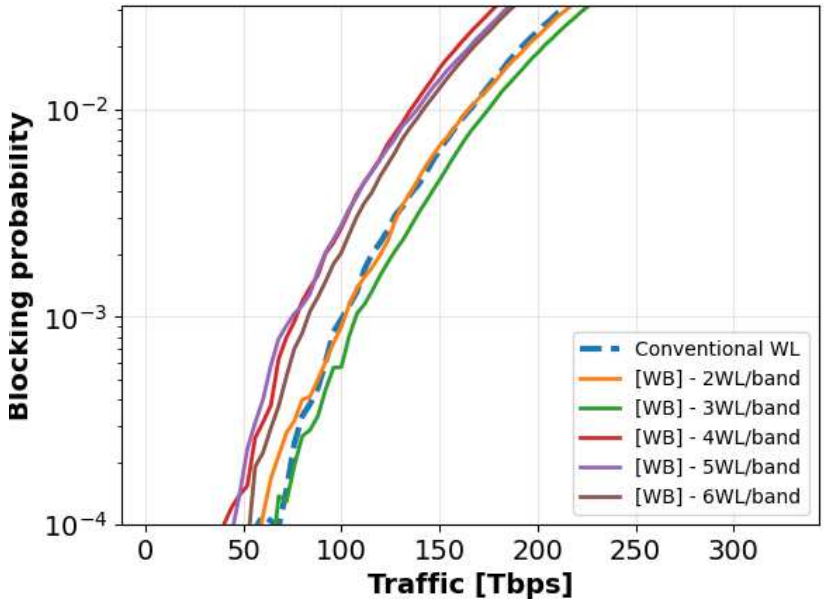

Figure 4.29: Blocking probability vs. traffic for wavelength and waveband enabled C+L network.

the distribution of network traffic across a spectrum of BP for conventional WL and WB architectures (M = 2, 3, 4, 5, 6), with each scenario accommodating a uniform traffic load of 4000 Gbps per request, within the C+L spectrum. Whereas Fig. 4.30 shows the overall network allocation against the BP for the C+L+S scenario. In Fig. 4.29, for BP = 10^{-2}, the traffic allocation for the WL case is 166 Tbps. Compared to the WB case (M = 2, 3, 4, 5, 6), the overall traffic allocation is 164 Tbps (1.2% lower), 177 Tbps (6.63% higher), 136 Tbps (22.9% lower), 139 Tbps (15.66% lower), and 141 Tbps (14.4% lower), respectively. In Fig. 4.30, for BP = 10^{-2}, the traffic allocation for the WL case is 241.5 Tbps. Compared to the WB case (M = 2, 3, 4, 5, 6), the overall traffic allocation is 248.5 Tbps (2.9% higher), 238 Tbps (1.3% lesser), 189 Tbps (21.5% lesser), 199 Tbps (17.4% lesser), and 189.5 Tbps (21.54% lesser), respectively.

Fig. 4.31 and Fig. 4.32 illustrate the network performance regarding the overall traffic allocation across a spectrum of traffic intensities, specifically with a fixed $BP = 10^{-2}$, within the context of the C+L and C+L+S scenarios, respectively. These figure presents a comparison of the overall network traffic capacity (measured in Tbps - y-axis) as a function of the waveband size (M) for a network

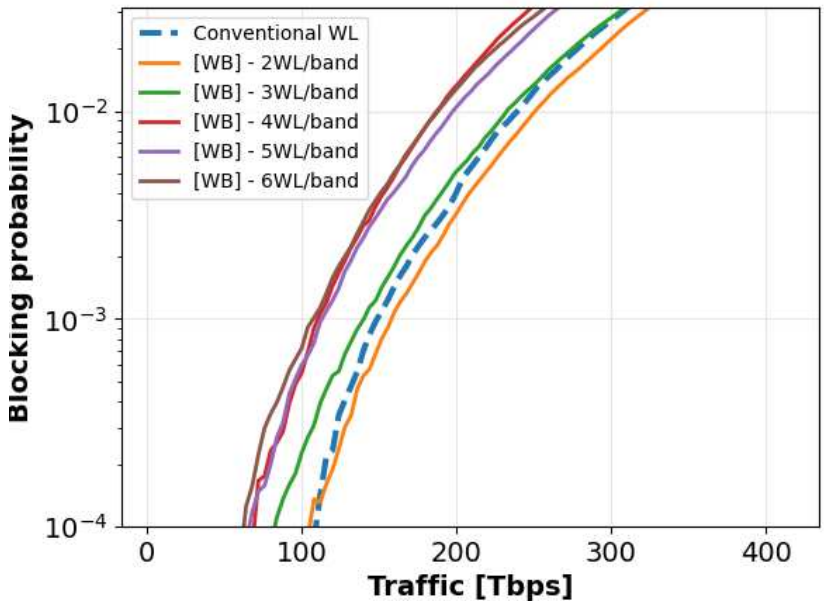

Figure 4.30: Blocking probability vs. traffic for wavelength and waveband enabled C+L+S network.

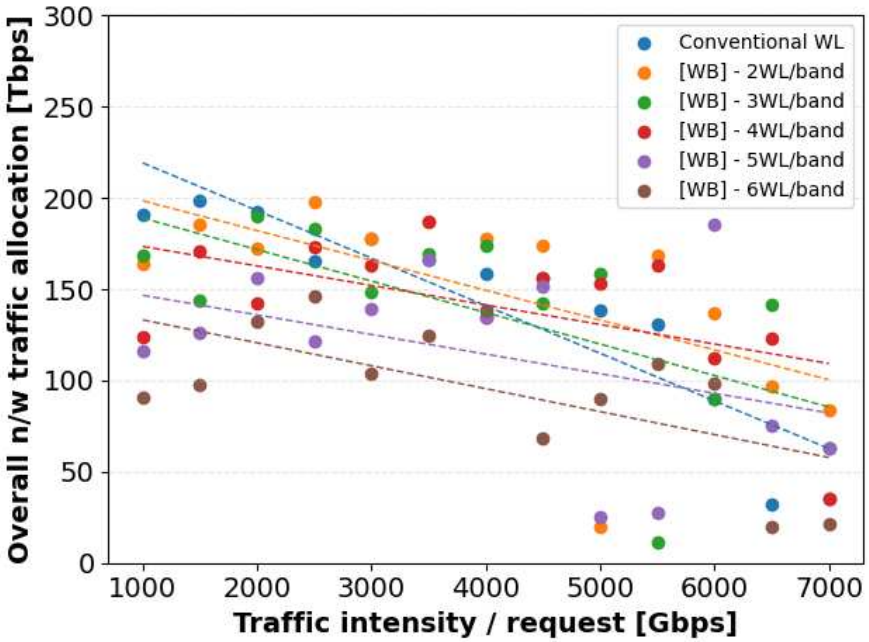

Figure 4.31: Impact of waveband size (M) on overall C+L Network Traffic.

utilizing the multi (C+L- and C+L+S-) bands. The configurations tested vary in the number of wavelengths grouped into a single waveband, ranging from 2 to 6 wavelengths per band for uniform traffic requests ranging from 1000 to 7000 Gbps

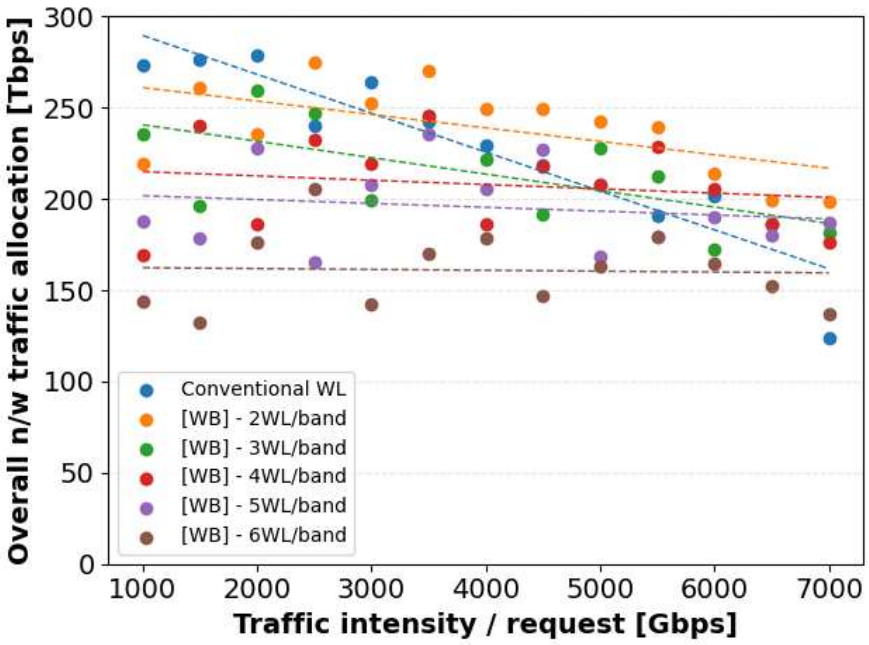

Figure 4.32: Impact of waveband size (M) on overall C+L+S Network Traffic.

(x-axis). The dots in the plot represents the actual simulation data and the dotted line shows the trend line for particular WB case for all the traffic profiles. As the waveband size increases for the increasing traffic intensity, there is a notable variation in the network's ability to handle traffic. The steeper downward slope in the conventional WL results in earlier blocking of traffic requests due to limited channel bandwidth. This variation is indicative of the trade-off between the flexibility of wavelength allocation and the efficiency of waveband switching. There is an optimal waveband size for the given traffic profiles, where the network achieves the highest traffic capacity. In Fig. 4.31, at 2000 Gbps traffic profile, conventional WL allocates around 190 Tbps network traffic, the allocation is of the order $conv.WL > 3WB/WL > 2WB/WL > 5WB/WL > 4WB/WL > 6WB/WL$. For 6000 Gbps case, overall network traffic allocation is of the order $5WB/WL > 2WB/WL > 4WB/WL > 6WB/WL > 3WB/WL$. At lower traffic intensities, the conventional WL switching offers superior granularity and flexibility in routing individual wavelength channels. This finer granularity allows for more efficient utilization of available spectral resources, minimizing wasted bandwidth and reducing the likelihood of blocking under moderate traffic loads. As traffic demand increases, the advantages of appropriately configured waveband switching become more evident, reducing fragmentation and maximizing spectral utilization, which translates to better overall network performance compared to the conventional WL approach. This indicates a balance between the granularity of switching and the overhead associated with waveband formation and management. Fig. 4.32 shows the same

scenarios for the C+L+S- bands, providing overall larger bandwidth. The impact of waveband size on traffic capacity differ from the C+L network scenario due to the added complexity and the potential for increased bandwidth which results in less blocking.

Both figures underscore the importance of WB size in optimizing network performance for multi-band optical networks. They highlight the need for a careful balance between the granularity of control offered by smaller wavebands and the efficiency and scalability benefits of larger wavebands. The analysis demonstrates that the optimal waveband size can significantly affect the network's capacity to manage traffic, with implications for network design and operation in bandwidth-intensive environments.

Chapter 5

Conclusions and future work

Overall, the thesis underscores the transformative impact of integrating advanced photonic technologies and machine learning into optical networking. The findings emphasize the potential for multi-band transmission systems to meet future network demands, offering scalable and efficient solutions. The research highlights the critical role of ongoing innovation in optical network technologies, paving the way for the development of next-generation optical transport systems that can handle increasing traffic demands while maintaining high performance and reliability. SUmmar of the key methods and their outcomes is summarized in Table.

Method/Tool	Description/Techniques Used	Purpose	Outputs
Network Simulation (SNAP Framework)	Simulates multi-band optical transport networks using real-world topologies (e.g., Germany, Italy, USA)	To evaluate network performance under different configurations and conditions	Network capacity, blocking probability, signal quality, bandwidth utilization
Photonic Integrated Wavelength Selective Switch (WSS)	A photonic integrated device enabling switching across C, L, and S bands	To optimize bandwidth allocation and routing in multi-band ROADM architectures	Enhanced spectral efficiency, lower insertion loss, and increased routing flexibility
Machine Learning Model (DNN and Heuristics)	Deep Neural Networks (DNN) with heuristic-based optimization for control state prediction and Quality of Transmission (QoT) evaluation	To dynamically manage traffic and predict routing control states in real-time	Reduced blocking probability, improved QoT, and lower latency in network operations
Comparison of SDM and BDM Systems	Compare Space Division Multiplexing (SDM) and Band Division Multiplexing (BDM) systems in terms of capacity, spectral efficiency, and network complexity	To evaluate the impact of SDM and BDM on network performance and capacity expansion in multi-band networks	Insights into system scalability, capacity gains, network complexity, and efficient resource allocation

Table 5.1: Summary of key methods/tools used

The thesis starts with a thorough examination of optical communication systems and the essential technologies that form the foundation of the worldwide communications infrastructure. With the continuous development of communication technologies, there is a persistent requirement for improved traffic control in optical communication networks. Chapter 2 presents a suggested switching device

specifically created to manage the growing requirements. This chapter presents the abstraction of the physical layer along with the fiber propagation impairments.

Chapter 3 of this thesis presents an implementation of the application of machine learning techniques to photonic devices, focusing on optimizing switching structures and evaluating their control states and QoT. The collaborative research with Synopsys, Inc. and Politecnico di Torino has led to significant advancements in enhancing the efficiency and reliability of optical network switching by harnessing the predictive and analytical power of machine learning. The chapter begins by introducing the fundamental concepts of Artificial Intelligence (AI) and Machine Learning (ML), setting a solid foundation for understanding their relevance in the context of optical networks.

The study evaluates a management model using machine learning applied to multistage crossover switches, which are essential for creating non-blocking networks. These networks can handle any input-output configurations without internal routing conflicts, making them ideal for implementing machine learning-based management models. The ability of machine learning techniques to predict routing control states accurately, even with limited training data, is demonstrated through various Beneš network configurations. This highlights the resilience and scalability of the machine learning model in managing larger and more complex networks, showcasing its potential to handle complex scenarios effectively.

Moreover, the chapter discusses the use of a Deep neural network (DNN) with optimized hyperparameters to predict QoT degradation. The deployment of a parallel DNN structure enhances both predictive accuracy and computational efficiency, ensuring optimal signal integrity across the network. This approach underscores the potential of machine learning to significantly improve the management and performance of optical networks.

The findings illustrate the transformative impact of integrating machine learning techniques within photonic networks. The developed models demonstrate high accuracy in predicting control states and QoT, even in large-scale networks, showcasing the potential for machine learning to revolutionize optical network management and optimization. This research highlights the critical role of ongoing innovation in machine learning applications to meet the increasing demands of modern optical networks, ensuring enhanced performance, reliability, and scalability. The study provides a robust framework for future advancements in photonic devices, contributing to the evolution of next-generation optical transport systems. By leveraging the capabilities of machine learning, this research paves the way for more efficient and flexible optical networks, capable of adapting to the dynamic demands of contemporary data transmission needs.

Chapter 4 of this thesis provided an in-depth analysis of network-level performance within multi-band optical transmission systems. Previous chapters discussed significant advancements in long-haul network technology, including improvements in optical switching. These developments have shifted bandwidth and operational

challenges toward metro and access networks. As demand for on-demand services increases, there is a pressing need for enhanced flexibility and rapid reconfiguration capabilities in optical networks. These improvements are essential to ensure continuous service delivery for critical operations. Spatial-division multiplexing (SDM) and Band division multiplexing (BDM) have emerged as pivotal technologies in enhancing optical system capacities. While SDM is already commercially viable (if redundant or dark fibers are considered), BDM—utilizing multi-band setups hows great potential for future scalability. The study employed the Statistical Network Assessment Process (SNAP) to evaluate the QoT by quantifying the impact of various network components on signal integrity, providing a robust framework for performance assessment.

The comparative analysis between SDM and BDM configurations revealed that BDM could achieve similar performance metrics with fewer fibers, highlighting its viability as an alternative in high-capacity network contexts. Evaluations of various network topologies, including real and random network topologies, demonstrated that BDM can effectively enhance network capacity without necessitating extensive modifications to the existing fiber infrastructure. This adaptability makes BDM particularly attractive for expanding current network capabilities cost-effectively.

Further analysis of traffic allocation and blocking probability underscored the efficiency of multi-band systems in managing higher volumes of data traffic while reducing operational expenses. Multi-band configurations showed marked improvements in traffic allocation and lower blocking probabilities compared to traditional single-band setups. These findings highlight the operational benefits and enhanced efficiency of adopting multi-band technologies in modern optical networks.

Projections for the growth of SDM over the next decade indicate a significant increase in the number of fiber pairs required to support rising traffic demands. This projection underscores the need for scalable and efficient network architectures to accommodate future growth.

Overall, the findings in provide a detailed evaluation of multi-band optical transmission systems, demonstrating their potential to meet future network demands through enhanced capacity and efficiency. The study underscores the importance of integrating advanced technologies, such as SDM and BDM, to optimize network performance and pave the way for next-generation optical transport systems. This study lays a strong foundation for future research focused on further enhancing the scalability and effectiveness of optical networks, ensuring they can meet the ever-growing demands of data traffic in a cost-effective and efficient manner.

In conlcusion, this study lays a robust foundation for future advancements in optical networking, with a focus on scalability and efficiency. The insights provided in this thesis are invaluable for researchers and industry professionals working towards the evolution of optical communication systems. By leveraging the capabilities of advanced photonic technologies and machine learning, this research paves the way for more efficient and flexible optical networks, ensuring they can adapt to the

dynamic demands of contemporary data transmission needs.

Future work

The research and findings presented in this thesis open several promising avenues for future work, particularly in the development and enhancement of multi-band systems. A key area of exploration involves the creation of hybrid multi-band systems. By combining the strengths of different multi-band technologies such as SDM and BDM, researchers can aim to maximize network capacity and flexibility. Hybrid systems can leverage the high spatial efficiency of SDM and the spectral efficiency of BDM, resulting in a more robust and scalable network architecture capable of meeting the diverse demands of future optical networks.

Another critical aspect of future research is the efficient spectrum sharing between different network operators and services. As the demand for bandwidth continues to grow, optimizing the utilization of available spectrum becomes paramount. Developing advanced techniques for spectrum sharing can ensure that multiple operators can coexist without interference, thereby improving the overall efficiency and capacity of the network.

In addition to theoretical advancements, real-world deployments and testing of the proposed technologies are essential to validate their performance and practicality. Conducting large-scale field trials and deployments will provide valuable empirical data, helping to refine the models and techniques based on practical feedback. This involves collaboration with industry partners and network operators to test the hybrid multi-band systems and spectrum sharing techniques in real-world scenarios. By focusing on these areas, future research can ensure that the advancements in multi-band optical systems are not only theoretically sound but also practically viable and ready for real-world implementation. This approach will pave the way for the next generation of optical networks, characterized by unprecedented capacity, flexibility, and efficiency. Through continuous innovation and collaboration, the optical networking community can address the ever-growing demands for high-speed, reliable communication, ultimately leading to more connected and efficient digital infrastructure.

Acronyms

ADC Analog-to-digital. 10

ADCs Analog-to-digital onverters. 25

AI Artificial intelligence. 41

APIs Application programming interfaces. 9, 48

ASE Amplified spontaneous emission. 29, 33, 62, 64, 69

AWGN Additive white Gaussian noise. 29

BDM Band division multiplexing. 60, 61, 69–78, 81, 82, 88, 100, 101

BER Bit error rate. 26, 50, 55

BP Back-propagation. 70–72, 86, 94

BPDs Balanced photodetectors. 25

CD Chromatic dispersion. 10, 60

CDCs Contra-directional couplers. 17, 19

CWDM Coarse Wavelength Division Multiplexing. 69

DAC Digital-to-analog. 10

DCUs Dispersion compensating units. 10

DD Direct-detection. 10

DFAs Doped Fiber Amplifiers. 32

DNN Deep neural network. 48, 52, 56, 99

DSP Digital signal processing. 10, 12, 25, 26, 28, 35

DWDM Dense Wavelength Division Multiplexing. 5, 14, 69

EDC Electronic dispersion compensation. 10

EDFA Erbium Doped Fiber Amplifier. 13, 23, 29, 69

EDFAs Erbium Doped Fiber Amplifiers. 15, 34

EONs Elastic optical networks. 12

FF First-fit. 62

FMF Few-Mode Fibers. 69

FSR Free spectral range. 20

FWM Four-wave mixing. 31

GGN Generalized gaussian noise. 14, 33

GSNR Generalized Signal-to-Noise Ratio. 33–36, 62–66, 68, 92

GVD Group-velocity dispersion. 27

ILAs Inline amplifiers. 32

IoT Internet Of Things. 12, 42

JPDF Joint Probability Distribution Function. 39

LCoS Liquid crystal on silicon. 16

LOGO Local-Optimization Global-Optimization. 64

LP Lightpath. 10, 34, 36, 37, 62, 70

LPs Light-paths. 35, 36

M2M Machine-to-machine. 12

MBT Multi band transmission. 2, 3, 12–15, 20, 22, 29, 30, 33–35, 60

MC Monte Carlo. 62, 63

MCF Multicore fiber. 61, 69

MEMS Microelectronicmechanical systems. 16

ML Machine learning. 41–44, 46–48, 52, 55–57

MMF Multimode fiber. 61

MPF Multiparallel fiber. 61

MRR Microring Resonator. 50

MRRs Micro-ring resonators. 17, 19, 45

MSE Mean square error. 52, 56, 57

MZI Mach-Zehnder Interferometer. 20, 45

MZMs Mach-Zehnder modulators. 24

NEs Network elements. 11

NF Noise figure. 30, 34

NFs Noise Figures. 34

NLI Nonlinear interference. 14, 33, 62, 69

NLP Natural language processing. 41

NOS Network operating system. 9

OAs Optical amplifiers. 31

OEO Optical-electro-optical. 10

OLO Optical local oscillator. 25

OLS optical line system. 12, 23, 32

OLSs optical line systems. 11

OSE Optical Switching Element. 56

OSEs Optical Switching Elements. 20, 44, 45

OSNR Optical Signal-to-Noise Ratio. 50, 55, 57

OXC Optical cross connect. 21, 23

PBSs Polarization beam splitters. 24, 25

PIC Photonic integrated circuit. 16, 46

PICs Photonic integrated circuits. 43

PMD Polarization-mode dispersion. 10, 26, 27, 60

PONs Passive optical networks. 6, 14

PS Probabilistic shaping. 60

QoT Quality of transmission. vi, 12, 27, 30, 33–35, 43, 44, 46, 47, 50, 56–58, 62, 64, 68, 69, 99, 100

ROADM Reconfigurable optical add-drop multiplexer. 15, 21, 23, 32, 35, 37, 62, 70

ROADMs Reconfigurable optical add-drop multiplexers. 6, 10, 11, 36, 42

RWA Routing and Wavelength Assignment. vi, 35–39, 62, 63

SDM Spatial-division multiplexing. 22, 23, 60, 61, 69–77, 81, 82, 88, 90, 91, 100, 101

SDN software-defined networking. 7–12, 21, 42, 43

SNAP Statistical Network Assessment Process. 62, 100

SNR Signal-to-Noise ratio. 30, 32, 33

SOAs Semiconductor Optical Amplifiers. 32

SRS Stimulated Raman Scattering. 14, 29, 32, 33, 61

SSMF Standard Single-Mode Fiber. 28, 33

TDFA Thulium Doped Fiber Amplifier. 15, 23, 30, 34, 69

TDFAs Thulium Doped Fiber Amplifiers. 34

TF *TensorFlow*©. 48

UWB Ultra wideband. 60

WB Waveband. 22, 23, 92, 94

WBSS Waveband selective switch. vi, 21

WDM Wavelength division multiplexing. 2, 13, 16, 25, 26, 28, 30, 31, 35, 36, 42, 59, 60, 62

WL Wavelength. 23, 92, 94

WSS Wavelength selective switch. 15, 16, 21, 23, 43, 68–70, 76, 88

Bibliography

[1] René-Jean Essiambre et al. "Capacity limits of optical fiber networks". In: *Journal of Lightwave technology* 28.4 (2010), pp. 662–701.

[2] Yoshihisa Yamamoto and Tatsuya Kimura. "Coherent optical fiber transmission systems". In: *IEEE Journal of Quantum Electronics* 17.6 (1981), pp. 919–935.

[3] G Ramesh, S Sundara Vadivelu, and Jose Anand. "A survey on wavelength division multiplexing (WDM) networks". In: *ICTACT Journal on Communication Technology* 1 (2010).

[4] Alessio Ferrari et al. "Assessment on the achievable throughput of multi-band ITU-T G. 652. D fiber transmission systems". In: *Journal of Lightwave Technology* 38.16 (2020), pp. 4279–4291.

[5] Rasoul Sadeghi et al. "Multi bands network performance assessment for different system upgrades". In: *2020 IEEE Photonics Conference (IPC)*. IEEE. 2020, pp. 1–2.

[6] Antonio Napoli et al. "Towards multiband optical systems". In: *Photonic Networks and Devices*. Optica Publishing Group. 2018, NeTu3E–1.

[7] Seiji Okamoto et al. "5-band (O, E, S, C, and L) WDM transmission with wavelength adaptive modulation format allocation". In: *ECOC 2016; 42nd European Conference on Optical Communication*. VDE. 2016, pp. 1–3.

[8] Alessio Ferrari, Emanuele Virgillito, and Vittorio Curri. "Band-division vs. space-division multiplexing: A network performance statistical assessment". In: *Journal of Lightwave Technology* 38.5 (2020), pp. 1041–1049.

[9] Alessio Ferrari et al. "Power control strategies in C+ L optical line systems". In: *Optical Fiber Communication Conference*. Optica Publishing Group. 2019, W2A–48.

[10] Daniela Moniz, Victor Lopez, and João Pedro. "Design strategies exploiting C+ L-band in networks with geographically-dependent fiber upgrade expenditures". In: *Optical Fiber Communication Conference*. Optica Publishing Group. 2020, M2G–3.

[11] Victor Lopez et al. “Optimized design and challenges for C&L band optical line systems”. In: *Journal of Lightwave Technology* 38.5 (2020), pp. 1080–1091.

[12] Jane M Simmons. *Optical network design and planning*. Springer, 2014.

[13] Rajiv Ramaswami, Kumar Sivarajan, and Galen Sasaki. *Optical networks: a practical perspective*. Morgan Kaufmann, 2009.

[14] Leonid G Kazovsky et al. “Next-generation optical access networks”. In: *Journal of lightwave technology* 25.11 (2007), pp. 3428–3442.

[15] Derek Nesset. “Next Generation PON Technologies: 50G PON and Beyond”. In: *2023 International Conference on Optical Network Design and Modeling (ONDM)*. IEEE. 2023, pp. 1–6.

[16] Glen Kramer and Gerry Pesavento. “Ethernet passive optical network (EPON): Building a next-generation optical access network”. In: *IEEE Communications magazine* 40.2 (2002), pp. 66–73.

[17] Bruno Astuto A Nunes et al. “A survey of software-defined networking: Past, present, and future of programmable networks”. In: *IEEE Communications surveys & tutorials* 16.3 (2014), pp. 1617–1634.

[18] Dany-Sebastien Ly-Gagnon et al. “Coherent detection of optical quadrature phase-shift keying signals with carrier phase estimation”. In: *Journal of lightwave technology* 24.1 (2006), p. 12.

[19] Michael G Taylor. “Coherent detection method using DSP for demodulation of signal and subsequent equalization of propagation impairments”. In: *IEEE Photonics Technology Letters* 16.2 (2004), pp. 674–676.

[20] JM Dugan et al. “All-optical, fiber-based 1550 nm dispersion compensation in a 10 Gbit/s, 150 km transmission experiment over 1310 nm optimized fiber”. In: *Optical Fiber Communication Conference*. Optica Publishing Group. 1992, PD14.

[21] MI Hayee and AE Willner. “NRZ versus RZ in 10-40-Gb/s dispersion-managed WDM transmission systems”. In: *IEEE photonics technology letters* 11.8 (1999), pp. 991–993.

[22] Han Sun, Kuang-Tsan Wu, and Kim Roberts. “Real-time measurements of a 40 Gb/s coherent system”. In: *Optics express* 16.2 (2008), pp. 873–879.

[23] Seb J Savory et al. “Electronic compensation of chromatic dispersion using a digital coherent receiver”. In: *Optics express* 15.5 (2007), pp. 2120–2126.

[24] Henning Bülow, Fred Buchali, and Axel Klekamp. “Electronic dispersion compensation”. In: *Journal of lightwave technology* 26.1 (2008), pp. 158–167.

[25] Seb J Savory. "Digital coherent optical receivers: Algorithms and subsystems". In: *IEEE Journal of selected topics in quantum electronics* 16.5 (2010), pp. 1164–1179.

[26] Xiang Zhou, Lynn E Nelson, and Peter Magill. "Rate-adaptable optics for next generation long-haul transport networks". In: *IEEE Communications Magazine* 51.3 (2013), pp. 41–49.

[27] Fernando P Guiomar et al. "Hybrid modulation formats enabling elastic fixed-grid optical networks". In: *Journal of Optical Communications and Networking* 8.7 (2016), A92–A100.

[28] Vittorio Curri et al. "Dispersion compensation and mitigation of nonlinear effects in 111-Gb/s WDM coherent PM-QPSK systems". In: *IEEE photonics technology letters* 20.17 (2008), pp. 1473–1475.

[29] Sheryl L Woodward, Mark D Feuer, and Paparao Palacharla. "ROADM-node architectures for reconfigurable photonic networks". In: *Optical Fiber Telecommunications* (2013), pp. 683–707.

[30] Dimitris Uzunidis et al. "Strategies for upgrading an operator's backbone network beyond the C-band: Towards multi-band optical networks". In: *IEEE Photonics Journal* 13.2 (2021), pp. 1–18.

[31] Andrew Lord, Andrea Soppera, and Arnaud Jacquet. "The impact of capacity growth in national telecommunications networks". In: *Philosophical Transactions of the Royal Society A: Mathematical, Physical and Engineering Sciences* 374.2062 (2016), p. 20140431.

[32] Seiji Okamoto et al. "5-band (O, E, S, C, and L) WDM transmission with wavelength adaptive modulation format allocation". In: *ECOC 2016; 42nd European Conference on Optical Communication*. VDE. 2016, pp. 1–3.

[33] Benjamin J Puttnam et al. "S, C and extended L-band transmission with doped fiber and distributed Raman amplification". In: *2021 Optical Fiber Communications Conference and Exhibition (OFC)*. IEEE. 2021, pp. 1–3.

[34] Lidia Galdino et al. "Optical fibre capacity optimisation via continuous bandwidth amplification and geometric shaping". In: *IEEE Photonics Technology Letters* 32.17 (2020), pp. 1021–1024.

[35] Antonio Napoli et al. "Towards multiband optical systems". In: *Photonic Networks and Devices*. Optica Publishing Group. 2018, NeTu3E–1.

[36] A Turukhin et al. "Power-efficient transmission using optimized C+ L EDFAs with 6.46 THz bandwidth and optimal spectral efficiency". In: *2018 European Conference on Optical Communication (ECOC)*. IEEE. 2018, pp. 1–3.

[37] Mattia Cantono et al. “Opportunities and challenges of C+ L transmission systems”. In: *Journal of Lightwave Technology* 38.5 (2020), pp. 1050–1060.

[38] *Meeting the 4 challenges of C+L*. https://www.infinera.com/blog/meeting-the-4-challenges-of-cl/tag/long-haul/?utm_source=SHP&utm_medium=Blog&utm_campaign=CLChallenges. [Accessed 05-03-2024].

[39] Johannes K Fischer et al. “Maximizing the capacity of installed optical fiber infrastructure via wideband transmission”. In: *2018 20th International Conference on Transparent Optical Networks (ICTON)*. IEEE. 2018, pp. 1–4.

[40] Alessio Ferrari et al. “Upgrade capacity scenarios enabled by multi-band optical systems”. In: *2019 21st International Conference on Transparent Optical Networks (ICTON)*. IEEE. 2019, pp. 1–4.

[41] *Optical Communication Band - FiberLabs Inc. — fiberlabs.com*. https://www.fiberlabs.com/glossary/optical-communication-band/. [Accessed 05-03-2024].

[42] Andrea D’Amico et al. “Scalable and disaggregated ggn approximation applied to a c+ l+ s optical network”. In: *Journal of Lightwave Technology* 40.11 (2022), pp. 3499–3511.

[43] Harmandeep Kaur and Kamajit Singh Bhatia. “Effect of Raman Amplifier and Cyclic Prefix on O-OFDM System Using Phase Modulation”. In: *Journal of Optical Communications* 36.3 (2015), pp. 197–203.

[44] Mattia Cantono et al. “On the interplay of nonlinear interference generation with stimulated Raman scattering for QoT estimation”. In: *Journal of Lightwave Technology* 36.15 (2018), pp. 3131–3141.

[45] Takeshi Hoshida et al. “Ultrawideband systems and networks: Beyond C+ L-band”. In: *Proceedings of the IEEE* 110.11 (2022), pp. 1725–1741.

[46] Robert Emmerich et al. “Enabling SCL-band systems with standard C-band modulator and coherent receiver using coherent system identification and nonlinear predistortion”. In: *Journal of Lightwave Technology* 40.5 (2022), pp. 1360–1368.

[47] Robert Emmerich et al. “Enabling SCL-band systems with standard C-band modulator and coherent receiver using coherent system identification and nonlinear predistortion”. In: *Journal of Lightwave Technology* 40.5 (2022), pp. 1360–1368.

[48] Gabriele Di Rosa et al. “Characterization, monitoring, and mitigation of the i/q imbalance in standard c-band transceivers in multi-band systems”. In: *Journal of Lightwave Technology* 40.11 (2022), pp. 3470–3478.

[49] Nicolas K Fontaine et al. “36-THz bandwidth wavelength selective switch”. In: *2021 European Conference on Optical Communication (ECOC)*. IEEE. 2021, pp. 1–4.

[50] Lorenzo Tunesi et al. “Design and performance assessment of modular multi-band photonic-integrated WSS”. In: *Optics Express* 31.22 (2023), pp. 36486–36502.

[51] Xiang Liu. “Enabling optical network technologies for 5G and beyond”. In: *Journal of Lightwave Technology* 40.2 (2022), pp. 358–367.

[52] *S-band amplifier (TDFA, Bench Top) - FiberLabs Inc. — fiberlabs.com*. https://www.fiberlabs.com/products/product_details/s-band-tdfa-bench-top/.

[53] Thomas A Strasser and Jefferson L Wagener. “Wavelength-selective switches for ROADM applications”. In: *IEEE journal of selected topics in quantum electronics* 16.5 (2010), pp. 1150–1157.

[54] Muhammad Umar Masood et al. “Networking assessment of ROADM architecture based on a photonics integrated WSS for 800G multi-band optical transport”. In: *Journal of Optical Communications and Networking* 15.10 (2023), E51–E62.

[55] Lorenzo Tunesi et al. “Modular Photonic-Integrated Device for Multi-Band Wavelength-Selective Switching”. In: *2022 27th OptoElectronics and Communications Conference (OECC) and 2022 International Conference on Photonics in Switching and Computing (PSC)*. IEEE. 2022, pp. 1–3.

[56] Lorenzo Tunesi et al. “Design and performance assessment of modular multi-band photonic-integrated WSS”. In: *Optics Express* 31.22 (2023), pp. 36486–36502.

[57] Xin Tu et al. “State of the art and perspectives on silicon photonic switches”. In: *Micromachines* 10.1 (2019), p. 51.

[58] Nicolas Dupuis et al. “Ultralow crosstalk nanosecond-scale nested 2× 2 Mach–Zehnder silicon photonic switch”. In: *Optics letters* 41.13 (2016), pp. 3002–3005.

[59] Zeqin Lu et al. “High-performance silicon photonic tri-state switch based on balanced nested Mach-Zehnder interferometer”. In: *Scientific reports* 7.1 (2017), p. 12244.

[60] Shengping Liu et al. “Thermo-optic phase shifters based on silicon-on-insulator platform: State-of-the-art and a review”. In: *Frontiers of Optoelectronics* 15.1 (2022), p. 9.

[61] Dan Yi et al. “Inverse design of multi-band and wideband waveguide crossings”. In: *Optics Letters* 46.4 (2021), pp. 884–887.

[62] Zejie Yu et al. “Inverse-designed low-loss and wideband polarization-insensitive silicon waveguide crossing”. In: *Optics Letters* 44.1 (2019), pp. 77–80.

[63] Sailong Wu et al. “State-of-the-art and perspectives on silicon waveguide crossings: A review”. In: *Micromachines* 11.3 (2020), p. 326.

[64] Siddharth Singh et al. “An MMI-based wavelength combiner employing non-uniform refractive index distribution”. In: *Optics Express* 22.7 (2014), pp. 8533–8540.

[65] Jinfeng Mu et al. “A low-loss and broadband MMI-based multi/demultiplexer in Si 3 N 4/SiO 2 technology”. In: *Journal of lightwave technology* 34.15 (2016), pp. 3603–3609.

[66] Hiroshi Hasegawa. “Bandwidth Abundant Optical Networking Enabled by Spatially-Jointed and Multi-Band Flexible Waveband Routing”. In: *IEICE Transactions on Communications* 107.1 (2024), pp. 16–26.

[67] Ryuji Munakata et al. “Architecture and performance evaluation of bundled-path-routing multi-band optical networks”. In: *2023 Optical Fiber Communications Conference and Exhibition (OFC)*. IEEE. 2023, pp. 1–3.

[68] Hai-Chau Le, Hiroshi Hasegawa, and Ken-ichi Sato. “Large capacity optical networks applying multi-stage hetero-granular optical path routing”. In: *Optical Switching and Networking* 11 (2014), pp. 105–112.

[69] Takahiro Ogawa, Hiroshi Hasegawa, and Ken-ichi Sato. “Optical fast circuit switching networks employing dynamic waveband tunnel”. In: *IEICE transactions on communications* 95.10 (2012), pp. 3139–3148.

[70] Takuma Kuno et al. “Experimental evaluation of optical cross-connects with flexible waveband routing function for SDM networks”. In: *2021 Optical Fiber Communications Conference and Exhibition (OFC)*. IEEE. 2021, pp. 1–3.

[71] Jingxin Wu, Suresh Subramaniam, and Hiroshi Hasegawa. “Comparison of OXC node architectures for WDM and flex-grid optical networks”. In: *2015 24th International Conference on Computer Communication and Networks (ICCCN)*. IEEE. 2015, pp. 1–8.

[72] Xiang Liu. “Evolution of fiber-optic transmission and networking toward the 5G era”. In: *Iscience* 22 (2019), pp. 489–506.

[73] Han Sun, Kuang-Tsan Wu, and Kim Roberts. “Real-time measurements of a 40 Gb/s coherent system”. In: *Optics express* 16.2 (2008), pp. 873–879.

[74] Michael G Taylor. “Coherent detection method using DSP for demodulation of signal and subsequent equalization of propagation impairments”. In: *IEEE Photonics Technology Letters* 16.2 (2004), pp. 674–676.

[75] S Walker. "Rapid modeling and estimation of total spectral loss in optical fibers". In: *Journal of lightwave technology* 4.8 (1986), pp. 1125–1131.

[76] Govind P Agrawal. *Fiber-optic communication systems*. John Wiley & Sons, 2012.

[77] GJ Foschini and CD Poole. "Statistical theory of polarization dispersion in single mode fibers". In: *Journal of Lightwave Technology* 9.11 (1991), pp. 1439–1456.

[78] Govind P Agrawal. "Nonlinear fiber optics". In: *Nonlinear Science at the Dawn of the 21st Century*. Springer, 2000, pp. 195–211.

[79] Erik Agrell et al. "Roadmap of optical communications". In: *Journal of Optics* 18.6 (2016), p. 063002.

[80] Five-Volume Set. "Encyclopedia of Modern Optics". In: (2005).

[81] Biswanath Mukherjee. *Optical WDM networks*. Springer Science & Business Media, 2006.

[82] AR Chraplyvy. "Optical power limits in multi-channel wavelength-division-multiplexed systems due to stimulated Raman scattering". In: *Electronics letters* 2.20 (1984), pp. 58–59.

[83] Govind P Agrawal. *Fiber-optic communication systems*. John Wiley & Sons, 2012.

[84] Emmanuel Desurvire. "Analysis of noise figure spectral distribution in erbium doped fiber amplifiers pumped near 980 and 1480 nm". In: *Applied optics* 29.21 (1990), pp. 3118–3125.

[85] Govind P Agrawal. "Nonlinear fiber optics". In: *Nonlinear Science at the Dawn of the 21st Century*. Springer, 2000, pp. 195–211.

[86] John Kerr. "XL. A new relation between electricity and light: Dielectrified media birefringent". In: *The London, Edinburgh, and Dublin Philosophical Magazine and Journal of Science* 50.332 (1875), pp. 337–348.

[87] Michael J Connelly. *Semiconductor optical amplifiers*. Springer Science & Business Media, 2007.

[88] Shoichi Sudo. *Optical fiber amplifiers: materials, devices, and applications*. Artech house, 1997.

[89] Clifford Headley and Govind P Agrawal. *Raman amplification in fiber optical communication systems*. Academic press, 2005.

[90] Vittorio Curri. "GNPy model for design of open and disaggregated optical networks". In: *2021 European Conference on Optical Communication (ECOC)*. IEEE. 2021, pp. 1–86.

[91] Mattia Cantono et al. “On the interplay of nonlinear interference generation with stimulated Raman scattering for QoT estimation”. In: *Journal of Lightwave Technology* 36.15 (2018), pp. 3131–3141.

[92] Alexei Pilipetskii et al. “The subsea fiber as a Shannon channel”. In: (2019).

[93] Vittorio Curri. “Software-defined WDM optical transport in disaggregated open optical networks”. In: *2020 22nd International Conference on Transparent Optical Networks (ICTON)*. IEEE. 2020, pp. 1–4.

[94] Alessio Ferrari et al. “GNPy: an open source application for physical layer aware open optical networks”. In: *Journal of Optical Communications and Networking* 12.6 (2020), pp. C31–C40.

[95] Jane M Simmons. *Optical network design and planning*. Springer, 2014.

[96] Asuman E Ozdaglar and Dimitri P Bertsekas. “Routing and wavelength assignment in optical networks”. In: *IEEE/ACM transactions on networking* 11.2 (2003), pp. 259–272.

[97] Ireneusz Szcześniak, Andrzej Jajszczyk, and Bożena Woźna-Szcześniak. “Generic Dijkstra for optical networks”. In: *Journal of Optical Communications and Networking* 11.11 (2019), pp. 568–577.

[98] Iguatemi E Fonseca et al. “Algorithms for FWM-aware routing and wavelength assignment”. In: *Proceedings of the 2003 SBMO/IEEE MTT-S International Microwave and Optoelectronics Conference-IMOC 2003.(Cat. No. 03TH8678)*. Vol. 2. IEEE. 2003, pp. 707–712.

[99] Akbar Ghaffarpour Rahbar. “Review of dynamic impairment-aware routing and wavelength assignment techniques in all-optical wavelength-routed networks”. In: *IEEE Communications Surveys & Tutorials* 14.4 (2011), pp. 1065–1089.

[100] Rudra Dutta, Ahmed E Kamal, and George N Rouskas. *Traffic grooming for optical networks: foundations, techniques and frontiers*. Springer Science & Business Media, 2008.

[101] Anshul Agrawal, Lev B Sofman, and Tarek S El-Bawab. “Enhancement of bandwidth efficiency by traffic grooming in optical-cross-connect based networks”. In: *Optical Transmission Systems and Equipment for WDM Networking II*. Vol. 5247. SPIE. 2003, pp. 196–202.

[102] Ihtesham Khan et al. “Automatic management of N× N photonic switch powered by machine learning in software-defined optical transport”. In: *IEEE Open Journal of the Communications Society* 2 (2021), pp. 1358–1365.

[103] Ihtesham Khan et al. “Machine Learning for Multi-Layer Open and Disaggregated Optical Networks”. In: (2022).

[104] Stephen Marsland. *Machine learning: an algorithmic perspective*. Chapman and Hall/CRC, 2011.

[105] Alvin Rajkomar, Jeffrey Dean, and Isaac Kohane. "Machine learning in medicine". In: *New England Journal of Medicine* 380.14 (2019), pp. 1347–1358.

[106] Fei Wang, Lawrence Peter Casalino, and Dhruv Khullar. "Deep learning in medicine—promise, progress, and challenges". In: *JAMA internal medicine* 179.3 (2019), pp. 293–294.

[107] Giuseppe Carleo et al. "Machine learning and the physical sciences". In: *Reviews of Modern Physics* 91.4 (2019), p. 045002.

[108] Vittorio Curri. "Software-defined WDM optical transport in disaggregated open optical networks". In: *2020 22nd International Conference on Transparent Optical Networks (ICTON)*. IEEE. 2020, pp. 1–4.

[109] Luis Velasco et al. "Building autonomic optical whitebox-based networks". In: *Journal of Lightwave Technology* 36.15 (2018), pp. 3097–3104.

[110] I. Khan et.al. "Machine-learning-aided abstraction of photonic integrated circuits in software-defined optical transport". In: *Next-Generation Optical Communication: Components, Sub-Systems, and Systems X*. Vol. 11713. International Society for Optics and Photonics. 2021, 117130Q.

[111] Ihtesham Khan et al. "Softwarized and Autonomous Management of Photonic Switching Systems Using Machine Learning". In: *2021 International Conference on Optical Network Design and Modeling (ONDM)*. IFIP. 2021.

[112] Ihtesham Khan et al. "Machine-learning-aided abstraction of photonic integrated circuits in software-defined optical transport". In: *Next-Generation Optical Communication: Components, Sub-Systems, and Systems X*. Vol. 11713. SPIE. 2021, pp. 145–150.

[113] Martín Abadi et al. "{TensorFlow}: a system for {Large-Scale} machine learning". In: *12th USENIX symposium on operating systems design and implementation (OSDI 16)*. 2016, pp. 265–283.

[114] Gavin Hackeling. *Mastering Machine Learning with scikit-learn*. Packt Publishing Ltd, 2017.

[115] Chihming Chang and Rami Melhem. "Arbitrary size benes networks". In: *Parallel Processing Letters* 7.03 (1997), pp. 279–284.

[116] Adel AM Saleh. "Transparent optical networking in backbone networks". In: *Optical Fiber Communication Conference*. Optica Publishing Group. 2000, ThD7.

[117] Adel AM Saleh and Jane M Simmons. "Evolution toward the next-generation core optical network". In: *Journal of lightwave Technology* 24.9 (2006), p. 3303.

[118] Xiang Liu. "Evolution of fiber-optic transmission and networking toward the 5G era". In: *Iscience* 22 (2019), pp. 489–506.

[119] Junho Cho et al. "Trans-atlantic field trial using high spectral efficiency probabilistically shaped 64-QAM and single-carrier real-time 250-Gb/s 16-QAM". In: *Journal of Lightwave Technology* 36.1 (2018), pp. 103–113.

[120] Dimitris Uzunidis et al. "Fifty Years of Fixed Optical Networks Evolution: A Survey of Architectural and Technological Developments in a Layered Approach". In: *Telecom*. Vol. 3. 4. MDPI. 2022, pp. 619–674.

[121] Sudhir K Routray et al. "The new frontiers of 800g high speed optical communications". In: *2020 4th International Conference on Electronics, Communication and Aerospace Technology (ICECA)*. IEEE. 2020, pp. 821–825.

[122] Yusuke Sasaki et al. "Optical-Fiber Cable Employing 200-μm-Coated Four-Core Multicore Fibers". In: *Journal of Lightwave Technology* 40.5 (2022), pp. 1560–1566.

[123] Hitoshi Takeshita et al. "Demonstration of uncoupled 4-core multicore fiber in submarine cable prototype with integrated multicore EDFA". In: *Journal of Lightwave Technology* 41.3 (2022), pp. 980–988.

[124] Mattia Cantono et al. "Opportunities and challenges of C+ L transmission systems". In: *Journal of Lightwave Technology* 38.5 (2020), pp. 1050–1060.

[125] Vittorio Curri. "GNPy model of the physical layer for open and disaggregated optical networking". In: *Journal of optical communications and networking* 14.6 (2022), pp. C92–C104.

[126] Emmanuel Desurvire and Michael N Zervas. *Erbium-doped fiber amplifiers: principles and applications*. 1995.

[127] Taban Qayoom, Gausia Qazi, and Hakim Najeeb-ud-din. "Design, characterization and performance evaluation of few-mode EDFA system with propagation up to six modes". In: *Optical and Quantum Electronics* 52 (2020), pp. 1–19.

[128] Benjamin J Puttnam et al. "High data-rate and long distance MCF transmission with 19-core C+ L band cladding-pumped EDFA". In: *Journal of Lightwave Technology* 38.1 (2020), pp. 123–130.

[129] Fady I El-Nahal, Abdel Hakeim M Husein, et al. "Thulium doped fiber amplifier (TDFA) for S-band WDM systems". In: *Open J. Appl. Sci* 2.04 (2012), pp. 5–9.

[130] Tiejun J Xia et al. "Transmission of 400G PM-16QAM channels over long-haul distance with commercial all-distributed Raman amplification system and aged standard SMF in field". In: *OFC 2014*. IEEE. 2014, pp. 1–3.

[131] Infinera. *Baud Rate, Modulation, and Maximizing Coherent Optical Performance*. Accessed: 2024-07-29. 2021. URL: https://www.infinera.com/wp-content/uploads/Baud-Rate-Modulation-and-Maximizing-Coherent-Optical-Performance-0294-WP-RevA-0921.pdf.

[132] Tingye Li, Alan E Willner, and Ivan Kaminow. *Optical Fiber Telecommunications VA: Components and Subsystems*. Elsevier, 2010.

[133] Rene Schmogrow. "Solving for scalability from multi-band to multi-rail core networks". In: *Journal of Lightwave Technology* 40.11 (2022), pp. 3406–3414.

This Ph.D. thesis has been typeset by means of the TEX-system facilities. The typesetting engine was pdfLATEX. The document class was `toptesi`, by Claudio Beccari, with option `tipotesi=scudo`. This class is available in every up-to-date and complete TEX-system installation.